2012

'Omic' Evaluation of the Region Specific Changes Induced by Non-Cholinergic Diisopropylfluorophosphate (DFP) Exposure in Fischer 344 Rat Brain

Deirdre A. Mahle
Wright State University

‘OMIC’ EVALUATION OF THE REGION SPECIFIC CHANGES INDUCED BY NON-CHOLINERGIC DIISOPROPYLFLUOROPHOSPHATE (DFP) EXPOSURE IN FISCHER 344 RAT BRAIN

A dissertation submitted in partial fulfillment of the
requirements for the degree of
Doctor of Philosophy

By

Deirdre A. Mahle
B.S., University of Dayton, 1987

2012
Wright State University

WRIGHT STATE UNIVERSITY

GRADUATE SCHOOL

July 5, 2012

I HEREBY RECOMMEND THAT THE DISSERTATION PREPARED UNDER MY SUPERVISION BY Deirdre A. Mahle ENTITLED 'Omic' Evaluation of the Region Specific Changes Induced by Non-Cholinergic Diisopropylfluorophosphate (DFP) Exposure in Fischer 344 Rat Brain BE ACCEPTED IN PARTIAL FULFILLMENT OF THE REQUIREMENTS FOR THE DEGREE OF Doctor of Philosophy.

_____

Nicholas V. Reo, Ph.D.
Dissertation Director

_____

Gerald Alter, Ph.D.
Director, Biomedical Sciences Ph.D. Program

_____

Andrew Hsu, Ph.D.
Dean, Graduate School

Committee on Final Examination

_____

Nicholas V. Reo, Ph.D.

_____

Adrian Corbett, Ph.D.

_____

James McDougal, Ph.D.

_____

James Olson, Ph.D.

_____

Michael Raymer, Ph.D.

ABSTRACT

Mahle, Deirdre A., PhD; Biomedical Sciences PhD program, Department of Biochemistry and Molecular Biology, Wright State University, 2012. 'Omic' Evaluation of the Region Specific Changes Induced by Non-Cholinergic Diisopropylfluorophosphate (DFP) Exposure in Fischer 344 Rat Brain

Organophosphorous compounds (OPs) are a class of serine esterase inhibitors that have widespread application as pesticides, veterinary pharmaceuticals and chemical warfare agents. Environmental contamination is ubiquitous. The threat of exposure is a concern for both military and civilian populations. Acute inhibition of acetylcholinesterase by OPs triggers a cholinergic crisis that results in muscle flaccidity, paralysis, convulsions and death. At low doses OPs can alter neuronal differentiation, cell signaling, behavior and cognition through unknown mechanisms. An imbalance of reactive oxygen species may be implicated in the adverse effects of OPs. An integrated approach using both metabolomic and transcriptomic techniques was used to reveal some of the non-cholinergic effects of diisopropylfluorophosphate (DFP), a model OP, in rat brain. Adult male Fischer 344 rats were administered 1 mg/kg DFP or saline via subcutaneous injection at 10 mL/kg. Cortex, brainstem, cerebellum and hippocampus were collected at multiple time points ranging from 0.5 - 48 hr. Total RNA was isolated from each region for differential gene expression analysis using the Affymetrix 1.0 ST gene array at 1 hr post dose. Lipid and aqueous extracts were prepared from each brain region at 2 hr post dose, and profiles of small molecule metabolites, lipids and phospholipids were measured using multinuclear NMR spectroscopy. Because the dose was below the threshold for cholinergic

toxicity, it was hypothesized that DFP exposure would up-regulate inflammatory pathways and down-regulate processes that result in cellular degradation, such as apoptosis, and that these changes would correlate with perturbations in the small molecule and lipid profiles as well as gene expression. All brain regions reached minimum acetylcholinesterase activity (40-55%) at 1-2 hr post dose with the exception of cortex, which had minimum activity at 12 hr post dose. No brain region showed significant increases in lipid peroxidation. After 1 hr, pathways associated with prostaglandin D2 synthesis were up-regulated in cortex. Brainstem showed increased expression of genes associated with an inflammatory response and ascorbate transport. Cortex showed the most changes in the lipid profile with significant decreases in phosphatidylcholine, phosphatidylethanolamine, cholesterol, n3 and n6 fatty acids. The mitochondrial phospholipid cardiolipin was significantly decreased after 2 hr in brainstem. By evaluating the impact of low level OP exposure on the neuronal phenotype of specific brain regions, we hope to gain a greater understanding of the non-cholinergic mechanisms of action and sensitive target areas in order to improve the development of therapeutic targets for individuals exposed to OPs.

TABLE OF CONTENTS

LIST OF FIGURES

LIST OF TABLES

ACKNOWLEDGEMENTS

I would like to thank my advisor, Dr. Nick Reo, for the opportunity to work in his lab and for teaching me so much. It has been an amazing experience. I would also like to thank my committee members, Dr. Adrian Corbett, Dr. Jim McDougal, Dr. Jim Olson and Dr. Mike Raymer. Your guidance and expertise have been invaluable. Thank you to the Biomedical Sciences PhD program for support, especially to Dr. Alter for encouraging me to apply to WSU and convincing me that I could do it.

Thank you to Dr. John Schlager for providing Air Force support as I pursued this advanced degree opportunity. Also, thank you to Dr. Victor Chan for patiently providing expertise in molecular biology. Finally, thank you to Dr. Jeff Gearhart, who was not a committee member, but certainly could have been for all the advice and support given to me. I will be forever grateful.

I also want to thank past and current members of the Reo lab, especially Andy Neuforth for always taking the time to help me in the lab and Dr. Mike Kent for always sparking scientific curiosity. From the Raymer lab, I want to thank Dr. Paul Anderson. I couldn't have done this without your help.

Last, I would like to thank my family: Andy, Lauren, Rachael and Elena. Your support and patience were everything to me.

DEDICATION

To my daughters Lauren, Rachael and Elena: you were my inspiration.

I. INTRODUCTION

1.1 Background

Sufficient evidence exists to suggest that organophosphates (OPs), as a class of compounds, exert toxicity by mechanisms that are non-cholinergic or are secondary to cholinergic activation. A variety of OPs exhibiting a range of acute toxicities have been reported to alter neuronal differentiation and migration, interfere with signaling cascades and impart learning and cognitive dysfunction at doses that do not significantly inhibit the enzyme acetylcholinesterase. Knowledge of the mechanisms of action, however, is limited. This dissertation investigates the off-target toxicity of the OP diisopropylfluorophosphate (DFP). A rat model was used to test the following hypothesis: **A non-cholinergic dose of DFP will initiate an inflammatory response, possibly mediated by oxidative stress, which perturbs the metabolic profile of the central nervous system.** Because of the low level nature of the dose, it was expected that the cellular response of the brain would be two-fold: protection and repair.

The experimental approach taken for this research relied on 'omic' technology, which allowed for a systems biology-focused analysis to integrate the complex biological responses in a complex biological system. Both transcriptomics and metabolomics provide a global picture of the cellular response to disease, injury or, in this case, toxic insult. While the transcriptome does not define a cell's physiology it reveals what potentially can happen. The physiological activity of the cell is triggered and regulated at the level of the metabolites. Therefore, the use of a multi-omic approach is advantageous since the results can be analyzed and interpreted in an integrated

manner. The etiology of nearly all central nervous system (CNS) diseases and dysfunctions is largely unknown but likely is a mix of conditions that are undefined (Kaddurah-Daouk and Krishnan, 2009). Therefore, transcriptomics and metabolomics are powerful and potentially synergistic tools that can provide a snapshot of the molecular impact of an OP exposure. By way of example, genomics has successfully been used to link motor neuron disease to a genomic mutation in superoxide dismutase (Rosen *et al*, 1993), while metabolic fingerprints have also been identified for the same disease (Rozen *et al*, 2005). Using both approaches can potentially bridge the gap between the changes in gene expression and the final phenotype of the cell.

No metabolomic approaches have investigated the changes in the brain's metabolic phenotype after exposure to an OP, though a few have looked at systemic fluids (Bevilacqua *et al*., 2005). Additionally, few transcriptomic studies have looked at the differential gene expression after OP exposure, and the results are incomplete, at best. However, one study, while limited, showed increased expression of both pro- and anti-apoptotic genes (Damodaran *et al*., 2006b), supporting the idea that the cellular response to low level exposure of an OP was balanced between protection and repair. The metabolomic and transcriptomic experiments described here increase the knowledge base toward improved understanding of the mechanistic basis of adverse effects of low level DFP exposure.

An important characteristic of this research effort is that the brain was not regarded as a single organ system. Because the brain is highly heterogeneous in chemistry, composition and function, it was divided into four major regions: cortex, brainstem, cerebellum and hippocampus. Each region represented a distinct structure and physiology, chemical and cellular makeup and, ultimately, a distinctive function. Therefore, it was reasonable to assume that each region's response to a low level exposure of DFP would have both characteristic similarities and unique differences. Additionally, investigating specific regions of the brain improved the likelihood of detecting slight perturbations that are significant responses for the region but may be diluted by

looking at the brain as a whole. In the rat brain, the hippocampus has been shown to be sensitive to nerve agent-induced seizures, while the frontoparietal cortex and cerebellum are sensitive regions in monkeys (Spradling *et al*., 2011). Because of the nature of nuclear magnetic resonance spectroscopy, a primary analytical tool for this research, sufficient tissue is unavailable from regions smaller than the hippocampus. Therefore, the selection of cortex, brainstem, cerebellum and hippocampus was based on regional sensitivity to OPs, size and uniqueness of function.

By understanding the mechanisms of DFP-induced inflammation and its impact on the metabolic functioning of specific brain regions, ongoing research can be focused on the sensitive areas of the brain to develop more effective therapeutic targets and preventative measures for individuals with neural dysfunction caused by OP exposure.

1.2 Transcriptomics and metabolomics

The research described here relied on the use of -omic techniques, specifically transcriptomics and metabolomics. A great deal of toxicological research is based on a reductionist approach, where a system is broken down to the smallest possible component in order to understand the component more fully. The use of a systems biology approach allowed the components to be integrated in order to understand more fully how the system was affected (Fig. 1). For the purpose of studying the mechanistic basis of a toxic insult, both transcriptomics and metabolomics can provide data-rich snapshots of the global cellular response.

Transcriptomics is the study of the transcriptome, or the set of all RNA molecules (mRNA, tRNA, rRNA and non-coding RNA) in a group of cells (Fig. 1). Traditionally, Northern blots have been performed to (semi) quantify the amount of mRNA in a biological sample. With the use of specific primers and a radiolabeled probe, RT-PCR (reverse transcriptase-polymerase chain reaction), can be employed to amplify a cDNA fragment for quantification. However, this could only be done with one gene at a time, until the advent of the microarray. Gene expression

in a biological sample was first profiled using a microarray in 1995 (Schena *et al*, 1995). A microarray is, in essence, thousands of Northern blots performed simultaneously in parallel. Using a gene array that probes for mRNA transcripts only, analyses can focus on the genes that are actively expressed or suppressed as a result of toxic insult. With the completion of the Human Genome Project in 2003, resulting in the identification of approximately 25,000 genes in human DNA, publicly available, comprehensive databases have facilitated the analysis and interpretation of gene expression data.

Metabolomics is, simply, the study of the metabolome, or the complete set of metabolites in a population of cells (Fig. 1). While metabolomics is often considered the newest of the 'omic' technologies, it has, in some sense, been used since the beginning of medicine when physicians used color, taste and smell of urine to diagnose disease (Wishart, 2007). The practice has evolved over time through the use of clinical chemistry, metabolic profiling and development of instrumentation such as HPLC (high pressure liquid chromatography), GC-MS (gas chromatography-mass spectrometry) and electrolyte analyzers.

Metabolites are intermediates or products of metabolism and are very dynamic. Approximately 2900 endogenous or common metabolites are estimated to be detectable in the human body, though not all are found in every cell type or fluid. Metabolomics was initially used to monitor specific metabolites or groups of metabolites associated with a known function (Wishart, 2007, Sweeley *et al*, 1974). This targeted approach has the advantage of being able to identify and quantify specific metabolites in order to determine a mechanistic basis of action for a disease, pharmaceutical or toxin. However, as more powerful tools have been developed, such as tandem mass spectrometry (MS-MS) and NMR spectroscopy, rapid analysis of hundreds of metabolites at a time has led to the popularity of a non-targeted approach, which has been further advanced by chemometric and multivariate methods to analyze and interpret spectra without identifying individual chemical species in a biofluid (Nicholson *et al*, 1999). Clustering

algorithms like principal component analysis (PCA) can identify metabolic signatures that classify spectra to a unique group. The benefit of a non-targeted approach is that unknown metabolites are not ignored or left out of the analysis, and metabolic patterns including previously unidentified metabolites have been successfully used to detect diseases and susceptibility to drug toxicity (Smith and Baert, 2003; Nicholson *et al*., 2002).

A significant problem for metabolomics is that, unlike the fully sequenced human genome, metabolic databases are still in their infancy. However, in 2007, scientists working under the support of Genome Alberta and Genome Canada completed the first draft of the Human Metabolome Project (www.metabolomics.ca). To date, the Human Metabolome Project has determined the normal concentration range of hundreds of metabolites specific for tissues, serum, urine and cerebrospinal fluid. Because the metabolic profile at any given time is a snapshot of that cell's physiology, metabolomics provides a unique tool to relate genomic changes to a cellular phenotype.

Both nuclear magnetic resonance (NMR) spectroscopy and liquid chromatography/mass spectrometry (LC/MS) are commonly-employed tools for studying and quantifying the metabolome. Each method has its own unique advantages and disadvantages. High resolution NMR-based metabolomics was used for this study because of the ability to capture a specific small molecule and lipid metabolite profile from one sample with minimal preparation. Instead of a classical approach of measuring an individual metabolite or a single kinetic parameter, NMR-based metabolomics gives a more complete picture of metabolic perturbations that can be more closely related to a biological process (Kaddurah-Daouk and Krishnan, 2009).

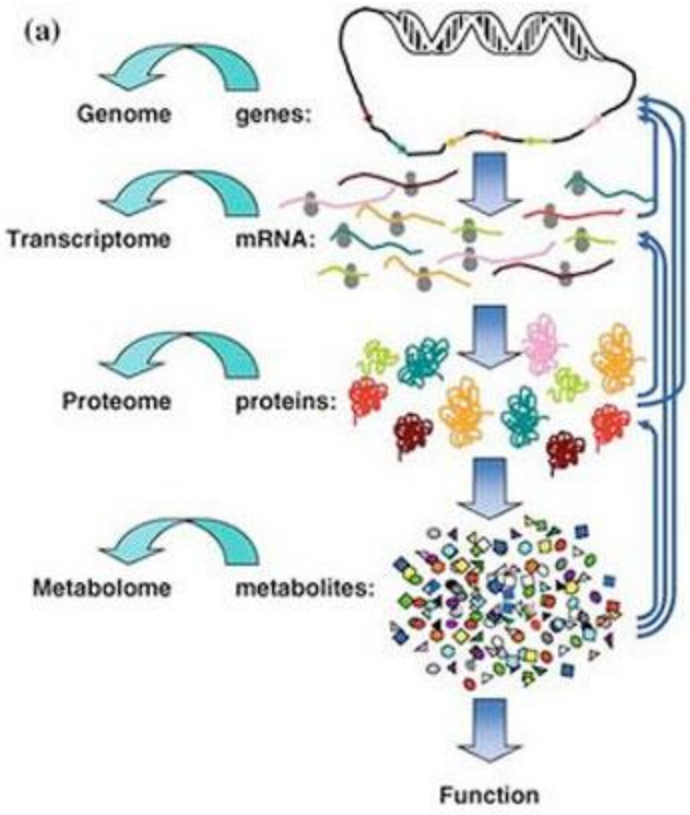

Figure 1. Hierarchy of omic techniques, showing the relationships between each discipline. The omic techniques are often described as: genomics – what can happen; transcriptomics – what appears to be happening; proteomics – how it happens; metabolomics – what happened. Image taken from the Royston Goodacre School of Chemistry, The University of Manchester.

1.3 Cholinergic toxicity of OP compounds

OPs are tri-ester derivatives of phosphoric or phosphorothioic acid. They are pentavalent tetrahedrons with three singly bound groups and an oxygen or sulfur atom doubly bound to a central phosphorous atom (Chambers and Oppenheimer, 2004). The general structure is shown in Figure 2; however, OPs exhibit a wide variety of chemistries as seen in Fig. 3.

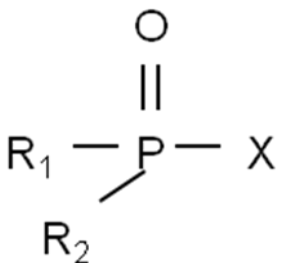

Figure 2. General organophosphate structure. R_1 and R_2 are typically alkyl or alkoxy groups. X denotes a leaving group and has diverse chemical identity. X is lost during the two step reaction with a serine esterase, allowing the remaining electrophilic chemical structure to bind with the hydroxyl group of a serine residue in the protein's active site.

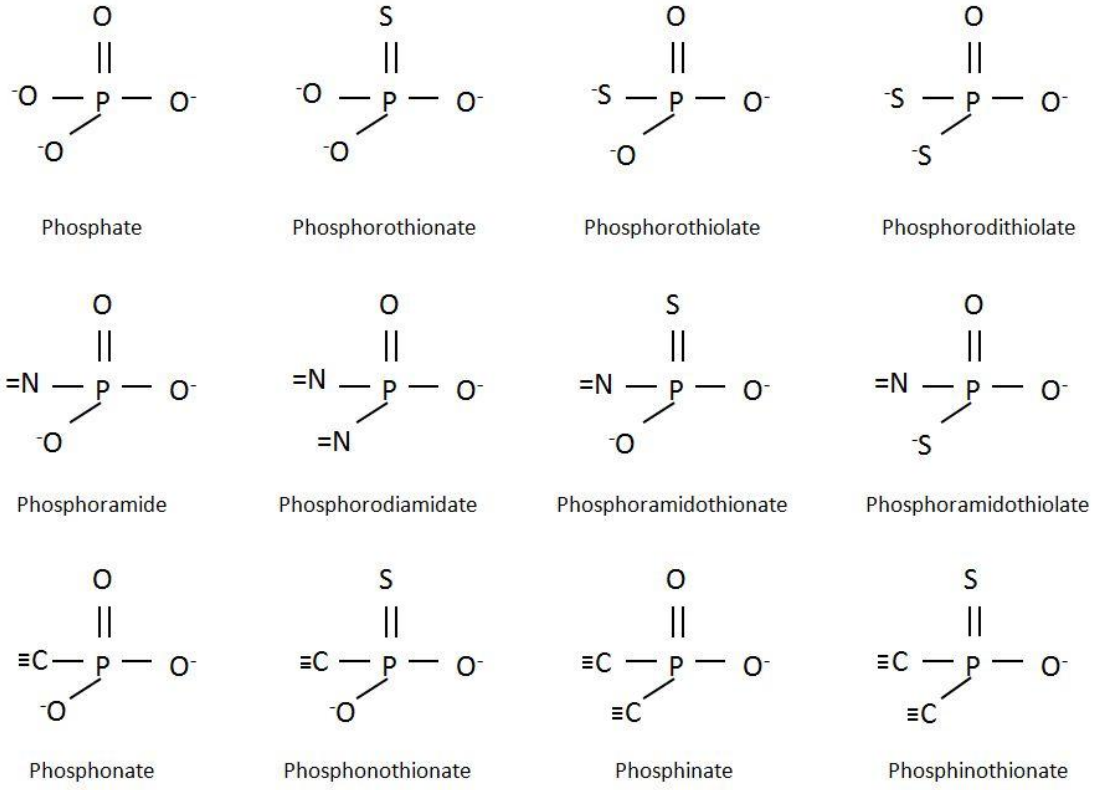

Figure 3. Examples of the wide variety of OP chemistry.

OPs are inhibitors of serine esterases and, most significantly, acetylcholinesterase (AChE). AChE is widely distributed in the central and peripheral nervous systems and is

responsible for the enzymatic cleavage of the neurotransmitter acetylcholine (ACh) to choline and acetate, part of the positive control feedback for normal neurological signaling (Figs. 4 and 5). The enzyme has a deep active site containing a catalytic triad of serine, histidine and glutamate, creating a strong nucleophile (Fig. 5a). The nucleophilic attack releases the choline group, forming an acetate-AChE intermediate (Fig. 5b). Hydrolysis frees the acetate moiety.

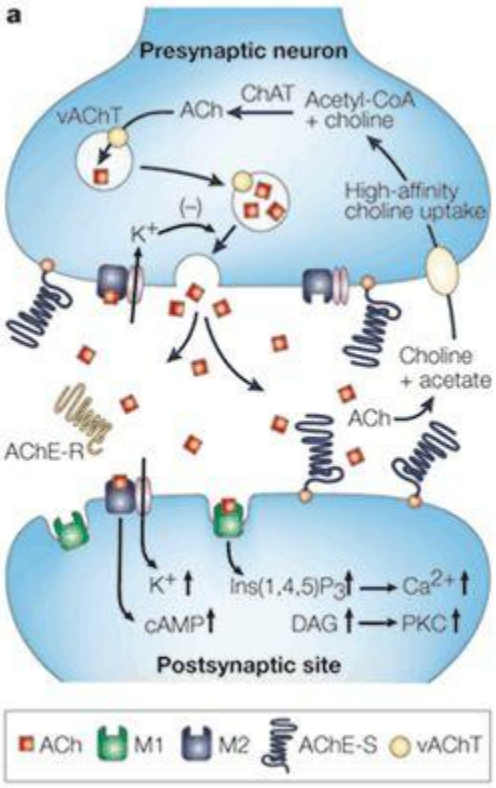

Figure 4. Schematic of cholinergic transmission and mechanism of action of acetylcholinesterase (AChE) in the cholinergic synapse. The neurotransmitter acetylcholine is released by a stimulated presynaptic neuron into the synaptic cleft. Acetylcholine binds to muscarininc or nicotinic receptors on the postsynaptic neuron or an end organ, typically muscle. Muscarininc receptors are metabotropic and use G proteins for signaling. Nicotininc receptors are ionotropic and open channels for Ca^{2+}, Na^{+} and K^{+}. AChE hydrolyzes acetylcholine to yield choline and acetate. Choline is taken back up by the presynaptic neuron through a high affinity choline transporter where it is recycled for acetylcholine synthesis via the enzyme choline acetyltransferase (ChAT). Image taken from Soreq and Seidman, 2001

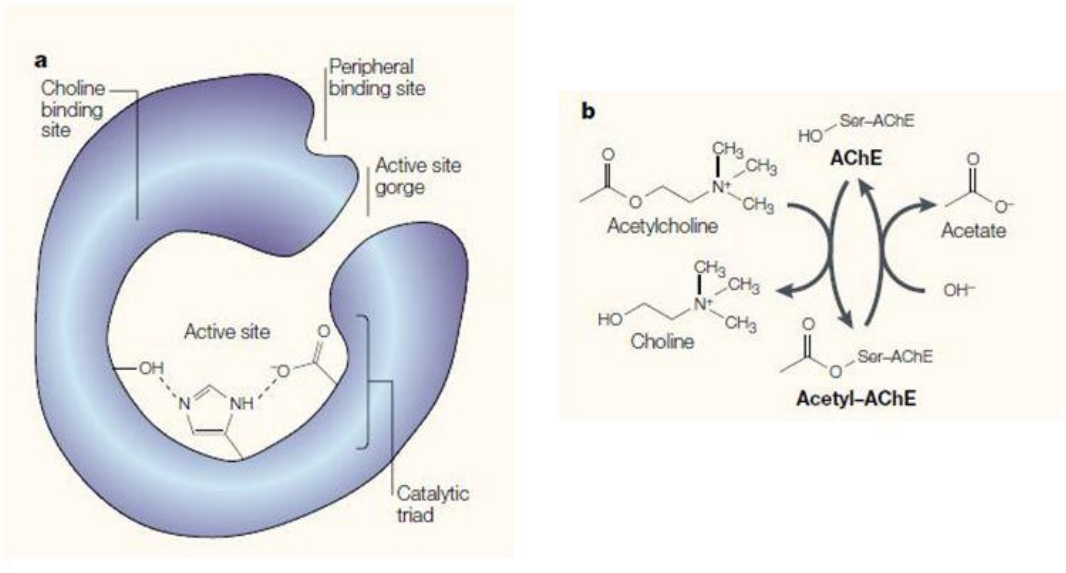

Figure 5. Breakdown of the neurotransmitter acetylcholine by acetylcholinesterase. a. catalytic triad of acetylcholinesterase. b. Hydrolysis of acetylcholine to choline and acetate. Image taken from Soreq and Seidman, 2001.

Inhibition of AChE is a two step process that involves the formation of an enzyme·OP complex in a transition state (Fig. 6).

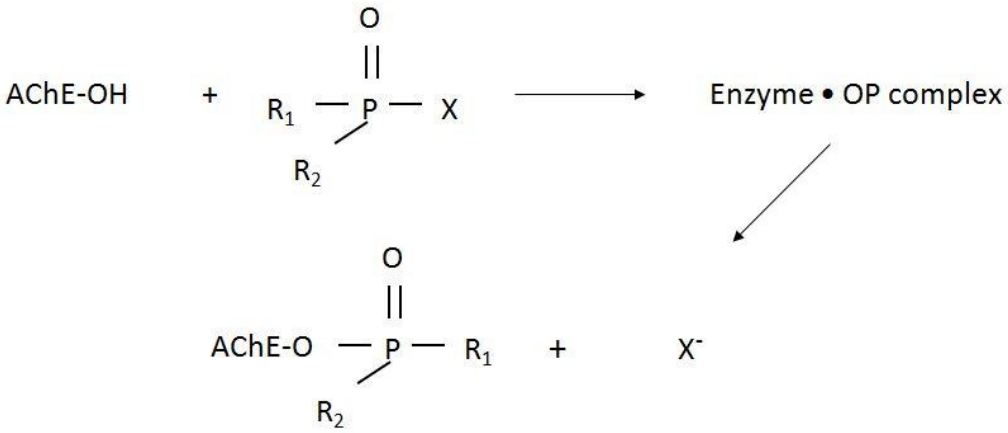

Figure 6. Two step inhibition of acetylcholinesterase, resulting in a phosphorylated enzyme.

Phosphorylation of the serine active site of AChE by an OP prevents the hydrolysis of ACh, resulting in a buildup of the neurotransmitter in the synapse and hyperstimulation of muscarinic and nicotinic receptors in the postsynaptic membrane. Figures 7 A, B and C show the binding of an OP, the transition state and the phosphorylation of the serine active site. OP binding to AChE is not irreversible, but takes hours to days to release; therefore, binding is considered essentially irreversible, as new enzymes are synthesized before the bound protein is spontaneously regenerated. However, certain OPs undergo 'aging', a process of dealkylation. The resulting monoalkyl renders the enzyme 'aged' and completely resistant to regeneration or reactivation.

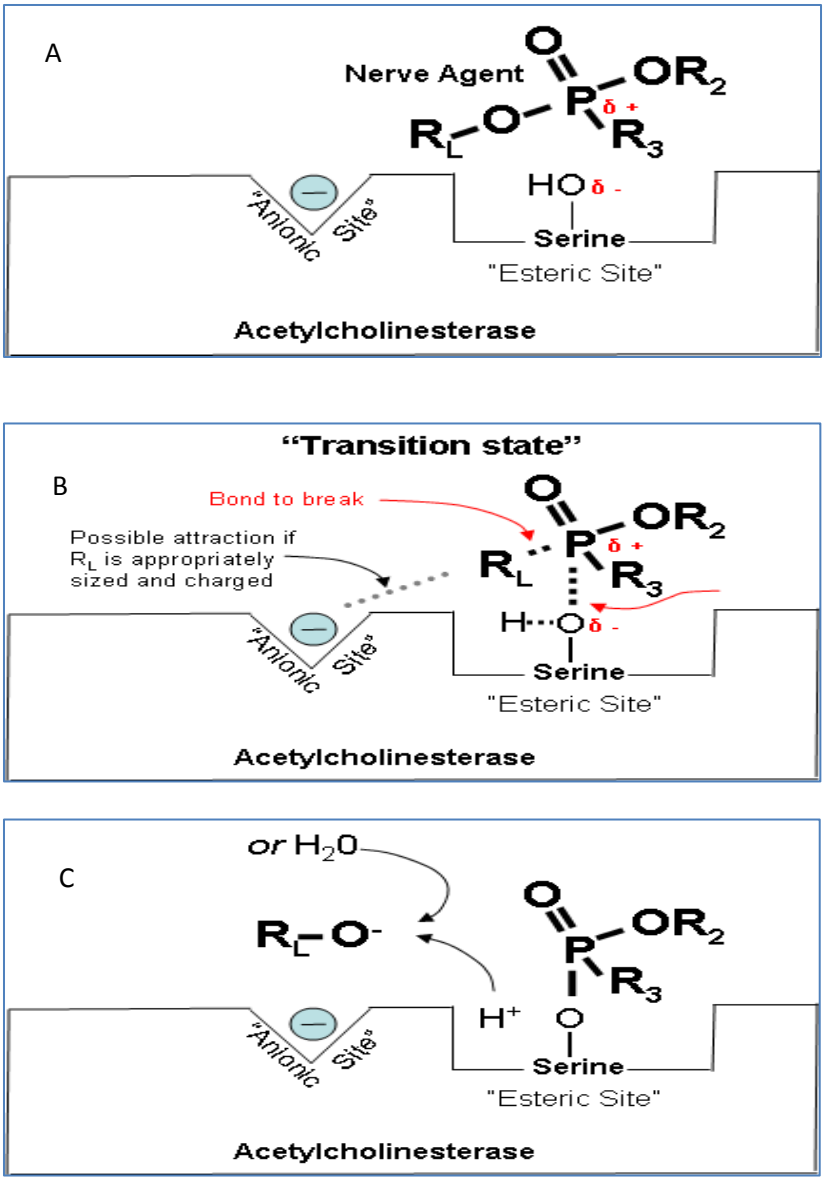

Figure 7. Mechanism of action of organophosphate (OP) inhibition of the enzyme acetylcholinesterase, using a nerve agent as a model OP. A.) Initial electrophilic attraction of the partially electropositive P of nerve agent to partially electronegative O of serine in the acetylcholinesterase active site. B.) Formation of OP·enzyme transition state. R_L is the leaving group. C.) Phosphorylation of serine active site of acetylcholinesterase. Binding of nerve agent prevents binding of acetylcholine in active site. Taken from Agency for Toxic Substances and Disease Registry (ATSDR).

Symptoms of cholinergic toxicity range from mild to severe and include blurred vision, muscle weakness, fasciculations, seizures, paralysis and death from respiratory failure. ACh receptor antagonists such as atropine can reduce or prevent excitotoxicity, while oxime

reactivators such as pralidoxime chloride can cleave the OP and restore enzyme activity. However, most therapeutically used oximes do not readily cross the blood brain barrier, leaving the brain vulnerable to long term effects of AChE inhibition (Garcia *et al*., 2010).

Because of the powerful ability to inhibit AChE activity, OPs have been exploited as pesticides, pharmaceuticals (treatment of glaucoma, primary degenerative dementia, schistosomiasis) and, more insidiously, as chemical warfare agents since the 1930s. The attacks on civilians with sarin (GB) in Japan made it clear that terrorist use of chemical weapons is no longer limited to military operations (Yokoyama *et al*., 1998; Yanagisawa *et al*., 2006). As a result, the risk of widespread contamination and human exposure, accidental or intentional, is high.

Cholinergic crisis is a catastrophic event that requires immediate life-saving treatment in the form of ACh receptor antagonists and enzyme reactivators. However, veterans of the Gulf War have been exposed to a variety of low level pesticides used in areas designated for eating and sleeping. Some were even exposed to low levels of GB and cyclosarin (GF) during the process of destroying a munitions dump (Proctor *et al*., 2006). It has been speculated that chronic exposure to these low levels of OPs may have contributed to the medically unexplainable physical symptoms experienced by many veterans of the first Gulf War. Indeed, the incidence of a neurodegenerative disease that strikingly resembles amyotrophic lateral sclerosis (ALS) was significantly increased in this group with onset at ages younger than typically seen with sporadic ALS (Haley, 2003; Horner *et al*., 2003; Weisskopf *et al*., 2005).

It has already been documented that chronic inhibition of the enzyme neurotoxic esterase (NTE) by some OPs is associated with OP-induced delayed neuropathy (OPIDN), though OP pesticides used in the United States are not significant inhibitors of NTE, and there is limited evidence to suggest that nerve agents target NTE (Pope, 1999; Richardson, 1992). Therefore,

OPIDN is not the focus of this research. However, in addition to anticholinesterase activity, evidence is mounting that OPs exert adverse neurological effects that may be secondary to or separate from inhibition of AChE with the potential to lead to neuronal dysfunction.

1.4 Non-cholinergic toxicity of OP compounds

Based on published data and for the purposes of this research, a non-cholinergic dose was considered to be a sub-acute dose that inhibits AChE to a level that does not elicit an overt response indicative of cholinergic toxicity such as salivation, lacrimation and seizures (muscarininc effects) or muscle weakness, fasciculation and flaccidity/paralysis (nicotinic effects). Substantial evidence exists to indicate that OPs elicit neurotoxic responses at non-cholinergic doses. Song *et al*. (1998) investigated the developmental neurotoxicity of chlorpyrifos (CPF), an organophosphothionate, using rat pheochromocytoma (PC12) cells, a cell line that can be induced to differentiate into cholinergic neurons. While the PC12 cells were in an undifferentiated state, subtoxic levels of CPF inhibited DNA synthesis in a dose dependent manner. Addition of ACh receptor antagonists had no effect on the inhibition of DNA synthesis, indicating that the effects were caused by non-cholinergic mechanisms. In the same cell line after treatment with nerve growth factor (NGF) to induce differentiation, CPF inhibited not only DNA synthesis but protein synthesis, as well, with a corresponding decrease in neurite extensions at the highest dose.

In vivo studies have also shown adverse developmental effects of OPs that raise concern over pediatric exposure. Early postnatal rats that were treated daily from postnatal day 1 to 6 by oral gavage with either a low or a high dose of CPF were evaluated for markers of neonatal brain growth (Betancourt, 2006). Although the chosen doses caused measurable levels of inhibition of brain AChE, they were below the NOEL (no observable effect level) for signs of overt toxicity. Both the low and high doses of CPF caused a decrease in the expression of NGF, reelin and

myelin-associated glycoprotein (MAG) mRNA. Because the protein reelin is involved with neuronal migration, it is possible that CPF can induce abnormal migration patterns which are associated with cognitive and mental dysfunction, as well as motor deficits. Additionally, decreases in MAG, a CNS specific protein, suggest that oligodendrocytes are a target of OPs and early formation of myelin in the CNS could be disrupted. It is important to note that while these changes in mRNA expression were dose dependent, the changes were significant from control even at the low dose.

Diazinon, another organophosphothionate, caused similar restrictive changes in neurite outgrowth as CPF in neonatal rats exposed to doses well below the maximum tolerated dose for 4 days (Slotkin *et al*., 2006). Choline acetyltransferase, the enzyme responsible for synthesis of ACh, was also decreased, although down regulation of muscarinic ACh receptors, a signal for excess cholinergic stimulation, was not evident. These results suggest that the developmental effects were independent from anticholinesterase activity. Song *et al*. (1997) compared the effects of CPF on adult rat forebrain, an area rich in cholinergic innervation, to the cerebellum, which has fewer cholinergic synapses than forebrain and to heart muscle, a non-neuronal tissue. The expression and activity of adenylyl cyclase (AC) as well as the activation of the G protein receptors coupled to AC were decreased in all three tissues. Interestingly, the actions of CPF were not immediate but were delayed for several days after cessation of treatment. The conclusion was that cholinergic synapses or even the CNS were not the specific target of CPF.

Lastly, it was determined from rat hippocampal cultures that nanomolar concentrations of the agent VX caused a release of glutamate and γ-aminobutyric acid (GABA) that was independent of action potential-induced opening of calcium channels (Rocha *et al*., 1999). Extracellular calcium was required for neurotransmitter release, suggesting that VX could interact with the calcium channels directly or through a second messenger. The release of neurotransmitters was unaffected by the complete inhibition of AChE by the nerve agent soman.

Therefore, independent of cholinesterase inhibition, VX was able to interfere with neuron to neuron communication, establishing dysfunctional transfer of information. In light of the evidence of non-cholinergic toxicity at the cellular level, do these effects translate into a phenotype of neurological dysfunction or disease?

1.5 Altered phenotypes after OP exposure

Genovese *et al*. (2006) investigated the effects of low level GF on the learned behavior of adult Sprague-Dawley rats that were operantly conditioned to press levers for food pellets. Rats receiving GF by inhalation at doses eliciting only mild signs of toxicity showed a significant deficit in the response time as compared to their baseline performances. However, the effects did not persist after 48 hr. This is in contrast, though, to cognitive studies carried out by Kassa *et al*. (2001). Learning and spatial memories of adult Wistar rats were significantly influenced by low level GB inhalation in a dose dependent manner as compared to control rats exposed to air only. Rats in the highest dose group that displayed some mild symptoms of toxicity but were non-convulsant showed a decrease in their performance for three weeks post exposure. The underlying reason for the deficit in memory, however, is unknown.

One interesting study investigated the short and long term changes in the hypothalamus-pituitary-adrenal (HPA) axis after low dose inhalation of GB in adult rats (Peña-Philippides *et al*., 2007). After repeated exposure to GB at doses that did not produce signs of cholinergic toxicity, serum cortisol levels decreased significantly and remained lower than control levels at eight weeks after treatment. To correlate the decrease in cortisol to inhibition of the HPA axis and not cholinergic toxicity, plasma levels of adrenocorticotropin hormone were measured and were found to be significantly decreased, as well. GB-induced suppression of the HPA axis has the potential to disrupt many of the functions under its control. In light of the fact that cortisol was

decreased for at least eight weeks hints at the long lasting effect that GB had on neuroendocrine function.

In 1994 and 1995 terrorists used GB on civilians in a Tokyo subway. Neurobehavioral tests conducted on survivors revealed significantly lower scores on psychomotor performances six to eight months after exposure when compared to unexposed individuals, possibly the result of permanent damage to the CNS (Yokoyama *et al*., 1998). In 1991 US troops destroyed a munitions dump that was later discovered in 1996 to have been a depot for the nerve agents GB and GF. Neuropsychological testing was performed to evaluate the impact of the exposure on neurobehavioral function on the returning troops (Proctor *et al*., 2006). It was found that low level exposure to GB and GF was significantly correlated to fine psychomotor dexterity and visuo-spatial deficiencies 4-5 years later.

It is clear that low level exposures to organophosphates have resulted in altered behavioral phenotypes, significantly affecting learning and memory functions. These deficits in cognitive function indicate the potential for long term damage caused by non-cholinergic doses of OPs.

1.6 OPs and oxidative stress

It is apparent that OPs can interact with a variety of enzymes and pathways, altering their function and changing the phenotype of the targeted cell. Because OPs are relatively lipophilic they can penetrate the blood brain barrier, target neurons and alter neuronal phenotype. What is not clear are the exact, non-cholinergic mechanisms by which OPs affect neural function and whether a non-lethal dose can result in adverse changes in brain function. It is possible that one means by which OPs exert non-cholinergic toxicity is through the induction of oxidative stress. In the privileged environment of the brain, generating oxidative stress can set off a chain of

adverse events that involves peroxidation of structural and signaling lipids, impaired function of membrane proteins and inflammation.

The adult human brain has a tremendously high O_2 and glucose consumption rate, using 20% of basal O_2 and 4 X 10^{21} molecules of glucose per min (Emerit *et al*., 2004). Mitochondrial respiration accounts for the majority of reactive oxygen species (ROS) produced, converting 1-2% of consumed oxygen into ROS. The production of ROS is a normal intermediate step of mitochondrial oxidation. However, oxidative stress occurs when there is an imbalance between generation and elimination of ROS. One of the major ROS produced from mitochondrial oxidation is superoxide anion, which has one unpaired electron, making it a free radical capable of removing an electron from a non-radical species. Polyunsaturated fatty acids (PUFAs), essential components of membranes and signaling lipids and highly abundant in the CNS, are sensitive targets of free radicals. Free radicals such as superoxide can extract hydrogen from a C-H bond, leaving an unpaired electron on the carbon atom (Fig. 8). The resulting carbon-centered free radical reacts quickly with O_2 to form peroxyl radicals. Peroxyl radicals are highly reactive and oxidize adjacent PUFA side chains, membrane proteins and cholesterol, propagating a chain reaction that is self sustaining and highly damaging to the cell.

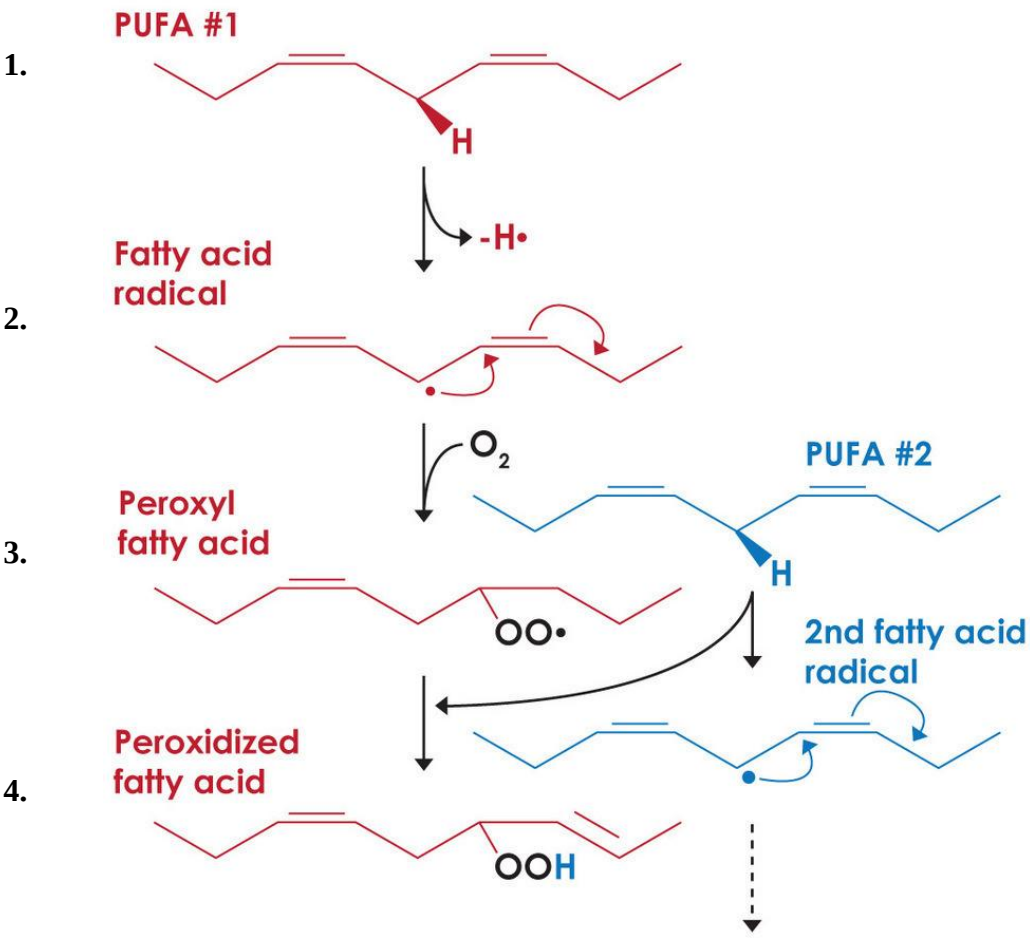

Figure 8. Steps involved in the chain reaction of lipid peroxidation. PUFA – polyunsaturated fatty acid. Step 1. Extraction of hydrogen from C-H bond. Step 2. Molecular rearrangement Step 3. Generation of lipid peroxyl radical, capable of extracting H from C-H from adjacent PUFA. Step 4. Peroxidized fatty acid. Taken from Oxidized Phospholipids: Of Whiskers and Razors, Brock, TG.

The adverse effects of lipid peroxidation include a decrease in membrane fluidity with a corresponding increase in membrane leakiness, as well as damage to the many membrane proteins, including receptors, enzymes and ion channels (Halliwell, 2006). Many OPs sequester in the cellular lipid domains with higher concentrations near the membranes as compared to other regions (Bagchi *et al*., 1995). Being localized in lipid dense regions provides an ideal environment for OPs to have maximum adverse effect, triggering oxidative stress-related impacts such as altered membrane structure, compromised membrane proteins or pro-inflammatory responses.

1.7 OPs and inflammation

DFP insult to the brain at a dose below the threshold for cholinergic toxicity would be considered an indirect or mild trauma, characterized by expression of M-CSF (macrophage colony stimulating factor), TGFβ-1 (transforming growth factor beta) and IL-6 (interleukin-6) (Raivich *et al*., 1999). Interestingly, an indirect trauma can activate microglia, cells of monocyte lineage, to a state of alert, priming them for a more graded response, if necessary (Raivich *et al*., 1999). Multiple reports have shown that acute, seizure-inducing doses of nerve agents elicit pro-inflammatory responses (Dhote *et al*., 2007; Chapman *et al*., 2006; Williams *et al*., 2003a). It is speculated that pro-inflammatory molecules are responsible for the secondary effects of OP poisoning and may be involved in long term neurodegeneration (Spradling *et al*., 2011). Limited data are available to indicate that non seizure-inducing doses of OPs also trigger inflammatory responses. However, after a 0.5 x LD_{50} dose of sarin, rat brain showed increased gene expression of cytokines that persisted 3 months post exposure (Damodaran *et al*., 2006a), evidence that low level OP exposures do induce an inflammatory response. It was hypothesized that a non-cholinergic dose of DFP would initiate an inflammatory response, possible mediated by oxidative stress, which would perturb the metabolic profile of the central nervous system. Because the dose level was low, it was expected that this should be a survivable insult and the cellular response would focus on protection and repair and the return to homeostasis. However, in an organ system as complex as the nervous system, particularly the brain, initiating an inflammatory cascade can set the stage for increased responses that may switch from neuroprotective to neurotoxic, resulting in long term dysregulation.

1.8 Diisopropylfluorophosphate

The OP selected for this research effort was diisopropylfluorophosphate (DFP). DFP was first synthesized in 1946 as a pesticide (McCombie and Saunders, 1946), though currently it has

little commercial value. This compound was selected because it is both structurally and mechanistically similar to highly toxic OPs such as activated insecticides and nerve agents (Taylor, 1980). The chemical structure of DFP is shown in Figure 9. DFP's leaving group is fluorine, a small, highly electronegative atom. In the two-step reaction with AChE, the loss of fluorine results in a strong electrophile that reacts readily with AChE.

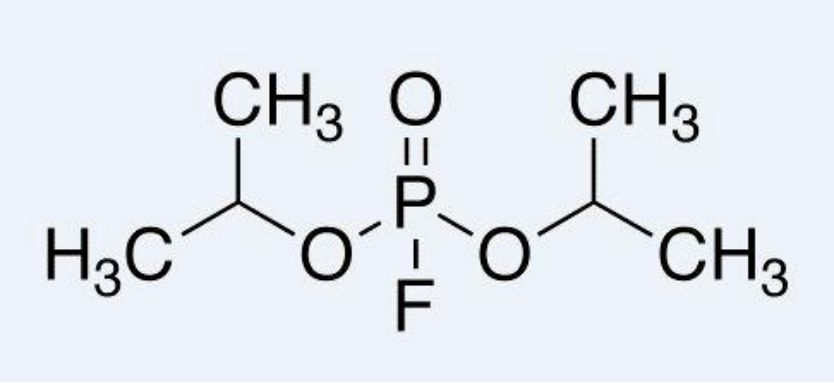

Figure 9. Chemical structure of the organophosphate diisopropylfluorophosphate (DFP). The leaving group is a fluorine atom, making DFP strongly electrophilic.

It is unclear if DFP-induced oxidative stress is dose-dependent or even if the generation of ROS occurs with low level exposure. Adult male rats exposed to a single dose of DFP had a significant increase in lipid peroxidation (measured by thiobarbituric acid-malondialdehyde complex) in diaphragm at 30, 60 and 120 minutes after exposure to 1.5 and 2.0 mg/kg but not 1 mg/kg (Yang and Dettbarn, 1996). The level of AChE activity after the 1 mg/kg dose was at approximately 47% of control while the two higher doses dropped enzyme activity to less than 15% of control. The muscle fasciculations caused by the hyperstimulation of ACh receptors could account for the increase in ROS (Reid *et al*., 1992; Yang and Dettbarn, 1996); therefore, it is unclear if the source of ROS was receptor hyperstimulation or increased muscle activity that correlated to an increase in mitochondrial output. This study also focused on measurements of AChE activity and lipid peroxidation in muscle with no report of brain-specific changes. In a

separate study, rats that were subcutaneously dosed with 1.25 mg/kg DFP in saline showed significant increases in cerebral F_2-isoprostanes and F_4-neuroprostanes, which are sensitive, specific markers of oxidative damage to arachidonic acid and docosahexaenoic acid, respectively, up to 2 hr post dose (Zaja-Milatovic *et al*, 2009). This dose elicited a severe yet nonlethal cholinergic response. Again, it cannot be determined if the generation of ROS was sparked by muscle activity or excitotoxicity that results from overstimulation of postsynaptic receptors. If receptor overstimulation was the primary source of oxidative stress, than it is possible that a DFP dose that inhibits AChE to a level that does not induce cholinergic crisis may still increase ROS through an increase in stimulation of excitatory receptors. Additionally, measurements of ROS for this study were done in whole brain which may mask specific regional changes in lipid peroxidation. To uncover compartmentalized effects and prevent diluted responses this research described changes in specific brain regions.

1.9 Selection of brain regions

An important aspect of this research was that the brain was not regarded as a single organ system. Because the brain is highly heterogeneous in chemistry, composition and function, it was divided into four major regions: cortex, brainstem, cerebellum and hippocampus. Each region represented a distinct structure and physiology, chemical and cellular makeup and, ultimately a distinctive function. Therefore, it was assumed that each region's response to a low level exposure of DFP would have both characteristic similarities and unique differences. By investigating specific regions of the brain, the likelihood of detecting slight, yet significant perturbations for a region was improved. In the rat brain, the hippocampus has been shown to be sensitive to nerve agent-induced seizures, while the frontoparietal cortex and cerebellum are sensitive regions in monkeys (Spradling *et al*., 2011). DFP has been reported to induce altered sleep-wake patterns controlled by the reticular formation in the brainstem (Deurveilher *et al*., 1999a, b). Because of the nature of nuclear magnetic resonance spectroscopy, a primary

analytical tool for this proposal, sufficient tissue was unavailable from regions smaller than the hippocampus. Therefore, the selection of cortex, brainstem, cerebellum and hippocampus was based on regional sensitivity to OPs, size and uniqueness of function.

1.10 Thesis focus and significance

This research has focused on understanding the mechanism of non-cholinergic toxicity and the means by which low level exposure to OPs contributes to long term effects. The data presented here support the hypothesis that a low level exposure to DFP induced an inflammatory response that was characterized by a graded cellular response of protection and repair and manifested by regional changes in lipid composition and small molecule metabolite profiles. Understanding the downstream effects of DFP-induced inflammation on specific regional metabolism will provide important knowledge for understanding the mechanistic basis for the development of neuroprotectants for individuals exposed to OPs.

II. MATERIALS AND METHODS

2.1 Animals and treatments

All animals used in this study were handled in accordance with the principles stated in the Guide for the Care and Use of Laboratory Animals, National Research Council, 1996 and the Animal Welfare Act of 1966, as amended. Male Fischer 344 rats (CDF® (F344)/CrlBR; 200-250g) were received from Charles Rivers Laboratory (Raleigh, NC) and housed individually with *ad libitum* access to food (Purina Certified Rat Chow #5002) and fresh conditioned reverse osmosis water. Rats were given a single subcutaneous injection at the dorsal base of the neck of DFP (Sigma Chemical Company) in 0.9% sterile saline at a dose of 1 mg/kg. Control rats received 0.9% sterile saline at 10 mL/kg. Animals were observed for signs of overt cholinergic toxicity for 1 hr post dosing. These signs included excess salivation, lacrimation, urination and defecation (SLUD), as well as the inability to maintain posture. Control and DFP-treated animals (N=5/time point) were euthanized by CO_2 inhalation and rapid decapitation at 0.5, 1, 2, 12, 24 or 48 hr post dose. One to two drops of trunk blood were collected into tubes containing a heparin ring and flash frozen in liquid nitrogen. Brains were removed, rinsed with ice cold saline and dissected on ice to collect cortex, brainstem, cerebellum and hippocampus. The first dissection cut, using a scalpel blade, was a coronal cut between the cerebrum and the cerebellum (Fig. 10 A, B). The portion of the brainstem attached to the cerebellum was gently pulled away to isolate the two regions (Fig. 10 C). A sagittal cut was then made between the two cerebral hemispheres, and the two hemispheres were laid medial side up (Fig. 10 A, D). The thalamus and midbrain were gently scraped away and added to the rest of the brainstem. An ice cold spatula was placed in the lateral ventricle underneath the hippocampus (Fig. 10 E). A cut was made superiorly and

inferiorly to free each end of the hippocampus. The hippocampus was rolled up and away from the cortex with the spatula (Fig. 10 F). It is important to note that because of the dissection technique it was undetermined if the corpus callosum was left in the cortex region. Each section was immediately flash frozen in liquid nitrogen and stored at -80°C.

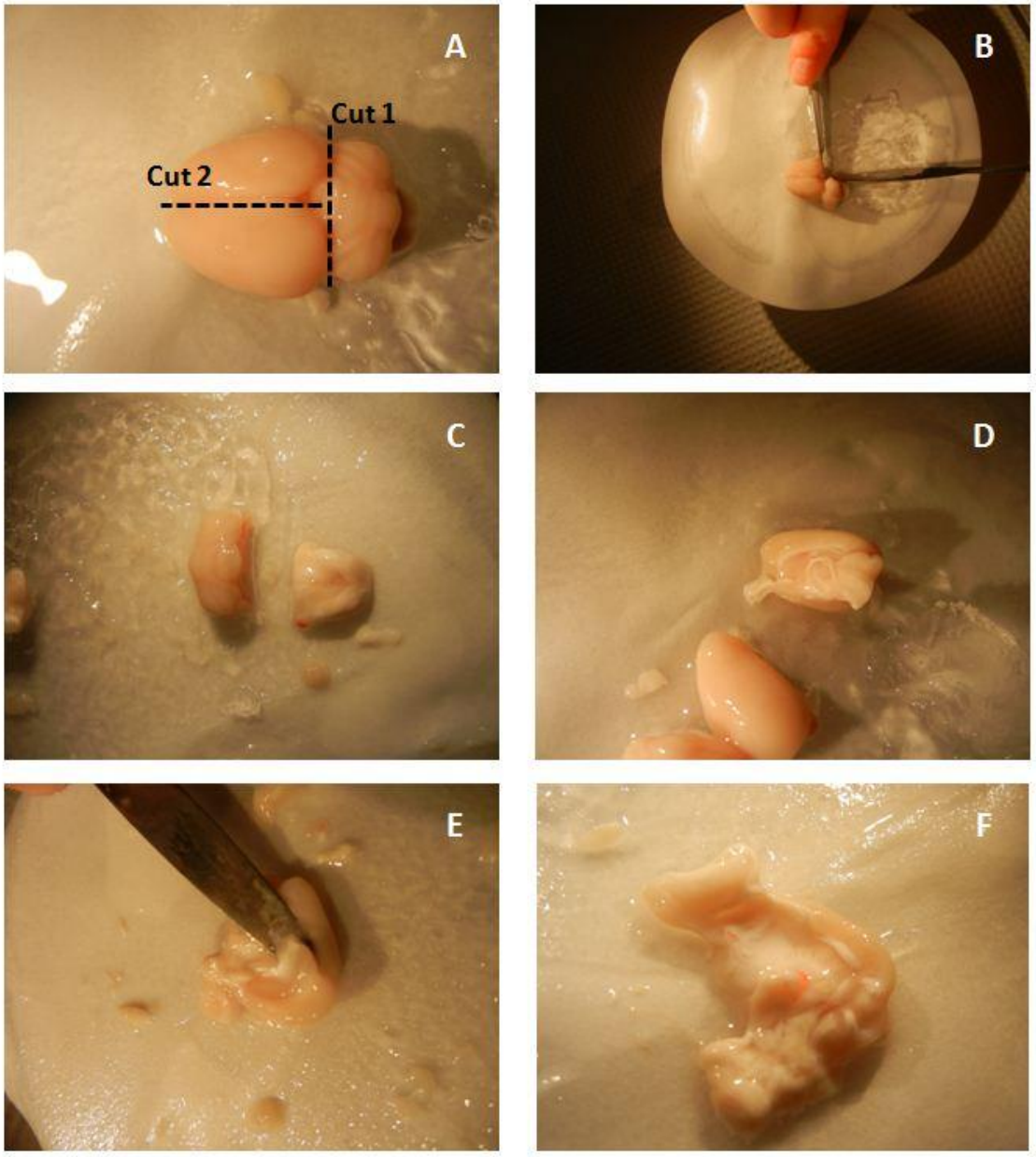

Figure 10. Diagram of rat brain dissection. A.) Cut 1 separated the cerebellum and portion of the brainstem from the rest of the brain. Cut 2 separated the two cerebral hemispheres to expose the remaining brainstem, thalamus and hippocampus. B.) Scalpel blade cutting cerebellum and portion of brainstem from cerebrum. C.) Separation of the cerebellum from portion of the brainstem. D.) Cerebral hemisphere displayed medial side up. E.) Isolation of the hippocampus. F.) Hippocampus rolled away from cerebral hemisphere. Photos courtesy of Dr. James Olson.

2.2 Biochemical assays

AChE activity was measured using a modified version of the Ellman assay (Ellman *et al*., 1961), using dithionitrobenzoic acid (DTNB) and acetylthiocholine as substrate. Brain samples were thawed on ice, and 15-20 mg sections of each region were homogenized in 200 µL buffer (0.1 M sodium phosphate, pH 7.4, containing 0.5% Tween-20), using a Dounce homogenizer with Teflon pestle. The homogenates were centrifuged at 13,000 rpm at 4°C for 5 min and supernatant transferred to a clean tube. To inhibit butyrylcholinesterase 1µL of 10 mM iso-OMPA (tetraisopropyl pyrophosphoramide) was added. Samples were incubated on ice for 45 min. Ten microliters of sample were added to wells of a 96 well flat bottom plate containing 150 µL of NaPO4, pH 8.0 buffer; samples were run in triplicate. Each well received 20 µL of 10 mM DTNB (prepared in 0.1 M $NaPO_4$ buffer, pH 7.0), and the reaction was started with the addition of 20 µL of 10 mM acetylthiocholine (prepared in double distilled water). Blank samples contained DTNB only. Hydrolysis of the acetylthiocholine substrate by AChE in the tissue homogenates produces thiocholine. The rate of this hydrolysis was determined by the reaction of thiocholine with dithionitrobenzoic acid to produce 5-thio-2-nitrobenzoate; therefore, the rate of hydrolysis was determined by measuring the change in absorbance at 412 nm over 6 min. Enzyme activity (µmol/min/ml) was calculated by dividing the slope of the absorbance values by the extinction coefficient (13600) and multiplying by the dilution factor (500). Data were normalized to protein concentration, which was determined in each brain region using the Pierce BCA method with bovine serum albumin for linear standard calibration (Thermo Fisher Scientific, Inc., Rockford, IL). A Dunnet's test was used to determine significant changes from the control value (averaged from all control animals at all time points).

Malondialdehyde (MDA) was determined for cortex samples using the Colorimetric Assay for Lipid Peroxidation kit (Oxford Biomedical Research, Oxford, MI) or for brainstem, cerebellum and hippocampus using the microplate version. Each whole brain region was

homogenized in ice cold PBS (1:1 w/v) at pH 7.4 with a Dounce homogenizer with Teflon pestle. Non-interference in the assay was confirmed for this buffer. Prior to homogenization, 10 µL of 0.5 M butylated hydroxytoluene (BHT) per mL of sample were added to prevent artifactual oxidation of any lipids. The samples were centrifuged at 3000 x g at 4°C for 10 min to remove large particles. An aliquot of the sample was removed for protein determination. The MDA standard was provided as a 10mM stock solution of 1, 1, 3, 3-tetramethoxypropane (TMOP) in Tris-HCl. A 20 µM standard stock was prepared from this by diluting the 10 mM stock 1:500 in dH_2O immediately before use. Standards for calibration were prepared in microcentrifuge tubes as described in Table 1.

Table 1. MDA standard curve preparation.

Standard	MDA conc (µM)	Vol of dH_2O (µL)	Vol of 20 µM MDA stock (µL)
S_0	0	200	-
S_1	0.5	195	5
S_2	1.0	190	10
S_3	2.5	175	25
S_4	5.0	150	50
S_5	10.0	100	100
S_6	15.0	50	150
S_7	20.0	-	200

A sample blank was prepared by adding 487.5 µL of acetonitrile and 162.5 µL of Diluent (provided in kit) to a microcentrifuge tube. The sample blank corrected for any contribution to the A_{586} caused by chromophore in the sample. The Reagent R1 (supplied in kit) was diluted 3:1 with Diluent immediately before use. The cuvette assay procedure was started by adding 200 µL of sample or standard, 650 µL of the diluted R1 and 150 µL of 12N hydrochloric acid to a microcentrifuge tube. The microplate assay procedure was started by adding 140 µL of sample or standard, 455 µL of the diluted R1 and 105 µL of 12N hydrochloric acid to a microcentrifuge tube. Samples and standards were run in triplicate. Standards, samples and the sample blank

were incubated at 45°C for 60 min. All tubes were centrifuged at 15,000 x g for 10 min to obtain a clear supernatant. For the cuvette assay, the clear supernatant was transferred to a cuvette and read at 586 nm. For the microplate assay, three 150 µL aliquots of the supernatant were transferred to the manufacturer supplied microplate and read at 586 nm. The net A_{586} for the standards were plotted against MDA concentration and a linear regression analysis was performed. The concentration of analyte was calculated for each unknown sample from the net A_{586} of the sample (Equation 1).

$$[\text{MDA}] = \frac{A-b}{m} \times df \qquad \text{Equation 1}$$

Where: [MDA] = µM concentration of MDA in sample

A = Net absorbance at 586 nm of the sample

m = regression coefficient (slope)

b = intercept

df = dilution factor (5)

Sample concentrations were normalized to protein content. Protein concentration was determined using the Pierce BCA method. Student's unpaired t-test was used to determine if there were significant changes ($p \leq 0.05$) in MDA after DFP exposure at each time point.

2.3 RNA preparation

2.3.1 RNA isolation

Before RNA isolation each brain region from the 1 hr time point was ground under liquid nitrogen using an RNase free frozen mortar and pestle to insure a homogeneous mix of the tissue sample. Total RNA was isolated from each brain region using a Qiagen RNeasy Mini Kit (Qiagen, Valencia, CA). Six-hundred microliters of Buffer RLT (from kit) with β-mercaptoethanol were added to a homogenization tube containing approximately 30 mg of tissue.

A stainless steel bead was added to each tube which was then homogenized on a Mix Mill MM 300 for 2 min at 20 Hz. The tube was rotated 180° and homogenized for another 2 min at 20 Hz. The sample was centrifuged at 15,000 rpm for 3 min. The supernatant was transferred to a QIAshredder spin column and centrifuged at 15,000 rpm for 2 min. After removing the column, the lysate was transferred to a new DNase RNase free microcentrifuge tube. Six-hundred microliters of 70% ethanol were added to the lysate and mixed by pipetting up and down 5 times. The sample was transferred to an RNeasy spin column fitted with a 2 mL collection tube and centrifuged for 20 sec at 10,000 rpm. The flow through was discarded. Seven-hundred microliters of Buffer RW1 (from kit) were added to the RNeasy spin column and centrifuged for 20 sec at 10,000 rpm. The flow through was discarded. Five-hundred microliters of Buffer RPE (from kit) were added to the RNeasy spin column and centrifuged for 20 sec at 10,000 rpm. The flow through was discarded. An additional 500 µL of Buffer RPE were added to the RNeasy spin column and centrifuged for 20 sec at 10,000 rpm. The flow through was discarded. The column and collection tubes were centrifuged for 1 min at 15,000 rpm to eliminate any possible carryover of Buffer RPE. The spin column was removed and placed in a new 1.5 mL collection tube. To elute the RNA, 30 µL of DNase RNase free water were added directly to the spin column and allowed to sit for 2 min at room temperature. The column and tube were centrifuged at 13,000 rpm for 1 min and flow through collected. The RNA concentration was measured using a NanoDrop 2000 spectrophotometer (Thermo Scientific, Wilmington, DE). In addition, RNA quality was determined spectrophotometrically from the A_{260}/A_{280} ratio (acceptable range of 1.9 to 2.1) and from gel electrophoretic separation of the 28S rRNA and 18S rRNA bands, using a freshly poured 1% agarose gel. Electrophoretic gel images and A_{260}/A_{280} ratios are shown in Appendix I. For the synthesis of cDNA through hybridization steps, refer to Figure 11.

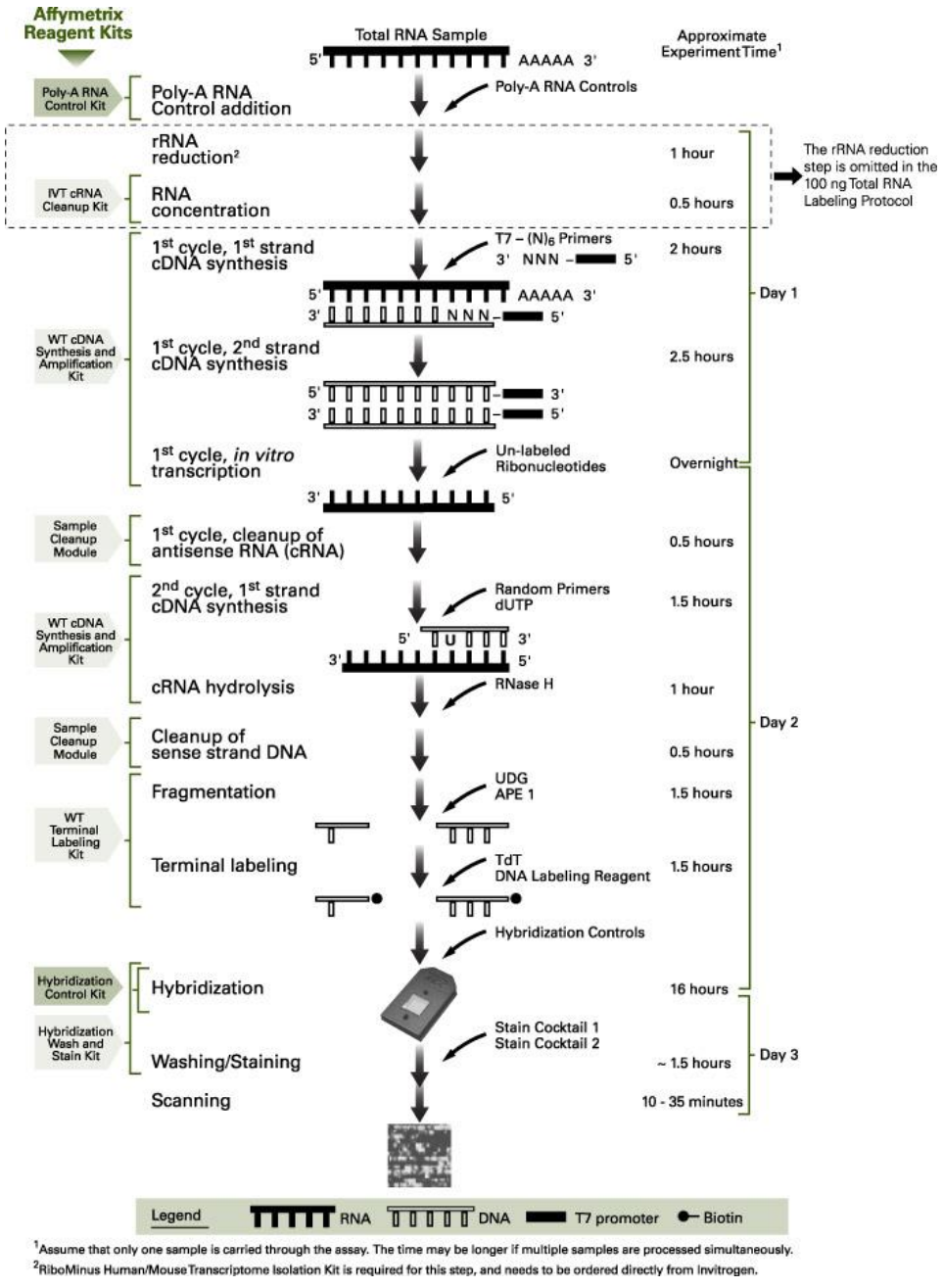

Figure 11. WT (Whole Transcript) Sense Target Labeling Assay. Schematic taken from Affymetrix.

2.3.2 1st strand cDNA synthesis

Amplification and target preparation of the RNA for microarray analysis were completed using the Ambion WT Expression Kit (Applied Biosystems), Affymetrix GeneChip WT Labeling

Kit and the Poly-A RNA Control kit. All tubes used were DNase and RNase free. All enzymes and buffers noted in the text were supplied with the kits. The Poly-A control stock was diluted 1:10, then 1:50, then 1:50 and finally 1:10 to yield a final 100 ng total RNA in 2 µL. The 1st strand master mix was prepared in bulk for all samples using the following mix ratio (for 1 sample): 4 µL 1st strand buffer mix; 1 µL 1st strand enzyme mix. The buffer mix contained T7-$(N)_6$ primers. Each sample was normalized to 100 ng RNA per 3 µL. To labeled PCR tubes, the following were added: 5 µL 1st strand master mix; 2 µL of the diluted Poly-A spike control; 3 µL of RNA-containing sample. Each tube was gently vortexed, quick spun and incubated in a Verti™ thermalcycler (Applied Biosystems) with a heated lid following the 1st Strand cDNA synthesis method (Table 2).

Table 2. Thermal Cycling Methods

Method	Heated Lid Temp (°C)	Step 1	Step 2	Step 3	Step 4
1st Strand cDNA Synthesis	50	25°C, 60 min	42°C, 60 min	4°C, 2 min	
2nd Strand cDNA synthesis	Room Temp	16°C, 60 min	65°C, 10 min	4°C, 2 min	
In Vitro Transcription cRNA synthesis	50	40°C, 16 hrs	4°C, hold		
2nd Cycle cRNA Denaturation	75	70°C, 5 min	25°C, 5 min	4°C, 2 min	
2nd Cycle cDNA synthesis	75	25°C, 10 min	42°C, 90 min	70°C, 10 min	4°C, 2 min
RNase H Hydrolysis	75	37°C, 45 min	95°C, 5 min	4°C, 2 min	
Fragmentation	105	37°C, 60 min	93°C, 2 min	4°C, 2 min	
Labeling	105	37°C, 60 min	70°C,10 min	4°C, 2 min	

2.3.3 2nd strand cDNA synthesis

The 2nd strand master mix was prepared on ice using the following mix ratio (for 1 sample): 32.5 µL DNase RNase free water; 12.5 µL 2nd strand buffer mix; 5 µL 2nd strand enzyme mix. Fifty microliters of the 2nd strand master mix were added to each of the 1st strand synthesis samples, gently vortexed, quick spun and incubated in a thermalcycler using the 2nd Strand Synthesis method (Table 2). At the end of the program, samples were removed, quick spun and placed on ice for 5 min before proceeding directly to *in vitro* transcription cRNA synthesis.

2.3.4 Synthesis of cRNA using in vitro transcription (IVT)

The IVT master mix was prepared at room temperature using the following mix ratio (for 1 sample): 24 µL IVT buffer mix; 6 µL IVT enzyme mix. Thirty microliters of the IVT master mix were added to each of the 2nd strand cDNA samples, gently vortexed, quick spun and incubated in a thermalcycler using the IVT method (Table 2). At the end of the IVT program, the samples were placed on ice before purification of the cRNA.

2.3.5 Purification of cRNA

The Elution Solution (provided with kit) was preheated at 55°C for at least 10 min before use. The cRNA binding master mix was prepared at room temperature using the following mix ratio (for 1 sample): 10 µL nucleic acid binding beads; 50 µL nucleic acid binding buffer. Sixty microliters of the cRNA binding master mix were added to each sample, pipetting up and down three times to mix. The samples were then transferred to a U-bottom plate. Sixty microliters of 100% isopropanol were added to each sample, pipetting up and down three times to mix. The plate was gently shaken on a plate shaker (Boekel Scientific) for 2 min and then moved to a magnetic stand for 5 min while the mixture became clear and the beads formed pellets against the magnets. The supernatant was removed and discarded. One-hundred microliters of nucleic acid

wash solution were added to each sample. The plate was shaken for 1 min, and the wash process was repeated a second time. The residual ethanol was allowed to evaporate by shaking the plate an additional minute at high speed. Forty microliters of the heated elution solution were added to each sample and allowed to incubate at room temperature for 2 min. The plate was vigorously shaken for 3 min and then moved to the magnetic stand for 5 min. The supernatant containing the cRNA was transferred to clean tubes, and cRNA yield was determined using a Nanodrop spectrophotometer and stored at -20°C before proceeding to the 2nd Cycle cDNA Synthesis.

2.3.6 2nd Cycle cDNA synthesis

Each sample was normalized to 455 ng/µL (equal to a total of 10 µg cRNA in a volume of 22 µL). Twenty-two microliters of the sample and 2 µL of Random Primers (from kit) were added to clean PCR tubes on ice. The samples were gently vortexed, quick spun and incubated in the thermalcycler, using the 2nd Cycle cRNA Denaturation program. The 2nd Cycle master mix was prepared at room temperature using the following mix ratio (for 1 sample): 8 µL of 2nd cycle buffer mix; 8 µL of 2nd cycle enzyme mix. At the end of the thermalcycler program, 16 µL of the 2nd Cycle master mix were added to the 2nd Cycle cRNA Denaturation product, gently vortexed, quick spun and incubated in the thermalcycler using the 2nd Cycle cDNA Synthesis program. The synthesis of second cycle cDNA in the presence of random primers and dUTP was performed to assure that regions encoded by all the exons on the gene were equally synthesized and that deoxyuridine was incorporated into the single-stranded DNA at pre-defined ratios relative to thymidine. Upon completion the samples were placed on ice for hydrolysis of the cRNA template. Two microliters of RNase H were added to each sample and mixed by pipetting up and down 3 times. Each sample was gently vortexed, quick spun and incubated on the thermalcycler using the RNase H program. The samples were removed and placed on ice for purification of the cDNA and removal of unincorporated nucleotides following the same procedure as in section 2.3.5.

2.3.7 Fragmentation, labeling and hybridization of single stranded cDNA

Fragmentation required the use of the Affymetrix GeneChip® WT Terminal Labeling kit. Each sample was normalized to 5.5 µg in 31.2 µL, using DNase RNase free water. Fragmentation master mix was prepared at room temperature using the following mix ratio (for 1 sample): 10 µL DNase RNase free water; 4.8 µL of 10X cDNA Fragmentation buffer; 1.0 µL of UDG (uracil-DNA glycosylase); 1.0 µL APE (apurinic/apyrimidinic endonuclease). Each sample tube containing 31.2 µL of normalized single stranded cDNA received 16.8 µL of fragmentation master mix. Tubes were gently vortexed, quick spun and incubated on the thermalcycler using the Fragmentation program. After the cDNA was fragmented 45 µL were transferred to clean PCR tubes, and 2 µL were used for gel electrophoresis to verify fragmented samples. Electrophoretic gel images are shown in Appendix I.

The labeling procedure required the use of the GeneChip® WT Terminal Labeling kit. Labeling master mix was prepared at room temperature using the following mix ratio (for 1 sample): 12 µL of 5X TdT (Terminal deoxynucleotidyl Transferase) buffer; 2 µL of TdT; 1 µL of 5 mM DNA labeling reagent (containing biotin label). Fifteen microliters of the master mix were added to the 45 µL aliquot of fragmented single-stranded DNA, gently vortexed, quick spun and incubated on the thermalcycler using the Labeling program.

Hybridization required the use of the GeneChip® Hybridization, Wash and Stain kit. The 20X GeneChip® Eukaryotic Hybridization Control stock was heated to 65°C for 5 min to resuspend the cRNA completely. The Hybridization Cocktail was prepared at room temperature using the following mix ratio (for 1 sample): 60 µL of fragmented and labeled DNA; 3.7 µL of control oligonucleotide B2 (3 nM); 11 µL of 20X Eukaryotic Hybridization controls (bioB, bioC, bioD, cre); 110 µL of 2X Hybridization mix; 15.4 µL of DMSO (dimethylsulfoxide); 19.9 µL of DNase RNase free water. The Hybridization Cocktail was heated at 99°C for 5 min and then

cooled to 45°C for 5 min. The samples were centrifuged at 15,000 rpm for 1 min. The Affymetrix GeneChip® Exon 1.0 ST (Sense Target) Arrays were equilibrated to room temperature and then injected with 200 µL of the sample for hybridization for 16 hr at 45°C using a rotating hybridization oven (Affymetrix) at 60 rpm. Using an Affymetrix Fluidics Station, the chips were washed and stained and then scanned with an Affymetrix GeneChip Scanner 3000. Expression Console™ software (Affymetrix) was used to evaluate overall quality of the arrays and to detect outliers.

2.38 Data processing procedures

Data processing required multiple steps to insure significant changes in gene expression in brain regions from DFP-treated rats as compared to control (Montgomery, 2006; Irizarry *et al*., 2003a; Irizarry *et al*, 2003b; Glantz, 1996; Holm, 1979). The following steps were used to process the gene array data.

Array Normalization: Normalization was performed using full quantile normalization (Irizarry *et al*., 2003). Each input array was normalized to the sum of the intensity from the 16^{th} to the 85^{th} percentile (removing higher level of noise from each end).

Probe Score Transformation and GC Filtering: The 4,021,734 probes on each array were filtered and transformed. Probes with a GC count less than 6 and greater than 17 were excluded from the analysis. Probe scores were then transformed by taking the Base-2 logarithm.

Background Correction: The background of each exon array was established from a pool of probes with no authentic hybridization targets. Each probe score was corrected for background by subtracting the median expression score of background probes with similar GC content.

Probe Summarization and Transformation: The Rat Exon 1.0 ST array contains 1,044,122 probe sets (4 probes/set). The expression score for each set was derived via the application of RMA

(Robust Multi-array Average) to the probe scores across all input hybridizations. Probe sets with fewer than three probes were excluded from further analysis.

Mixed model, nested analysis of variance was used to identify the genes with group specific expression (Montgomery, 2006). For the mixed model, the CEL file (stores the results of intensity calculations) is the random factor. The exons and the groups are the fixed effects. The data are then analyzed by ANOVA according to a linear model. For each gene tested, the probability of a false-positive was 0.05. Because a large number of independent genes were tested, this significance value was misleading since the probability of finding a false-positive grows as more genes are tested (Glantz, 1996). To correct for this, the Holm's method (step-down Bonferroni) was used.

2.4 GeneChip analysis

The gene chip data were stringently evaluated by a variety of quality assessment metrics before statistical analysis was completed (Affymetrix, Gentleman *et al*., 2005). Quality assessment measures included: (i) comparison of the mean raw intensity for all probes to the background intensity, (ii) a Pearson's correlation to check for variability in gene expression relative to other chips, and (iii) evaluation of the polyA spike probeset to confirm expected behaviors, such as constant expression levels and rank order of signals between spike sets, were observed. Cell intensities of the genechip arrays were evaluated and statistical analyses were performed using XRAY for Exon and GeneArray analysis software (Biotique Systems, Inc., Reno, NV) with a significance threshold of $p<0.05$ and an initial stringency filter of fold change > 1.15x. To determine the presence or absence of expression for a particular gene in a group, the p-value was derived to test the null hypothesis that the average of the CEL files (intensity files) belonging to the group was not above background. Rejection of the null hypothesis occurred when the p-value was less than the significance level of 0.05, in which case it is inferred that the

gene was expressed in the given group. The NIH NIAID DAVID (Database for Annotation, Visualization and Integrated Discovery, http://david.abcc.ncifcrf.gov/tools.jsp) database was used to generate the lists of pathways and biological processes with significant enrichment of up- and down-regulated genes to infer modulation/perturbation of specific biological pathways and processes in DFP-treated brain regions as compared to control (Dennis *et al*., 2003; Huang *et al*., 2009a, b). Significance was determined using a modified (more conservative) Fisher Exact test which subtracted one from the total number of genes affected by treatment. The Gene Ontology website (http://www.geneontology.org) was used in conjunction with DAVID to characterize the biological processes, molecular functions and cellular components that had altered regulation as a result of DFP exposure. PubMed Gene (www.ncbi.nlm.nih.gov/pubmed/) was used to identify specific gene functions and descriptions. To visualize the biological interactions of the significant genes, pathway analysis on the combined lists of up and down regulated genes for each brain region was performed using GeneSpring bioinformatic software (version 11.5.1; Agilent Technologies, Santa Clara, CA).

The low stringency filter was justifiable and even preferred over a higher fold change (FC) threshold. Because gene chips and RNA preparation chemistry have substantially improved, noise in the microarray is minimal, alleviating the need for a high FC filter which would lose true positives while reducing false positives. Also, the degree of fold change does not correlate to biological significance linearly, emphasizing the need for pathway analysis and determining biological interactions. The datasets went through a second level of filtering with the pathway analyses, making the need for a high stringency FC filter unnecessary. Use of the DAVID database shifted the analysis of the microarray from individual genes changes to changes in pathways.

2.5 NMR sample preparation

Each brain region from the 2 hr time point and cortex samples from the 48 hr time point were extracted by the dual phase method of Tyagi *et al*. (1996). Frozen brain sections were ground to a fine powder under liquid nitrogen using a frozen mortar and pestle. The frozen powder was quickly transferred to a tared 20 mL glass homogenizer tube, and the weight recorded. Ice cold methanol (MeOH) was immediately added to the tube at 0.7 mL/100 mg tissue, and the mixture was homogenized on ice with a chilled Teflon pestle in reverse mode at 20 rpm. The homogenate was allowed to stand on ice for 15 min. Chilled chloroform ($CHCL_3$) at 0.7 mL/100 mg tissue was added, and the mixture was homogenized at 20 rpm. Chilled double distilled water (ddH_2O) was added at 0.7 mL/100 mg tissue, and the mixture was homogenized at 20 rpm. The mixture was transferred to an ice cold 50 mL glass centrifuge tube and allowed to stand on ice for 15 min before centrifuging at 2000 x g for 25 min at 4°C. In the meantime, a separatory flask and funnel were placed in a refrigerator at 4°C. A #1 filter paper disc was placed in the funnel and primed with 0.5 mL each of MeOH, $CHCL_3$ and ddH_2O, in that order. The supernatant was transferred to the flask. The homogenizer tube was washed with 0.5 mL each of MeOH, $CHCL_3$ and ddH_2O and the mixture was re-homogenized. The mixture was allowed to stand on ice for 5 min, transferred to the same centrifuge tube and centrifuged at 2000 x g for 5 min at 4°C, transferring the supernatant to the separatory funnel. This procedure was repeated 2 more times. After the supernatant was completely filtered, the mixture was allowed to stand at 4°C for 17-24 hr to allow complete separation of the 2 liquid phases.

Once separation was complete, the funnel was moved to room temperature and allowed to sit for 2 hr. The upper aqueous phase was carefully aspirated with a disposable pipet and transferred to a 60 mL lyophilizer flask. The lower organic phase was drained into a pre-weighed 10 mL amber vial. The funnel was washed 3 times with 0.5 mL each of ddH_2O, $CHCL_3$ and

MeOH (in this order), allowing funnel to sit for 45 min between each wash to allow the phases to separate. Aqueous and organic phases were removed each time as before.

The lyophilizer flask containing the aqueous extract and the amber vial containing the organic extract were attached to clamps and placed in a 25°C water bath. A gentle stream of nitrogen was blown over the top of the flask or vial to evaporate the MeOH or $CHCL_3$. After most of the MeOH was evaporated the lyophilizer flask was placed in liquid nitrogen to freeze the aqueous extract and then lyophilized to dryness overnight. After the $CHCL_3$ was evaporated the vial was sealed with a black Viton septum (Fisher Scientific) and placed on vacuum overnight and then weighed. The lipid sample was reconstituted in 600 µL of 99.8% deuterated chloroform ($CDCl_3$) or, if the lipid weight was greater than 30 mg, then enough $CDCl_3$ was added to yield a lipid concentration of 50 mg/ml. Each vial was then crimp-sealed and stored at -20°C until analysis.

The dried aqueous sample was reconstituted in 2 mL of ddH_2O, and 5 g/100 mL of Chelex 100 were added to remove divalent ions. The mixture was stirred at 4°C for 1 hr, then transferred to a 15 mL disposable centrifuge tube and centrifuged at 2000 x g for 10 min at 4°C to remove the Chelex. The supernatant was transferred to a pre-weighed 20 mL clear serum vial and covered with filter paper. The lyophilizer flask was rinsed 3 times with 2 mL of ddH_2O, transferring each washing to the same centrifuge tube. The tube was centrifuged at 2000 x g for 5 min at 4°C, transferring the supernatant to the same vial each time. The vial was placed in liquid nitrogen to freeze the aqueous extract and placed on a lyophilizer overnight. Once dry, the dried sample was weighed, crimp-sealed and stored at -20°C for subsequent NMR analysis.

The dried aqueous extracts were reconstituted in 750 µL of 1.04 mM 2, 2`, 3, 3`-deuterotrimethylsilylpropionic acid (TSP) solution prepared in 99.99% deuterium oxide (D_2O). TSP was added as a chemical shift reference (set at 0.0 ppm) and internal standard for metabolite

quantification (^{1}H NMR). For ^{1}H analysis, 650 µL of the reconstituted solution were added to a 5 mm NMR tube. Upon completion of ^{1}H acquisition, 75 µL of 30.4 mM methylene diphosphonic acid (MDPA) in a 141.5 mM Na_2(EDTA) solution were added to the NMR tube as a standard for ^{31}P NMR analysis of aqueous samples. For NMR analysis, lipid extracts were prepared in a three-part solvent system consisting of $CDCl_3$, MeOH and 90 mM aqueous Cs_2(EDTA) (Meneses and Glonck, 1988). The final lipid sample composition was 12/4/1 $CDCl_3$:MeOH:H_2O (v/v/v). Samples were placed into 5 mm NMR tubes.

2.6 NMR analyses

All NMR analyses were performed using a Varian INOVA 600 MHz spectrometer (14.1 T). High-resolution ^{1}H and proton-decoupled ^{31}P and ^{13}C NMR spectra of brain region extracts were acquired in field-lock mode using a 5 mm broadband probe operating at 600, 243 and 151 MHz, respectively. The sample temperatures were maintained at 20°C for lipid extracts to optimize spectral resolution and 25°C for aqueous extracts. Data acquisition parameters for ^{1}H included 8000 Hz spectral bandwidth, 4 s acquisition time, 1 s interpulse delay and 45 min of signal averaging. C-13 parameters included a 70° pulse, 35 kHz spectral bandwidth and 2 s acquisition time, using a waltz ^{1}H-decoupling sequence with nuclear Overhauser enhancement (NOE) and approximately 20 hr of signal averaging. P-31 aqueous data were acquired using a ^{1}H-decoupling sequence with NOE using a 70° pulse, 12 kHz bandwidth, 1.6 s acquisition time, 2 s interpulse delay and 20 hr of signal averaging. P-31 lipid data were acquired using a 90° pulse, 800 Hz bandwidth, 1.6 s acquisition time, 13 s interpulse delay and 6 hr of signal averaging (full T_1 relaxation and no NOE).

2.7 NMR data analysis and quantification of specific metabolites

Using a Sun Microsystems computer and VNMR v6.1 software, NMR data were processed using exponential multiplication, Fourier transformation, manual phasing and baseline

correction (5^{th} order polynomial and spline correction). The ^{1}H and ^{13}C NMR spectra were adaptively binned using a dynamic programming technique in MATLAB® (MathWorks, Inc., R2011b) that sets the minimum distance between peaks to 0.002 ppm and the maximum distance between peaks in a bin to 0.04 ppm (Anderson *et al*., 2010). Adaptively binned spectra were then deconvolved, if necessary, and integrated for quantification of individually identified metabolites.

NMR chemical shift assignments for lipid resonances in the ^{13}C spectrum were taken from Forgacs *et al*. (2012), Halliday *et al*. (1988) and Sillerud *et al*. (1986). The $CDCl_3$ signal was set at 77.79 ppm for reference and was used as the internal standard for quantification. The C18, C19 and C14 carbons of cholesterol at 12.5, 19.7 and 57.2 ppm, respectively, were averaged for quantification. The signal in the range of 20.9 – 21.03 ppm represented the n2 carbon from all n3-fatty acids (FA), and the signal within the range of 32.03 – 32.29 ppm represented the n3 carbon of the n6-FA. These carbon signals shift slightly within this range because of the differences in carbon chain lengths of these fatty acids. The signal generated from the magnetically equivalent resonances of the 3 methyl carbons of the choline headgroup of phosphatidylcholine (PtdC), $(CH_3)_3N$-, at 54.4 ppm was used to quantify PtdC. This concentration of PtdC was then used as the internal standard for quantification of the ^{31}P lipid spectra. The terminal methyl carbon of fatty acids at 14.8 ppm was used as a measure of total FA. The signal at 27.3 ppm represented the polyunsaturated fatty acids (PUFA), specifically allylic carbons, C=C-$\underline{C}H_2$- C=C. While this signal was integrated for a quantitative value of PUFA, it is important to note that its intensity is dependent upon both concentration and composition, and, therefore, is not an accurate measure of concentration.

For quantification purposes the ^{1}H, ^{31}P and ^{13}C NMR signal intensities were corrected for T_1 saturation and NOE, when necessary. To correct for T_1saturation and NOE data were acquired for a representative cortex and brainstem sample under fully relaxed conditions ($5T_1$ with no NOE; interpulse delay of 250 µsec for ^{13}C and 59 µsec for ^{1}H). The ratio of the intensity of each

signal selected to the $CDCl_3$ or TSP intensity was calculated for both fully relaxed (R_{FR}) and partially saturated (R_{PS}) spectra. Calculation of the R_{FR}/R_{PS} ratio provided the saturation factor for each signal of interest. For all analyses metabolite concentrations were normalized to tissue weight.

Principal component analysis (PCA) was used as an unsupervised method to visualize NMR-derived data from control animals by transforming the data into a new coordinate system, where each new dimension was computed as a linear combination of the original values in order to demonstrate the uniqueness and/or similarities of each brain region best explained by the overall variance in the data (Jolliffe, 1986; Mahle *et al*., 2010). For PCA, adaptively binned ^1H aqueous spectra were normalized to tissue weight and autoscaled to the mean and standard deviation of the control spectra, equalizing the importance of small and large signal metabolites (Van den Berg *et al*., 2006). The signals for water and TSP were removed before autoscaling.

In order to evaluate differences between metabolites from each group, a targeted approach was used to focus on the NMR signals that were identifiable as known metabolites, making a direct comparison between control and DFP-treated groups. Because the NMR spectra represented individual rat metabolite profiles and were independent measures, Student's 2-tailed t test (unpaired) was used to determine significant differences in metabolite concentration between treatment and control groups.

III. RESULTS

3.1 Basal regional differences

3.1.1 Basal AChE activity

AChE data from control animals were compiled in order to provide comparative information regarding the normal, basal activity of the enzyme in each brain region measured (Fig. 12). AChE activity in brainstem was significantly higher than all other brain regions, while activity in cerebellum was significantly lower than all other brain regions ($p<0.01$). Enzyme activity levels in cortex and hippocampus were not different from each other.

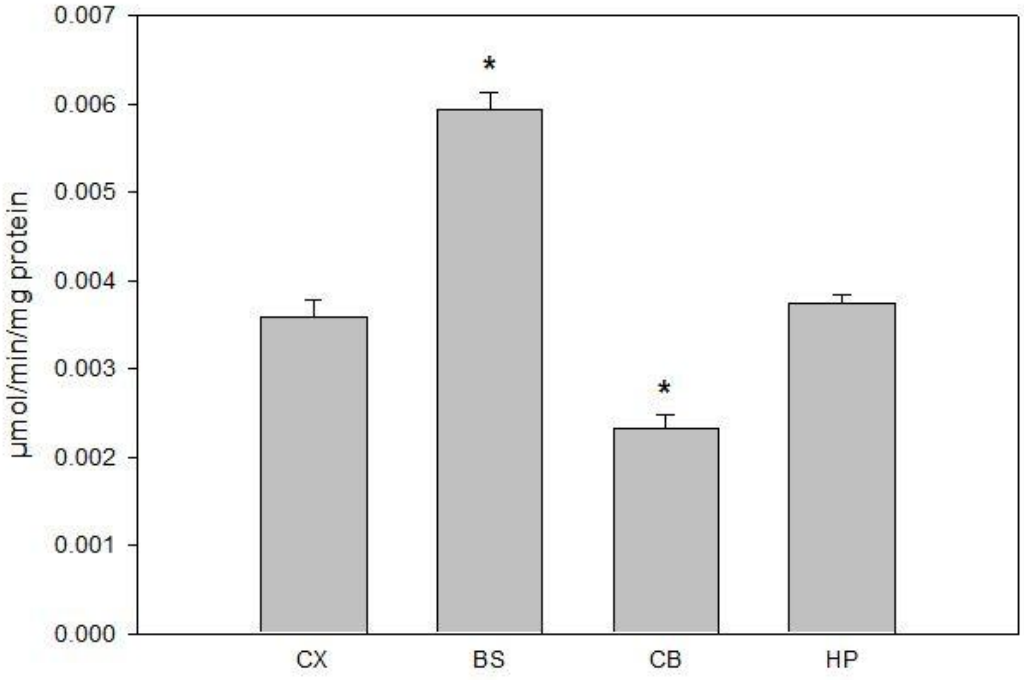

Figure 12. Basal acetylcholinesterase activity in measured brain regions. Abbreviations: CX – cortex; BS –brainstem; CB – cerebellum; HP - hippocampus. Data are from all control animals averaged over all time points (Mean ± SE; n=30). *Significantly different from all other regions ($p<0.01$).

3.1.2 Basal lipid profiles

The normal regional composition of several measured lipid species in cortex, brainstem, cerebellum and hippocampus are shown in Figure 13. The brainstem had the greatest amount of FA per g tissue and was significantly higher than all other regions measured. The hippocampus had the least amount of FA per g tissue and was significantly lower than all other regions. Cortex was lower than cerebellum. The brainstem also had the greatest amount of cholesterol, averaging about 145, 120 and 230% greater than cortex, cerebellum and hippocampus, respectively. The hippocampus had the lowest amount of cholesterol as compared to the other three regions. Cholesterol in the cerebellum was 13% higher than cortex. The intensity of the NMR signal at

27.3 ppm (PUFA) can be altered by changes in concentration and composition (number of double bonds in the FA); therefore, changes in the intensity of this NMR signal are not truly reflective of PUFA concentration alone. Overall, PUFA differences between regions were minimal. The hippocampus had lower levels of PUFA than cortex, brainstem and cerebellum, while the cortex had lower levels than brainstem and cerebellum. There was no statistical difference in PUFA levels between brainstem and cerebellum.

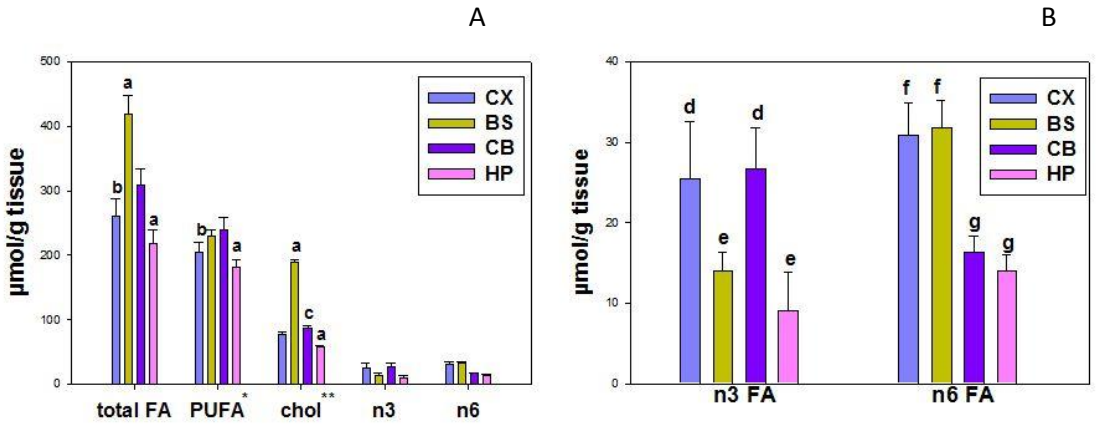

Figure 13. Normal regional composition of lipid species in measured brain regions from vehicle-treated control rats. Significant differences ($p \leq 0.05$) noted as: [a]different than all other regions; [b]less than BS, CB; [c]greater than CX, HP; [d]greater than BS, HP; [e]less than CX, CB; [f]greater than CB, HP, [g]less than CX, BS. *PUFA signal intensity is subject to changes in both concentration and composition. **Average of 3 cholesterol carbon signals (C18 at 12.5 ppm, C19 at 19.7 ppm and C14 at 57.2 ppm). Abbreviations: CX – cortex; BS – brainstem; CB – cerebellum; HP – hippocampus; FA – fatty acid; PUFA – polyunsaturated fatty acid. A) full scale profile B) expanded scale for display of n3 and n6 FA.

The n3 and n6 FA data are displayed at an expanded scale in the inset of Figure 13. The levels of n3 FA in the hippocampus were approximately 35% of cortex and cerebellum levels and 65% of brainstem. Brainstem levels of n3 FA were also significantly lower than cortex and cerebellum. There was no statistical difference in n3 FA levels between cortex and cerebellum. The levels of n6 FA in both the cerebellum and the hippocampus were about half the levels in the

cortex and brainstem. There was no difference in n6 FA levels between cortex and brainstem or cerebellum and hippocampus.

Figure 14 shows the normal regional composition of the major phospholipids in cortex, brainstem, cerebellum and hippocampus from vehicle-treated control animals. With the exception of phosphatidylethanolamine (PtdE) and phosphatidylinositol (PtdI), brainstem had significantly higher levels of all phospholipids than cortex, cerebellum and hippocampus. Levels of phosphatidic acid (PA) were 6-10 fold greater in the brainstem than the other three regions, while levels of PtdC were 2-4 fold greater. On average, brainstem levels of all other phospholipids averaged about 3, 3 and 5 fold greater than cortex, cerebellum and hippocampus, respectively. The hippocampus had significantly lower levels of sphingomyelin (SM), PtdI, choline plasmalogen (ChPl), ethanolamine plasmalogen (EthPl), PtdE and PtdC and phosphatidylserine (PtdS) than all other brain regions (inset of Fig. 14). The levels of PtdI, ChPl, PtdE, PtdS and PtdC were significantly lower in cerebellum as compared to cortex and brainstem and higher than hippocampus. There was no significant difference in levels of PA between cortex and cerebellum or hippocampus. No differences existed between cortex and cerebellum or cerebellum and hippocampus for cardiolipin (CL). Levels of SM were also the same in cortex and cerebellum.

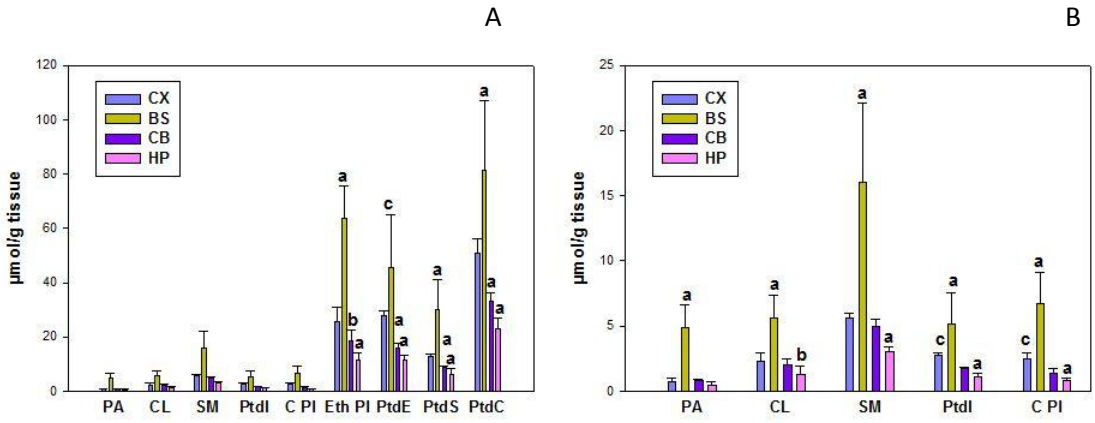

Figure 14. Normal regional composition of major phospholipids in measured brain regions from vehicle-treated control rats. Significant differences ($p \leq 0.05$) noted as: [a]different than all other regions; [b]less than CX; [c]greater than CB, HP. Abbreviations: CX – cortex; BS – brainstem; CB – cerebellum; HP – hippocampus; PA – phosphatidic acid; CL – cardiolipin; SM – sphingomyelin; PtdI – phosphatidylinositol; ChPl – choline plasmalogen; EthPl – ethanolamine plasmalogen; PtdE – phosphatidyethanolamine; PtdS – phosphatidylserine; PtdC – phosphatidylcholine. A) full scale profile B) expanded scale for display of PA, CL, SM, PtdI and ChPl.

3.1.3 Aqueous metabolite profile

The intensities from adaptively binned ^{1}H-NMR spectra of aqueous extracts of each brain region from control animals provided multivariate data input to principal component analysis (PCA). The PCA scores plot (PC1 vs. PC2) for the four brain regions is shown in Figure 15. Differences in the mapping position on the plot reflect differences in the biochemical composition of the aqueous extract. ^{1}H-NMR spectra for each brain region displayed tight clustering in PC space with distinct grouping within and between each region. No region overlapped with another region.

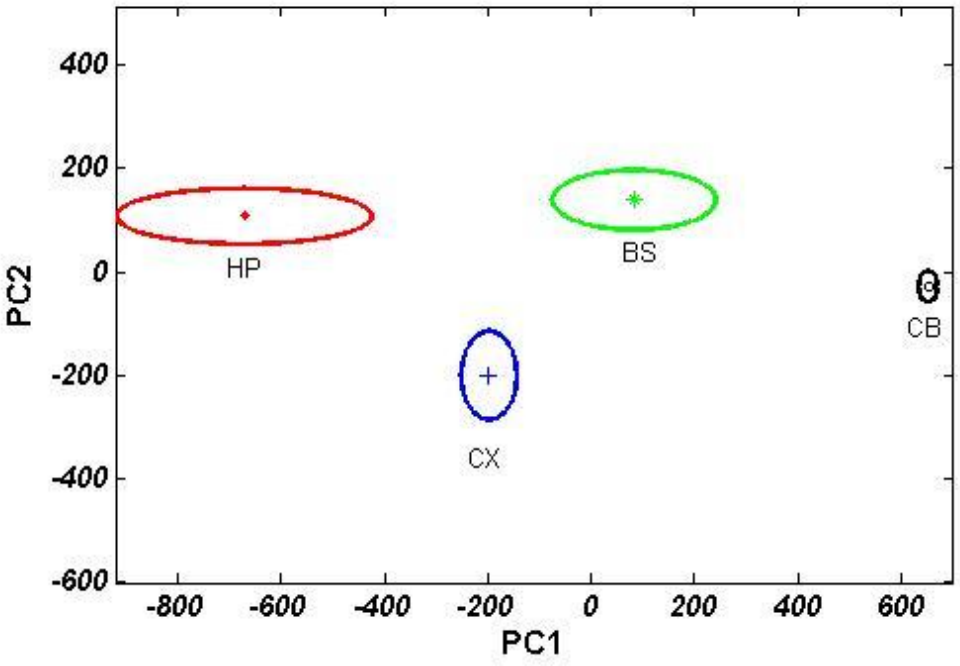

Figure 15. Principal component plot of ^{1}H-NMR spectra of aqueous metabolites from control animals. Abbreviations: CX – cortex; BS – brainstem; CB – cerebellum; HP – hippocampus. Data are plotted as the mean value for the first two principal components (PC1 vs. PC2) ± 1 SE (ellipse). Adaptively binned ^{1}H aqueous spectra were normalized to tissue weight and autoscaled to the mean and standard deviation of the control spectra specific to each brain region.

3.2 Cortex

3.2.1 Biochemical assays

Inhibition of AChE in the cortex reached a maximum at 12 hr post dose with activity levels at 55% of control activity (Fig. 16). The cortex showed a trend toward recovery by 48 hr post dose; however, enzyme activity levels did not reach control levels by 48 hr post dose.

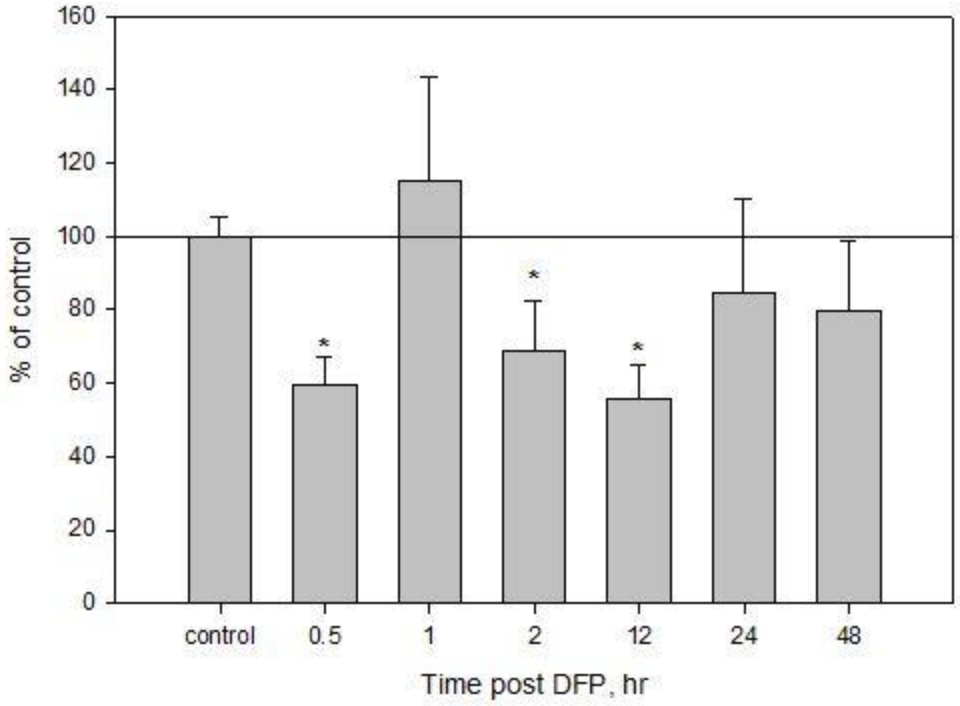

Figure 16. Inhibition of acetylcholinesterase activity reported as a percentage of the control value in cortex after a single subcutaneous dose of 1 mg/kg DFP. Data are mean ± SE; n=5/time point. *Significantly different from control at $p<0.05$.

MDA was measured in the cortex at 0.5, 1, 2, 12, 24 and 48 hr post DFP dose. None of the cortex samples from rats treated with DFP showed any significant change in the level of MDA at any time point post dose (Fig. 17).

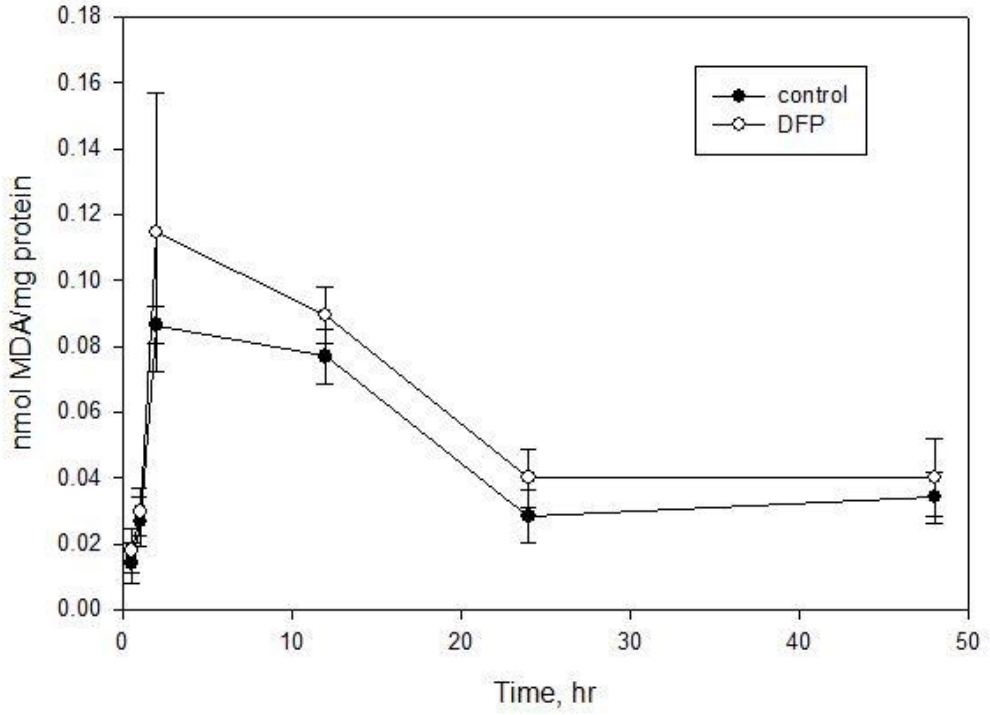

Figure 17. Time course measurement of levels of malondialdehyde in cortex. Data are Mean ± SE; n=5/time point.

3.2.2 Differential gene expression in cortex

Complete results of the quality control analysis of the gene arrays are shown in Appendix II. Based on the quality control analyses, the data from the gene chip from one cortex sample (animal #72, DFP group, n = 4 for this group) was excluded from the dataset. The final differential gene expression changes in the cortex 1 hr post DFP exposure included 28 up and 319 down-regulated genes ($p<0.05$ with fold change > 15% regardless of annotation status). The total number of annotated genes that were differentially expressed was 319 (genes with a known protein product are designated as annotated). The expression of 20 genes was present in the control group but absent in the DFP group, while 5 genes were not expressed in the control group but were in the DFP group. The full list of differentially expressed genes in the cortex can be found in Appendix III. Only the genes that were annotated were included in the final list.

In order to understand the biological relevance of the many gene expression changes caused by DFP exposure, complete lists of up- and down-regulated genes were used separately to search the DAVID web site. This analysis produced a large number of biological processes, cellular components and molecular functions that were affected by DFP exposure. The results of the database search are summarized in Table 3. Among the many down-regulated biological processes were: protein localization and transport, regulation of apoptosis/ programmed cell death, cellular signaling, synaptic transmission, regulation of neurotransmitter levels and secretion of neurotransmitters. The database search also identified down-regulated cellular components, specifically plasma membrane, synapse and cellular projections. The molecular function termed 'disulfide bond' was significantly up-regulated and consisted of the genes coding for neuromedin U receptor (*Nmur2*) and prostaglandin D2 synthase (*Ptgds*). The molecular functions of ATP and nucleotide binding were significantly down-regulated.

Table 3. Gene expression changes in specific cellular pathways of the cortex 1 hr post 1 mg/kg DFP exposure.

Category	Pathway	Regulation	# genes changed	%[a]	p-value*
Biological Process	cell-cell signaling	Down	13	5.1	0.0038
	cellular protein catabolic process	Down	10	3.9	0.0450
	establishment of protein localization	Down	19	7.5	0.0014
	generation of a signal involved in cell-cell signaling	Down	7	2.7	0.0052
	intracellular protein transport	Down	10	3.9	0.0270
	memory	Down	4	1.6	0.0500
	mRNA transport	Down	4	1.6	0.0480
	neurotransmitter secretion	Down	5	2.0	0.0073
	protein amino acid phosphorylation	Down	17	6.7	0.0190
	protein localization	Down	22	8.6	0.0007
	protein modification by small protein conjugation or removal	Down	7	2.7	0.0094
	protein transport	Down	19	7.5	0.0013
	protein ubiquitination	Down	5	2.0	0.0340
	regulation of apoptosis	Down	17	6.7	0.0400
	regulation of cell death	Down	17	6.7	0.0460
	regulation of neuron differentiation	Down	7	2.7	0.0360

	regulation of neurotransmitter levels	Down	6	2.4	0.0084
	regulation of programmed cell death	Down	17	6.7	0.0450
	regulation of protein catabolic process	Down	5	2.0	0.0063
	response to electrical stimulus	Down	3	1.2	0.0180
	RNA localization	Down	5	2.0	0.0150
	synaptic transmission	Down	11	4.3	0.0015
	transmission of nerve impulse	Down	12	4.7	0.0031
Cellular Component	cell junction	Down	14	5.5	0.0068
	cell projection	Down	19	7.5	0.0096
	cell projection part	Down	10	3.9	0.0070
	cell soma	Down	10	3.9	0.0069
	cortical actin cytoskeleton	Down	3	1.2	0.0410
	dendrite	Down	9	3.5	0.0140
	dendritic spine	Down	7	2.7	0.0002
	endosome	Down	10	3.9	0.0052
	filopodium	Down	4	1.6	0.0039
	Golgi apparatus part	Down	9	3.5	0.0220
	intracellular organelle lumen	Down	26	10.2	0.0190
	late endosome	Down	4	1.6	0.0360
	membrane-enclosed lumen	Down	26	10.2	0.0380
	neuron projection	Down	12	4.7	0.0350
	nuclear lumen	Down	21	8.2	0.0300
	nuclear pore	Down	4	1.6	0.0360
	nucleolus	Down	12	4.7	0.0015
	plasma membrane	Down	48	18.8	0.0037
	plasma membrane part	Down	30	11.8	0.0080
	postsynaptic membrane	Down	9	3.5	0.0006
	synapse	Down	15	5.9	0.0006
	synapse part	Down	12	4.7	0.0008
Molecular Function	Disulfide bond	Up	3	50	0.0220
	adenyl nucleotide binding	Down	37	14.5	0.00005
	adenyl ribonucleotide binding	Down	37	14.5	0.00002
	ATP binding	Down	37	14.5	0.00001
	ATPase activity	Down	10	3.9	0.01100
	ATPase activity, coupled	Down	8	3.1	0.02000
	ATP-dependent helicase activity	Down	4	1.6	0.04300
	ephrin receptor activity	Down	3	1.2	0.01000
	helicase activity	Down	8	3.1	0.00025
	ion channel activity	Down	10	3.9	0.03900
	nucleoside binding	Down	38	14.9	0.00004
	nucleotide binding	Down	49	19.2	0.00002
	phosphatase binding	Down	4	1.6	0.02000
	protein complex binding	Down	8	3.1	0.03600
	protein kinase activity	Down	18	7.1	0.00190
	protein phosphatase binding	Down	4	1.6	0.01500
	protein tyrosine kinase activity	Down	6	2.4	0.02700

	purine NTP-dependent helicase activity	Down	4	1.6	0.04300
	purine nucleoside binding	Down	37	14.5	0.00008
	purine nucleotide binding	Down	43	16.9	0.00003
	purine ribonucleotide binding	Down	43	16.9	0.00001
	substrate specific channel activity	Down	10	3.9	0.04600
	DEAD-like helicase, N-terminal	Down	4	1.6	0.02100
	DNA/RNA helicase, C-terminal	Down	5	2.0	0.00460
	DNA/RNA helicase, DEAD/DEAH box type, N-terminal	Down	4	1.6	0.00760
	Ephrin receptor, ligand binding	Down	3	1.2	0.00570
	Fibronectin, type III subdomain	Down	3	1.2	0.02300
	Helicase, superfamily 1 and 2, ATP-binding	Down	4	1.6	0.02100
	RNA helicase, ATP-dependent, DEAD-box, conserved site	Down	3	1.2	0.03700
	RNA helicase, DEAD-box type, Q motif	Down	4	1.6	0.00450
	Tyrosine-protein kinase, ephrin receptor	Down	3	1.2	0.00570
	Axon guidance	Down	6	2.4	0.04100

*p-value derived from modified Fisher's Exact test.
[a]Percentage calculated by number of genes differentially expressed/total number of genes involved in process, cellular component or molecular function*100.

3.2.3 Metabolic changes in cortex

Lipid metabolite changes at 2 hr post DFP exposure are detailed in Table 4. In cortex, all lipid species measured decreased significantly after DFP treatment, except phosphatidic acid and cardiolipin. The lipids showing the greatest decreases were EthPl and ChPl (45 and 56%), as well as n3 fatty acids (48%). The n6 fatty acids were also decreased by 43%. The average decrease after DFP exposure for the remaining lipid species was about 30%, ranging from 16% for sphingomyelin to 44% for phosphatidylinositol. Lipid metabolite changes at 48 hr post DFP exposure were also measured. However, the decoupling parameters used were no longer accurate for the ^{13}C acquisition, making the ^{13}C lipid spectra difficult to quantify. The remaining lipids in $CDCl_3$ were re-analyzed, although the total amount of lipid was small and did not necessarily correlate back to the original lipid weight. Therefore, while lipid signals were quantified the

results are only qualitative. The qualitative results reveal no significant differences in any of the measured lipids. The quantified results are available in Appendix IV.

Table 4. Changes in lipid metabolite concentrations in the cortex 2 hr post 1 mg/kg DFP dose.

	Metabolite Concentration (μmol/g tissue)	
Metabolite	**Control**	**DFP**
Total Tissue Weight (g)	0.841 ± 0.036	0.808 ± 0.043
Phosphatidic acid	0.7 ± 0.3	0.5 ± 0.0
Cardiolipin	2.3 ± 0.6	2.2 ± 0.5
Ethanolamine plasmalogen	25.6 ± 5.2	14.2 ± 1.3*
Choline plasmalogen	2.5 ± 0.5	1.1 ± 0.4**
Phosphatidylserine	12.7 ± 1.2	8.4 ± 0.2**
Phosphatidyl-ethanolamine	27.8 ± 2.0	16.8 ± 0.5**
Phosphatidylinositol	2.7 ± 0.3	1.5 ± 0.1**
Phosphatidylcholine	50.8 ± 5.3	33.3 ± 1.6**
Sphingomyelin	5.6 ± 0.4	4.7 ± 0.1*
Cholesterol[a]	77.5 ± 3.3	57.9 ± 4.1**
n3 Fatty acids	25.4 ± 7.1	13.2 ± 5.1*
n6 Fatty acids	30.9 ± 4.0	17.7 ± 2.4**
Polyunsaturated fatty acids[b]	205.2 ± 14.1	155.2 ± 3.3**
Total fatty acids	261.1 ± 27.4	200.2 ± 17.4*

Control n = 4; DFP n = 3
* $p<0.05$
** $p<0.01$
[a]Average of 3 cholesterol carbon signals (C18 at 12.5 ppm, C19 at 19.7 ppm and C14 at 57.2 ppm.
[b]Polyunsaturated fatty acid signal intensity is subject to changes in both concentration and composition

Aqueous, small molecule metabolites were measured in extracts of the cortex at the 2 hr time point by ^{1}H and ^{31}P NMR. N-acetylaspartate (NAA) was decreased by approximately 11% in response to DFP treatment (Table 5). Small molecule metabolites from extracts of the cortex at 48 hr post dose were also measured (Table 5). The amino acids valine and isoleucine were increased 4 and 5 fold, respectively. GABA was increased by 55%. G3P and dihydroxyacetone

phosphate (DHAP) were both decreased 2 fold. Decreases in phosphocholine, glucose and G6P were approximately 25-35%.

Table 5. Changes in aqueous metabolite concentrations in the cortex 2 and 48 hr post 1 mg/kg DFP dose.

Metabolite (chem. shift in ppm)	Metabolite Concentration (μmol/g tissue)			
	2 hr post dose		48 hr post dose	
	Control	DFP	Control	DFP
Valine (0.98)	0.03 ± 0.01	0.08 ± 0.06	0.05 ± 0.03	0.26 ± 0.08**
Isoleucine (1.01)	0.08 ± 0.01	0.07 ± 0.01	0.09 ± 0.01	0.38 ± 0.13**
β-hydroxybutyrate (1.24)	0.44 ± 0.05	0.44 ± 0.00	0.66 ± 0.27	0.58 ± 0.07
Lactate[a] (1.33, 4.11)	12.3 ± 1.1	11.9 ± 0.7	12.8 ± 1.6	13.6 ± 1.8
Alanine (1.41)	0.51± 0.03	0.48 ± 0.02	2.0 ± 0.5	0.69 ± 0.05**
NAA (2.02)	8.7 ± 0.3	7.7 ± 0.2**	8.7 ± 1.0	9.4 ± 1.2
Methionine (2.13)	0.09 ± 0.01	0.08 ± 0.01	ND	ND
Succinate (2.41)	0.75 ± 0.05	0.74 ± 0.02	0.71 ± 0.11	0.74 ± 0.20
Trimethylamine (2.92)	0.05 ± 0.00	0.04 ± 0.00	0.09 ± 0.01	0.09 ± 0.02
GABA (2.98)	2.6 ± 0.3	2.1 ± 0.8	2.6 ± 0.2	3.7 ± 0.3*
Ornithine (3.07)	1.3 ± 0.23	0.95 ± 0.04	1.21 ± 0.29	1.28 ± 0.20
Cis-aconitate (3.21)	0.39 ± 0.08	0.27 ± 0.01	1.2 ± 0.8	2.7 ± 1.1*
Choline (3.22)	0.52 ± 0.02	0.47 ± 0.06	0.51 ± 0.06	0.43 ± 0.18
Phosphocholine (3.23)	0.94 ± 0.06	0.87 ± 0.02	0.89 ± 0.13	0.66 ± 0.08*
Myo-inositol[a] (3.53, 4.06)	6.4 ± 0.8	5.8 ± 0.8	8.1 ± 1.4	7.8 ± 0.5
Glucose (3.41)	3.86 ± 3.80	3.07 ± 0.21	3.5 ± 1.3	2.2 ± 0.1*
Fumarate (6.52)	0.02 ± 0.01	0.03 ± 0.01	0.02 ± 0.01	0.02 ± 0.01
Tyrosine (7.13)	0.1± 0.04	0.05 ± 0.05	0.14 ± 0.02	0.18 ± 0.07
Formate (8.46)	1.4 ± 0.4	1.2 ± 0.1	0.59 ± 0.37	0.44 ± 0.13
Nicotinate[a] (8.71, 8.94)	0.10 ± 0.06	0.04 ± 0.03	0.2 ± 0.04	0.2 ± 0.04
GPC[b] (3.06)	0.59 ± 0.02	0.55 ± 0.06	0.52 ± 0.07	0.49 ± 0.07
GPE[b] (3.73)	0.28 ± 0.01	0.27 ± 0.02	0.29 ± 0.03	0.28 ± 0.02
G3P[b] (7.05)	3.95 ± 0.18	3.85 ± 0.19	3.6 ± 0.6	1.7 ± 1.3*
G6P[b] (7.11)	3.34 ± 0.2	3.28 ± 0.05	3.0 ± 0.5	2.2 ± 0.3*
DHAP[b] (8.04)	0.09 ± 0.03	0.06 ± 0.00	0.13 ± 0.04	0.07 ± 0.02*

Control n = 5; DFP n = 2
*p<0.05
**p<0.01
[a]average of multiple signals
[b]metabolite signals are from ^{31}P aqueous spectra. GPC set at 3.082 ppm for reference
Abbreviations: NAA – N-acetylaspartate; GABA – γ-aminobutyric acid; GPC – glycerophosphocholine; GPE – glycerophosphoethanolamine; G3P – glycerol-3-phosphate; G6P – glucose-6-phosphate; DHAP – dihydroxyacetone phosphate; ND – Not detectable

3.3 Brainstem

3.3.1 Biochemical assays

Inhibition of AChE in the brainstem reached a maximum at 1 hr post dose with activity levels at 40% of control activity (Fig. 18). The cortex showed a trend toward recovery by 48 hr post dose; however, enzyme activity levels did not reach control levels by 48 hr post dose.

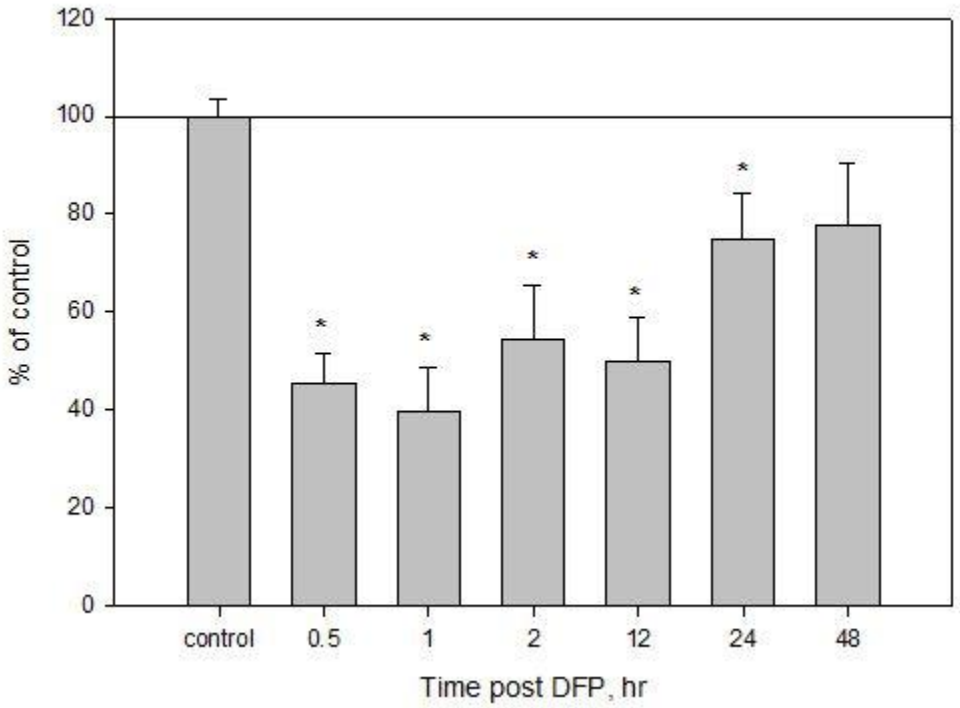

Figure 18. Inhibition of acetylcholinesterase activity reported as a percentage of the control value in brainstem after a single subcutaneous dose of 1 mg/kg DFP. Data are mean ± SE; n=5/time point. *Significantly different from control at $p<0.05$.

MDA was measured in the brainstem at 0.5, 1, 2, 12, 24 and 48 hr post DFP dose. None of the brainstem samples from rats treated with DFP showed any significant change in the level of MDA at any time point post dose (Fig. 19).

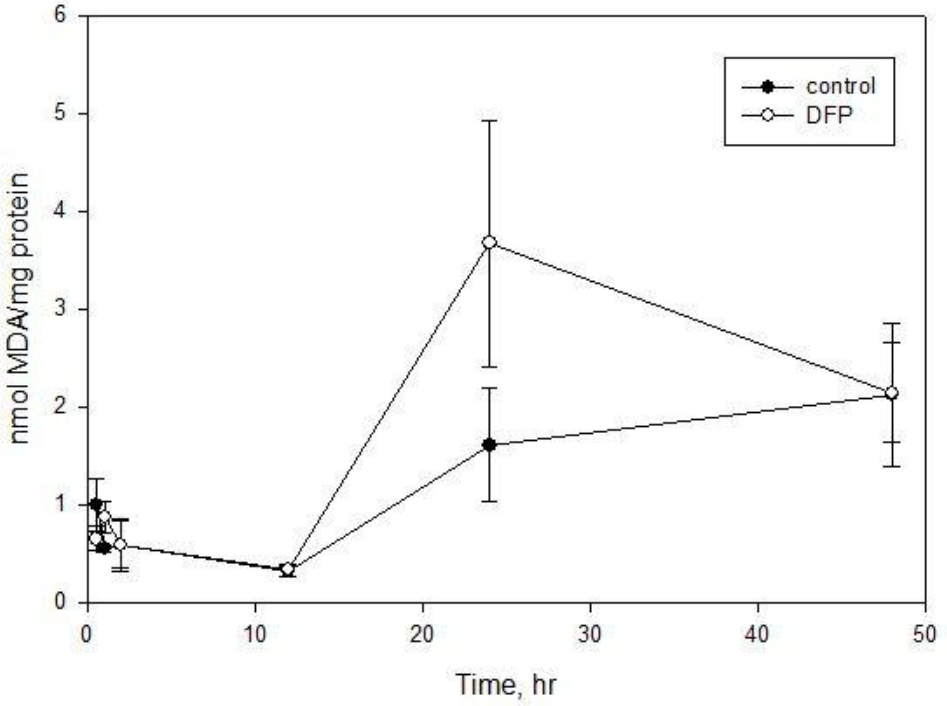

Figure 19. Time course measurement of levels of malondialdehyde in brainstem. Data are Mean ± SE; n=5/time point.

3.3.2 Differential gene expression in brainstem

Complete results of the quality control analysis of the gene arrays are shown in Appendix II. Based on the quality control analyses, the data from all gene chips were included in the dataset. However, one array from the DFP group was lost during preparation (n=4 for DFP group). The final differential gene expression changes in the brainstem 1 hr post DFP exposure included 57 up and 107 down-regulated genes ($p<0.05$ with fold change > 15% regardless of

annotation status). The total number of annotated genes that were differentially expressed was 121. The expression of 19 genes was present in the control group but absent in the DFP group, while 19 genes were not expressed in the control group but were in the DFP group. The full list of differentially expressed genes in the brainstem can be found in Appendix III. Only the genes that were annotated were included in the final list.

In order to understand the biological relevance of the many gene expression changes caused by DFP exposure, complete lists of up- and down-regulated genes were used separately to search the DAVID web site. The results of the database search are summarized in Table 6. In the brainstem vitamin transport was up-regulated. Among the down-regulated biological processes were protein localization, regulation of exocytosis and cellular homeostasis. The database search identified cellular components that were up-regulated (brush border and cell projections) and down-regulated (nucleus and synapse associated components). As in the cortex, the molecular functions of ATP and nucleotide binding were down-regulated in the brainstem.

Table 6. Gene expression changes in specific cellular pathways of the brainstem 1 hr post 1 mg/kg DFP exposure.

Category	Pathway	Regulation	# genes changed	%[a]	p-value*
Biological Process	vitamin transport	Up	2	12.5	0.0200
	cellular homeostasis	Down	6	7.5	0.0500
	establishment of protein localization	Down	7	8.8	0.0370
	intracellular receptor-mediated signaling pathway	Down	3	3.8	0.0220
	modification-dependent protein catabolic process	Down	5	6.2	0.0390
	nuclear import	Down	3	3.8	0.0360
	protein folding	Down	4	5.0	0.0170
	protein import into nucleus	Down	3	3.8	0.0330
	protein localization in nucleus	Down	3	3.8	0.0420
	regulation of exocytosis	Down	3	3.8	0.0200
	regulation of secretion	Down	5	6.2	0.0240
	steroid hormone receptor signaling pathway	Down	3	3.8	0.0110
	ubiquitin-dependent protein catabolic process	Down	4	5.0	0.0390
Cellular Component	brush border	Up	3	18.8	0.0016
	cell projection	Up	4	25.0	0.0440
	nuclear lumen	Down	10	12.5	0.0098
	nuclear matrix	Down	3	3.8	0.0150
	synapse	Down	6	7.5	0.0160
	synaptic vesicle	Down	3	3.8	0.0400
Molecular Function	vitamin transporter activity	Up	2	12.5	0.0120
	ATP binding	Down	12	15.0	0.0150
	heat shock protein binding	Down	3	3.8	0.0420
	purine ribonucleotide binding	Down	15	18.8	0.0048

*p-value derived from modified Fisher's Exact test
[a]Percentage calculated by number of genes differentially expressed/total number of genes involved in process, cellular component or molecular function*100.

3.3.3 Metabolic changes in brainstem

Lipid metabolite changes in the brainstem at 2 hr post DFP exposure are detailed in Table 7. In brainstem cardiolipin was significantly decreased by 38% ($p<0.05$). No other measured lipids were significantly changed after DFP exposure.

Table 7. Changes in lipid metabolite concentrations in the brainstem 2 hr post 1 mg/kg DFP dose.

Metabolite	Metabolite Concentration (µmol/g tissue)	
	Control	**DFP**
Total Tissue Weight (g)	0.523 ± 0.017	0.529 ± 0.043
Phosphatidic acid	4.9 ± 1.7	2.9 ± 1.2
Cardiolipin	5.6 ± 1.8	3.5 ± 0.8*
Ethanolamine plasmalogen	63.7 ± 11.7	54.0 ± 13.1
Choline plasmalogen	6.7 ± 2.4	5.1 ± 0.8
Phosphatidylserine	30.0 ±11.2	26.7 ± 3.7
Phosphatidyl-ethanolamine	45.5 ± 9.4	38.1 ± 7.1
Phosphatidylinositol	5.2 ± 2.3	4.7 ± 0.8
Phosphatidylcholine	81.4 ± 5.5	71.2 ± 9.5
Sphingomyelin	16.1 ± 6.0	14.3 ± 2.0
Cholesterol[a]	189.8 ± .9	184.0 ± 8.6
n3 Fatty acids	14.0 ± 2.4	13.3 ± 2.6
n6 Fatty acids	31.7 ± 3.4	35.0 ± 5.0
Polyunsaturated fatty acids[b]	229.5 ± 9.5	230.3 ± 20.9
Total fatty acids	419.3 ± 28.5	457.6 ± 88.1

Control n = 5; DFP n = 5

*Denotes significance at $p<0.05$

[a]Average of 3 cholesterol carbon signals (C18 at 12.5 ppm, C19 at 19.7 ppm and C14 at 57.2 ppm.

[b]Polyunsaturated fatty acid signal intensity is subject to changes in both concentration and composition

Aqueous, small molecule metabolites were measured in extracts of the brainstem at the 2 hr time point by ^{1}H and ^{31}P NMR. Brainstem showed no significant changes in any measured small molecule metabolites 2 hr post 1 mg/kg DFP exposure (Table 8).

Table 8. Changes in aqueous metabolite concentrations in the brainstem 2 hr post 1 mg/kg DFP dose.

Metabolite (chem. shift in ppm)	Metabolite Concentration (µmol/g tissue)	
	2 hr post dose	
	Control	DFP
Valine (0.98)	0.01 ± 0.00	0.02 ± 0.01
Isoleucine (1.01)	0.08 ± 0.02	0.10 ± 0.04
β-hydroxybutyrate (1.24)	0.33 ± 0.08	0.5 ± 0.2
Lactate[a] (1.33, 4.11)	11.7 ± 2.7	13.6 ± 0.8
Alanine (1.41)	0.11 ± 0.05	0.12 ± 0.03
NAA (2.02)	6.8 ± 1.6	7.8 ± 0.9
Methionine (2.13)	0.06 ± 0.01	0.07 ± 0.00
Succinate (2.41)	0.69 ± 0.21	0.85 ± 0.13
Trimethylamine (2.92)	0.05 ± 0.05	0.02 ± 0.01
GABA (2.98)	2.4 ± 0.7	3.0 ± 0.4
Ornithine (3.07)	ND	ND
Cis-aconitate (3.21)	0.3 ± 0.2	0.3 ± 0.03
Choline (3.22)	0.6 ± 0.2	0.7 ± 0.1
Phosphocholine (3.23)	1.2 ± 0.3	1.4 ± 0.1
Myo-inositol[a] (3.53, 4.06)	8.0 ± 2.2	9.2 ± 1.3
Glucose (3.41)	3.6 ± 3.0	1.5 ± 0.8
Fumarate (6.52)	0.03 ± 0.01	0.03 ± 0.01
Tyrosine (7.13)	0.15 ± 0.03	0.09 ± 0.05
Formate (8.46)	1.4 ± 0.9	1.6 ± 0.5
Nicotinate[a] (8.71, 8.94)	0.11 ± 0.03	0.21 ± 0.18
GPC[b] (3.06)	0.89 ± 0.33	1.19 ± 0.28
GPE[b] (3.73)	0.35 ± 0.14	0.42 ± 0.22
G3P[b] (7.05)	2.7 ± 1.2	3.4 ± 1.0
G6P[b] (7.11)	8.7 ± 3.8	10.9 ± 3.4
DHAP[b] (8.04)	0.05 ± 0.06	0.08 ± 0.06

Control n = 5; DFP n = 5

[a]average of multiple signals

[b]metabolite signals are from ^{31}P aqueous spectra. GPC set at 3.082 ppm for reference

Abbreviations: NAA – N-acetylaspartate; GABA – γ-aminobutyric acid; GPC – glycerophosphocholine; GPE – glycerophosphoethanolamine; G3P – glycerol-3-phosphate; G6P – glucose-6-phosphate; DHAP – dihydroxyacetone phosphate; ND – Not detectable

3.4 Cerebellum

3.4.1 Biochemical assays

Inhibition of AChE in the cerebellum reached a maximum at 2 hr post dose with activity levels at 50% of control activity (Fig. 20). The cerebellum showed a trend toward recovery by 48 hr post dose; however, enzyme activity levels did not reach control levels by 48 hr post dose.

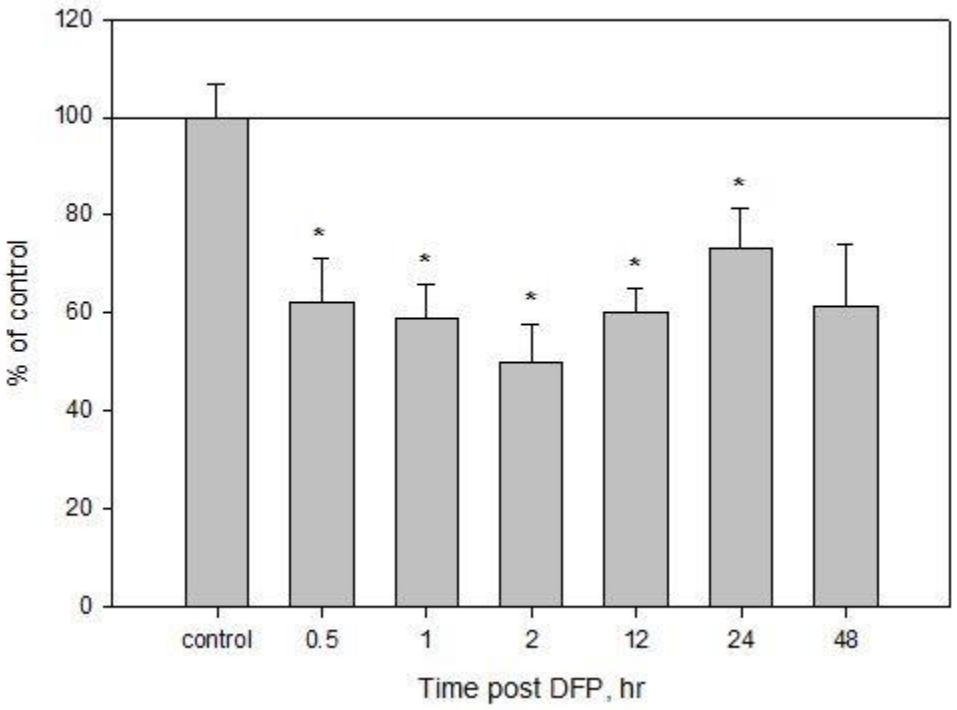

Figure 20. Inhibition of acetylcholinesterase activity reported as a percentage of the control value in cerebellum after a single subcutaneous dose of 1 mg/kg DFP. Data are mean ± SE; n=5/time point. *Significantly different from control at $p<0.05$.

MDA was measured in the cerebellum at 0.5, 1, 2, 12, 24 and 48 hr post DFP dose. None of the cerebellum samples from rats treated with DFP showed any significant change in the level of MDA at any time point post dose (Fig. 21).

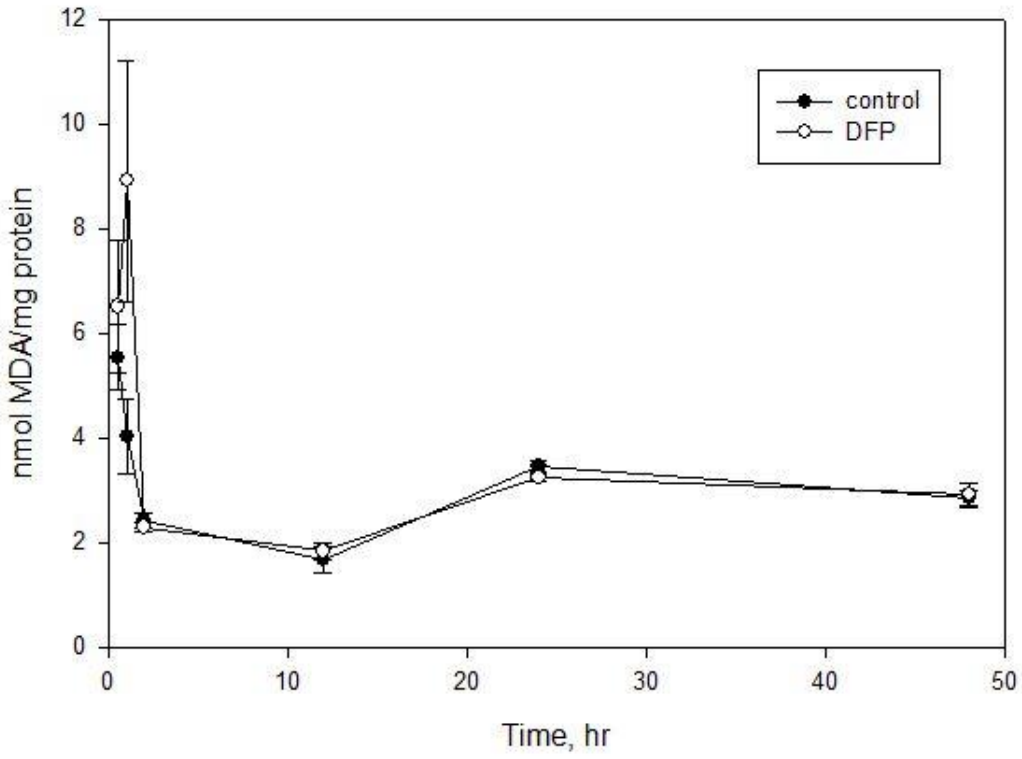

Figure 21. Time course measurement of levels of malondialdehyde in cerebellum. Data are mean ± SE; n=5/time point.

3.4.2 Differential gene expression in cerebellum

Complete results of the quality control analysis of the gene arrays are shown in Appendix II. Based on the quality control analyses, the data from two gene chips (one control and one DFP-treated; n = 4 for each group) were excluded from the dataset. The final differential gene expression changes in the cerebellum 1 hr post DFP exposure included 65 up and 158 down-regulated genes ($p<0.05$ with fold change > 15% regardless of annotation status). The total number of annotated genes that were differentially expressed was 163. The expression of 12 genes was present in the control group but absent in the DFP group, while 17 genes were not expressed in the control group but were in the DFP group. The full list of differentially expressed genes in the cerebellum can be found in Appendix III. Only the genes that were annotated were included in the final list.

In order to understand the biological relevance of the many gene expression changes caused by DFP exposure, complete lists of up- and down-regulated genes were used separately to search the DAVID web site. The results of the database search are summarized in Table 9. Among the many up-regulated biological processes in the cerebellum were anti-apoptosis, response to stimuli, response to oxidative stress and regulation of gene expression/ RNA metabolism/ RNA polymerase. Down-regulated biological processes included negative regulation of apoptosis, protein folding/ catabolism, purine nucleoside triphosphate synthesis and ribosome synthesis. Cellular components were down-regulated and consisted of intracellular organelles and the nucleus. Phosphatase activity associated with the mitogen activated protein kinase (MAPK) pathway was up-regulated. ATPase activity and DNA repair processes were down-regulated.

Table 9. Gene expression changes in specific cellular pathways of the cerebellum 1 hr post 1 mg/kg DFP exposure.

Category	Pathway	Regulation	# genes changed	%[a]	p-value*
Biological Process	adult behavior	Up	3	16.7	0.0052
	behavior	Up	5	27.8	0.0012
	negative regulation of transcription factor activity	Up	2	11.1	0.0470
	positive regulation of anti-apoptosis	Up	2	11.1	0.0320
	positive regulation of gene expression	Up	4	22.2	0.0250
	positive regulation of RNA metabolic process	Up	4	22.2	0.0160
	positive regulation of transcription from RNA polymerase II promoter	Up	4	22.2	0.0096
	regulation of anti-apoptosis	Up	2	11.1	0.0430
	regulation of cell proliferation	Up	4	22.2	0.0410
	regulation of RNA metabolic process	Up	6	33.3	0.0110
	regulation of transcription	Up	7	38.9	0.0064
	response to endogenous stimulus	Up	4	22.2	0.0270
	response to extracellular stimulus	Up	4	22.2	0.0048
	response to oxidative stress	Up	3	16.7	0.0180
	transcription	Up	5	27.8	0.0070
	cellular protein catabolic process	Down	6	5.5	0.0280
	cellular response to stress	Down	7	6.4	0.0300
	chromatin organization	Down	5	4.5	0.0450
	DNA repair	Down	7	6.4	0.0005
	modification-dependent protein catabolic process	Down	6	5.5	0.0190
	negative regulation of apoptosis	Down	8	7.3	0.0020
	negative regulation of cell death	Down	8	7.3	0.0023
	negative regulation of programmed cell death	Down	8	7.3	0.0022
	nucleoside triphosphate biosynthetic process	Down	4	3.6	0.0190
	nucleotide-excision repair	Down	3	2.7	0.0290
	positive regulation of ligase activity	Down	4	3.6	0.0044
	positive regulation of ubiquitin-protein ligase activity	Down	3	2.7	0.0410
	protein catabolic process	Down	6	5.5	0.0350
	protein folding	Down	5	4.5	0.0041
	proteolysis involved in cellular protein catabolic process	Down	6	5.5	0.0270
	purine nucleoside triphosphate biosynthetic process	Down	4	3.6	0.0180
	purine ribonucleoside triphosphate biosynthetic process	Down	4	3.6	0.0180
	regulation of apoptosis	Down	9	8.2	0.0280
	regulation of cell death	Down	9	8.2	0.0300
	regulation of ligase activity	Down	4	3.6	0.0058
	regulation of programmed cell death	Down	9	8.2	0.0300
	regulation of ubiquitin-protein ligase	Down	3	2.7	0.0490

	activity				
	response to DNA damage stimulus	Down	7	6.4	0.0027
	ribonucleoprotein complex biogenesis	Down	4	3.6	0.0350
	ribosome biogenesis	Down	4	3.6	0.0130
	rRNA metabolic process	Down	3	2.7	0.0450
	rRNA processing	Down	3	2.7	0.0420
	sulfur metabolic process	Down	4	3.6	0.0210
	transcription-coupled nucleotide-excision repair	Down	2	1.8	0.0330
	transmembrane transport	Down	4	3.6	0.0330
Cellular Component	chromosome	Down	7	6.4	0.0380
	intracellular organelle lumen	Down	19	17.3	0.0016
	membrane-enclosed lumen	Down	20	18.2	0.0013
	nuclear lumen	Down	15	13.6	0.0062
	nucleolus	Down	7	6.4	0.0140
	nucleoplasm	Down	11	10.0	0.0270
	organelle lumen	Down	20	18.2	0.0009
	mitochondrion inner membrane	Down	5	4.5	0.0120
Molecular Function	MAP kinase phosphatase activity	Up	2	11.1	0.0120
	MAP kinase tyrosine/serine/threonine phosphatase activity	Up	2	11.1	0.0120
	protein heterodimerization activity	Up	3	16.7	0.0300
	protein tyrosine/serine/threonine phosphatase activity	Up	2	11.1	0.0350
	transcription activator activity	Up	3	16.7	0.0450
	transcription factor activity	Up	4	22.2	0.0360
	transcription regulator activity	Up	5	27.8	0.0300
	Dual specificity protein phosphatase (MAP kinase phosphatase)	Up	2	11.1	0.0110
	MAP kinase phosphatase	Up	2	11.1	0.0110
	MAPK signaling pathway	Up	3	16.7	0.0210
	PIRSF002524:nerve growth factor IB-like nuclear receptor	Up	2	11.1	0.0063
	ATPase activity	Down	6	5.5	0.0190
	ATPase activity, coupled	Down	5	4.5	0.0290
	hydrogen ion transmembrane transporter activity	Down	4	3.6	0.0140
	Chaperone	Down	4	3.6	0.0390
	DNA damage	Down	4	3.6	0.0290
	DNA repair	Down	4	3.6	0.0190

*p-value derived from modified Fisher's Exact test

[a]Percentage calculated by number of genes differentially expressed/total number of genes involved in process, cellular component or molecular function*100.

3.4.3 Metabolic changes in cerebellum

Lipid metabolite changes in the cerebellum at 2 hr post DFP exposure are detailed in Table 10. In cerebellum phosphatidylinositol was 11% lower in the DFP-treated group as compared to control while n3 fatty acids were about 33% lower.

Table 10. Changes in lipid metabolite concentrations in the cerebellum 2 hr post 1 mg/kg DFP dose.

	Metabolite Concentration (µmol/g tissue)	
Metabolite	**Control**	**DFP**
Total Tissue Weight (g)	0.249 ± 0.032	0.218 ± 0.022
Phosphatidic acid	0.8 ± 0.1	0.8 ± 0.2
Cardiolipin	2.1 ± 0.4	1.9 ± 0.3
Ethanolamine plasmalogen	18.5 ± 3.9	17.0 ± 2.2
Choline plasmalogen	1.4 ± 0.4	1.4 ± 0.1
Phosphatidylserine	8.6 ± 0.8	8.2 ± 0.7
Phosphatidyl-ethanolamine	15.9 ± 1.7	15.0 ± 2.4
Phosphatidylinositol	1.8 ± 0.1	1.6 ± 0.2*
Phosphatidylcholine	33.2 ± 3.2	32.5 ± 1.6
Sphingomyelin	4.9 ± 0.6	4.9 ± 0.3
Cholesterol[a]	87.7 ± 2.2	81.8 ± 2.8
n3 Fatty acids	26.7 ± 5.1	17.8 ± 6.3**
n6 Fatty acids	16.3 ± 1.9	15.6 ± 2.3
Polyunsaturated fatty acids[b]	240.1 ± 18.7	221.3 ± 10.0
Total fatty acids	308.9 ± 25.6	289.1 ± 13.3

Control n = 5; DFP n = 5

*Denotes significance at $p<0.05$

**Denotes significance at $p<0.01$

[a]Average of 3 cholesterol carbon signals (C18 at 12.5 ppm, C19 at 19.7 ppm and C14 at 57.2 ppm.

[b]Polyunsaturated fatty acid signal intensity is subject to changes in both concentration and composition

Aqueous, small molecule metabolites were measured in extracts of the cerebellum at the 2 hr time point by ^{1}H and ^{31}P NMR. Alanine was increased 3 fold in cerebellum while succinate was increased by about 30%. Trimethylamine was decreased by approximately 50% (Table 11).

Table 11. Changes in aqueous metabolite concentrations in the cerebellum 2 hr post 1 mg/kg DFP dose.

Metabolite (chem. shift in ppm)	Metabolite Concentration (μmol/g tissue)	
	2 hr post dose	
	Control	DFP
Valine (0.98)	ND	ND
Isoleucine (1.01)	ND	ND
β-hydroxybutyrate (1.24)	0.16 ± 0.03	0.16 ± 0.02
Lactate[a] (1.33, 4.11)	15.8 ± 1.9	17.3 ± 2.3
Alanine (1.41)	0.02 ± 0.00	0.06 ± 0.00*
NAA (2.02)	6.3 ± 0.9	7.0 ± 0.8
Methionine (2.13)	0.05 ± 0.01	0.05 ± 0.01
Succinate (2.41)	0.7 ± 0.1	0.9 ± 0.2**
Trimethylamine (2.92)	0.007 ± 0.001	0.004 ± 0.00*
GABA (2.98)	ND	ND
Ornithine (3.07)	ND	ND
Cis-aconitate (3.21)	0.09 ± 0.03	0.1 ± 0.06
Choline (3.22)	0.56 ± 0.17	0.56 ± 0.04
Phosphocholine (3.23)	0.78 ± 0.09	0.93 ± 0.12
Myo-inositol[a] (3.53, 4.06)	7.6 ± 4.2	6.3 ± 6.3
Glucose (3.41)	0.36 ± 0.3	0.16 ± 0.04
Fumarate (6.52)	0.01 ± 0.01	0.01 ± 0.01
Tyrosine (7.13)	0.02 ± 0.01	0.02 ± 0.01
Formate (8.46)	3.2 ± 2.5	3.7 ± 0.4
Nicotinate[a] (8.71, 8.94)	0.15 ± 0.03	0.16 ± 0.05
GPC[b] (3.06)	0.58 ± 0.08	0.71 ± 0.11
GPE[b] (3.73)	0.13 ± 0.03	0.29 ± 0.11
G3P[b] (7.05)	2.6 ± 0.5	2.8 ± 0.2
G6P[b] (7.11)	1.1 ± 0.2	1.0 ± 0.1
DHAP[b] (8.04)	0.05 ± 0.04	0.07 ± 0.05

Control n = 5; DFP n = 5

*Denotes significance at $p<0.01$

**Denotes significance at $p<0.05$

[a]average of multiple signals

[b]metabolite signals are from ^{31}P aqueous spectra. GPC set at 3.082 ppm for reference

Abbreviations: NAA – N-acetylaspartate; GABA – γ-aminobutyric acid; GPC – glycerophosphocholine; GPE – glycerophosphoethanolamine; G3P – glycerol-3-phosphate; G6P – glucose-6-phosphate; DHAP – dihydroxyacetone phosphate; ND – Not detectable

3.5 Hippocampus

3.5.1 Biochemical assays

Inhibition of AChE in the hippocampus reached a maximum at 2 hr post dose with activity levels at 55% of control activity (Fig. 22). The hippocampus showed a trend toward recovery by 48 hr post dose; however, enzyme activity levels did not reach control levels by 48 hr post dose.

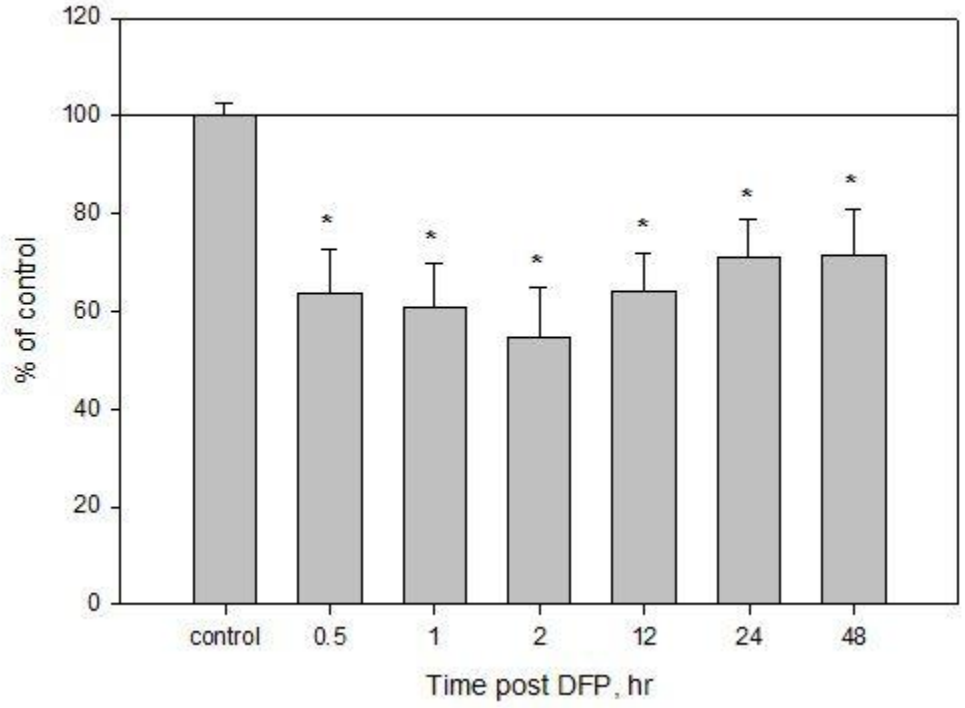

Figure 22. Inhibition of acetylcholinesterase activity reported as a percentage of the control value in hippocampus after a single subcutaneous dose of 1 mg/kg DFP. Data are mean ± SE; n=5/time point. *Significantly different from control at $p<0.05$.

MDA was measured in the hippocampus at 0.5, 1, 2, 12, 24 and 48 hr post DFP dose. None of the hippocampus samples from rats treated with DFP showed any significant change in the level of MDA at any time point post dose (Fig. 23).

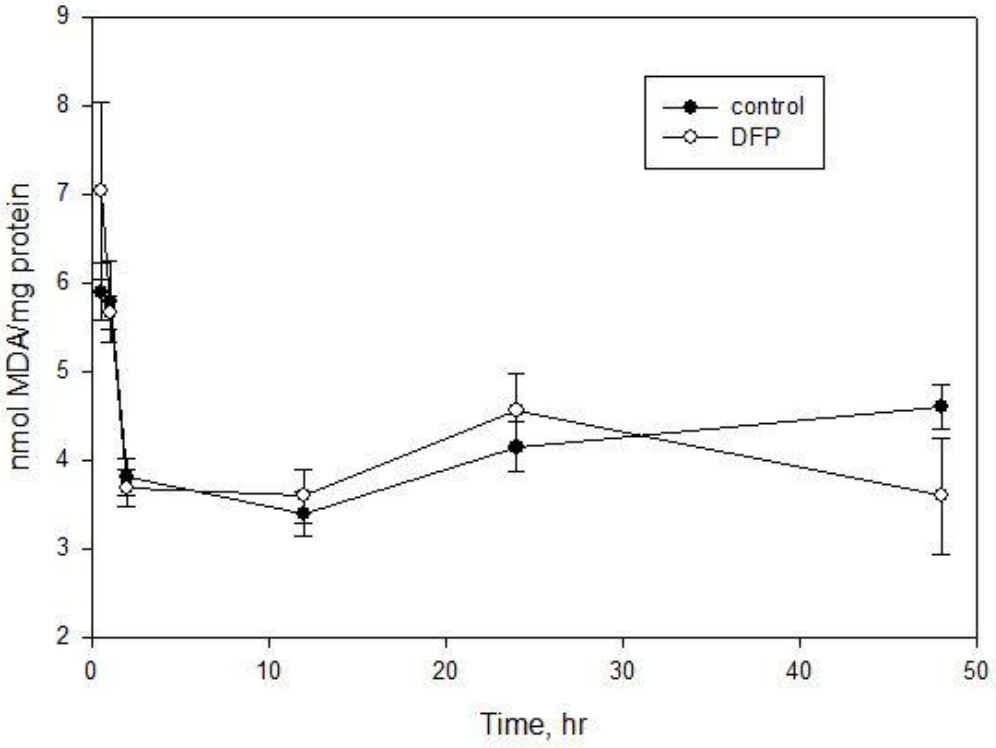

Figure 23. Time course measurement of levels of malondialdehyde in hippocampus. Data are Mean ± SE; n=5/time point.

3.5.2 Differential gene expression in hippocampus

Complete results of the quality control analysis of the gene arrays are shown in Appendix II. Based on the quality control analyses, the data from one gene chip (DFP-treated; n=4 for DFP group) were excluded from the dataset. One sample was lost during preparation (n=4 for control group). The final differential gene expression changes in the hippocampus 1 hr post DFP exposure included 18 up- and 105 down-regulated genes ($p<0.05$ with fold change >

15% regardless of annotation status). The total number of annotated genes that were differentially expressed was 105. The expression of 22 genes was present in the control group but absent in the DFP group, while 9 genes were not expressed in the control group but were in the DFP group. The full list of differentially expressed genes in the hippocampus can be found in Appendix III. Only the genes that were annotated were included in the final list.

In order to understand the biological relevance of the many gene expression changes caused by DFP exposure, complete lists of up- and down-regulated genes were used separately to search the DAVID web site. The results of the database search are listed in Table 12. All biological processes and cellular components in the hippocampus were down-regulated. The cellular pathways affected by DFP exposure were I-kappaB kinase cascade and Wnt signaling pathways. The down-regulated cellular components were cytoplasmic vesicles.

Table 12. Gene expression changes in specific cellular pathways of the hippocampus 1 hr post 1 mg/kg DFP exposure.

Category	Pathway	Regulation	# genes changed	%	p-value*
Biological Process	I-kappaB kinase/NF-kappaB cascade	Down	3	3.8	0.0110
	Protein kinase cascade	Down	5	5.2	0.035
Cellular Component	cytoplasmic vesicle	Down	7	8.8	0.0300
Molecular Function	Wnt signaling pathway	Down	5	5.2	0.0055

*p-values derived from modified Fisher's Exact test

3.5.3 Metabolic changes in hippocampus

Lipid metabolite changes in the hippocampus at 2 hr post DFP exposure are detailed in Table 13. The hippocampus had no significant changes after DFP treatment in any of the lipid species measured.

Table 13. Changes in lipid metabolite concentrations in the hippocampus 2 hr post 1 mg/kg DFP dose.

	Metabolite Concentration (µmol/g tissue)	
Metabolite	**Control**	**DFP**
Total Tissue Weight (g)	0.113 ± 0.031	0.130 ± 0.017
Phosphatidic acid	0.5 ± 0.2	0.3 ± 0.2
Cardiolipin	1.2 ± 0.7	1.5 ± 0.6
Ethanolamine plasmalogen	11.3 ± 2.6	10.0 ± 4.2
Choline plasmalogen	0.8 ± 0.2	0.7 ± 0.4
Phosphatidylserine	6.3 ± 2.0	5.4 ± 1.7
Phosphatidyl-ethanolamine	11.3 ±1.9	10.5 ± 2.9
Phosphatidylinositol	1.1 ± 0.3	1.1 ± 0.4
Phosphatidylcholine	22.9 ± 4.0	20.8 ± 6.2
Sphingomyelin	3.0 ± 0.4	2.8 ± 0.7
Cholesterol[a]	58.1 ± 2.2	55.1 ± 3.6
n3 Fatty acids	9.1 ± 4.7	8.8 ± 2.3
n6 Fatty acids	14.0 ± 1.9	12.1 ± 5.6
Polyunsaturated fatty acids[b]	181.0 ± 11.6	175.8 ± 49.1
Total fatty acids	218.1 ± 20.4	199.6 ± 50.9

Control n = 5; DFP n = 4

[a]Average of 3 cholesterol carbon signals (C18 at 12.5 ppm, C19 at 19.7 ppm and C14 at 57.2 ppm.

[b]Polyunsaturated fatty acid signal intensity is subject to changes in both concentration and composition

Aqueous, small molecule metabolites were measured in extracts of the hippocampus at the 2 hr time point by ^{1}H and ^{31}P NMR (Table 14). In the hippocampus, the amino acids valine, isoleucine and alanine were increased 4-5 fold, while cis-aconitate, fumarate and nicotinate were

increased 2-3 fold after exposure to DFP. Succinate and γ-aminobutyric acid (GABA) were decreased approximately 57%.

Table 14. Changes in aqueous metabolite concentrations in the hippocampus 2 hr post 1 mg/kg DFP dose.

Metabolite (chem. shift in ppm)	Metabolite Concentration (μmol/g tissue)	
	2 hr post dose	
	Control	DFP
Valine (0.98)	0.05 ± 0.01	0.26 ± 0.05**
Isoleucine (1.01)	0.11 ± 0.06	0.43 ± 0.06**
β-hydroxybutyrate (1.24)	0.51 ± 0.42	0.38 ± 0.21
Lactate[a] (1.33, 4.11)	11.1 ± 2.0	12.1 ± 1.5
Alanine (1.41)	0.03 ± 0.01	0.16 ± 0.02**
NAA (2.02)	5.2 ± 1.3	5.4 ± 0.6
Methionine (2.13)	ND	ND
Succinate (2.41)	0.69 ± 0.01	0.27 ± 0.01**
Trimethylamine (2.92)	ND	ND
GABA (2.98)	1.3 ± 0.3	0.6 ± 0.5*
Ornithine (3.07)	ND	0.28 ± 0.17
Cis-aconitate (3.21)	0.36 ± 0.2	0.83 ± 0.24*
Choline (3.22)	0.53 ± 0.13	0.51 ± 0.07
Phosphocholine (3.23)	0.53 ± 0.07	0.48 ± 0.04
Myo-inositol[a] (3.53, 4.06)	3.9 ± 0.9	3.9 ± 0.4
Glucose (3.41)	1.3 ± 0.2	1.6 ± 0.6
Fumarate (6.52)	0.04 ± 0.03	0.1 ± 0.03*
Tyrosine (7.13)	0.06 ± 0.04	0.1 ± 0.02
Formate (8.46)	3.2 ± 2.8	8.3 ± 6.5
Nicotinate[a] (8.71, 8.94)	0.10 ± 0.04	0.19 ± 0.06**
GPC[b] (3.06)	0.43 ± 0.16	0.42 ± 0.06
GPE[b] (3.73)	0.28 ± 0.01	0.26 ± 0
G3P[b] (7.05)	ND	ND
G6P[b] (7.11)	ND	ND
DHAP[b] (8.04)	ND	ND

Control n = 4; DFP n = 4

*Denotes significance at $p<0.05$

**Denotes significance at $p<0.01$

[a]Average of multiple signals

[b]Metabolite signals are from ^{31}P aqueous spectra. GPC set at 3.082 ppm for reference

Abbreviations: NAA – N-acetylaspartate; GABA – γ-aminobutyric acid; GPC – glycerophosphocholine; GPE – glycerophosphoethanolamine; G3P – glycerol-3-phosphate; G6P – glucose-6-phosphate; DHAP – dihydroxyacetone phosphate; ND – Not detectable

IV. DISCUSSION

The aim of this research was to gain insight into the possible mechanistic basis of non-cholinergic toxicity induced by the OP, DFP, in the rat brain. The –omic approach to investigating the off-target toxicity of DFP provided a global picture of the effects triggered by low level exposure. The use of a multi-omic approach was advantageous since the results could be analyzed and interpreted in an integrated manner. It was expected that the cellular response to a low dose insult of DFP would be protection and repair with an effort to return to homeostasis. The greatest effects at 1 hr (gene expression) and 2 and 48 hr (metabolic) after DFP exposure were seen in the cortex, although each region had similar and distinctive changes in metabolic and gene expression profiles.

4.1 Normal regional lipid composition

The use of NMR to generate full lipid profiles of the cortex, brainstem, cerebellum and hippocampus provided an insightful view of the normal regional lipid differences (Figs 13, 14). The brainstem showed the most unique lipid profile as compared to the other three regions, being much higher in all measured phospholipids and cholesterol. With the exception of the substantia nigra, red nucleus and olivary and cranial nuclei, the brainstem is predominantly white matter, corresponding to the increased levels of these lipids. Interestingly, the levels of n6 fatty acids were comparable in brainstem relative to other regions, but the level of n3 fatty acids was significantly lower than in cortex and cerebellum. In the ^{13}C spectrum of all brain extracts, the n3 fatty acid signal was a single peak, likely representing a single lipid species, presumably docosahexaenoic acid (DHA), the major n3 fatty acid in mammalian brain. Though not a single peak, the n6 fatty acid signal was dominated by one peak and assumed to be arachidonic acid

(AA). These signals corresponded to NMR spectra from reference standards of DHA and AA that were acquired in this laboratory. DHA is specific to the CNS and is particularly enriched in grey matter (Halliwell and Whiteman, 2004; Milatovic *et al*., 2006). Approximately 50% of CNS plasma membrane PUFAs is DHA, with a concentration in the synapses (Bazan *et al*., 2011). AA is a known precursor of pro-inflammatory eicosanoids and also increases production of interleukins 1 and 6 as well as TNF-α (tumor necrosis factor alpha) (Yao *et al*., 2009). n3 fatty acids such as DHA, however, suppress the production of AA-derived eicosanoids by competitively inhibiting cyclooxygenase and through a negative feedback mechanism on Δ-desaturase, the rate limiting enzyme in the formation of AA; n3 fatty acids thus are considered to be anti-inflammatory or immunosuppressive (Muakkassa *et al*., 1991; Yao *et al*., 2009). It is unknown if the brainstem has higher levels of most lipid species solely because of greater myelination or if there is functional importance associated with these elevated lipid species. It has been thought that the high levels of ethanolamine plasmalogen in the brainstem may serve as scavengers for ROS, protecting critical membrane phospholipids from peroxidation (Brosche and Platt, 1998; Engelmann *et al*., 1994; Hahnel *et al*., 1999; Kuczynski and Reo, 2006). The high n6:n3 (or AA:DHA) FA ratio, calculated to be 2.32 ± 0.51, in the brainstem would favor a pro-inflammatory response. Irrespective, the high lipid density of the brainstem does create an attractive target for lipid soluble toxins, such as OPs. Correspondingly, this region was also found to have the highest basal level of AChE activity (Fig. 12)

Cortex, cerebellum and hippocampus were relatively similar and unremarkable in the lipid profiles with the exception of the n3 and n6 FA which, again, may reflect the inflammatory response tendencies of those regions. The calculated n6:n3 ratios for the cortex, cerebellum and hippocampus were 1.26 ± 0.27, 0.62 ± 0.08 and 2.07 ± 1.4, respectively. The relatively equal ratio between AA and DHA in the cortex would balance the pro- and anti-inflammatory response, while the hippocampus may behave similarly to the brainstem with a pro-inflammatory tendency.

With an AA:DHA ratio less than 1, the cerebellum was unique and likely favors an anti-inflammatory response.

4.2 Regional metabolomes

PCA is a commonly used unsupervised method to visualize NMR-derived metabolomic data. Various reports have described the use of PCA to illustrate the clustering of NMR spectral intensities using top principal components (Anthony *et al*, 1994; Holmes *et al*, 1992, 1998a,b; Williams *et al*., 2003b). One of the stated reasons for the selection of cortex, brainstem, cerebellum and hippocampus as the brain regions for the investigation of low level OP toxicity was because of the assumption that each region had distinct function, and therefore, would have distinct chemical makeup. Since the physiological activity of the cell is defined and regulated by the metabolites, then the cellular chemistry would be a driver of that region's specific physiology. PCA of the ^{1}H NMR spectra of control brain extracts illustrated the biochemical uniqueness of the four brain regions investigated (Fig. 15). Each region displayed tight clustering within each group and no overlap between regions. This result demonstrates that, unlike the lipid composition which was relatively similar for cortex, cerebellum and hippocampus, the biochemical makeup of each region was unique. The systemic distribution of DFP delivered enough dosage to cause comparable and significant levels of inhibition of AChE in each region (Figs. 16, 18, 20, 22). With such different metabolic profiles each region's cellular response to the insult would be expected to reflect these variations.

4.3 Acetylcholinesterase inhibition

For the purposes of this research, a non-cholinergic dose was considered to be a sub-acute dose that inhibited AChE to a level that did not elicit an overt response indicative of cholinergic toxicity such as salivation, lacrimation and seizures (muscarinic effects) or muscle weakness, fasciculation and flaccidity/paralysis (nicotinic effects). All animals showed none of these cholinergic symptoms post dosing. The inhibition of AChE in each of the brain regions was positive indication of systemic distribution of DFP to the brain. The large amount of variability

in the cortex likely stems from non-homogeneous sampling of the large cortical region. All other regions were subsequently homogenized before removal of sample for analysis. Knowing that the level of maximum inhibition for all four regions was approximately 50%, and that the brainstem had the highest level of basal activity, more of the DFP dose reached the brainstem. Because of the substantially higher lipid content in the brainstem this may be caused, in part, by higher partitioning of DFP in this region. Many OPs are highly lipophilic, although DFP is water soluble, as well. The K_{ow} (octanol/water partition coefficient) of DFP is 14.8, compared to the highly lipid soluble soman which has a K_{ow} of 66.1. This increased affinity for lipids may make the brainstem a target for OPs. Each brain region showed a trend toward recovery by 48 hr which is similar to previous reports in whole brain (Gearhart *et al*., 1990; Martin, 1985), though none of the regions reached control levels by 48 hr. New enzyme production depends on protein synthesis only and not mRNA synthesis, and the appearance of new AChE occurs over a period of days to weeks (Chippendale *et al*., 1974; Lanks *et al*., 1974) which is consistent with the lack of complete recovery seen at 48 hr. Therefore, even in the absence of cholinergic symptoms, delayed synthesis of AChE can prolong mild hyperstimulation of postsynaptic receptors. In addition to this, it is important to note that while neuronal and astrocytic metabolism differ, neuronal health and function is dependent on the surrounding astrocytes. While the initial response may occur at the synapse, the cascade of effects is not limited to the neuron.

4.4 Determination of oxidative stress

It has not been previously shown if a 1 mg/kg dose of DFP would trigger oxidative stress through the formation of ROS. We were unable to measure any significant increases in MDA, the selected marker of lipid peroxidation, in any of the four brain regions. The MDA assay itself may also be unreliable, as there were significant differences between data generated from the cuvette method and the microplate method (Figs. 17, 19, 21, 23), although it is believed that comparisons between treated and control for each tissue were valid as they were run together with linear standard calibration. If mild lipid peroxidation occurs at this dose of DFP, then more

sensitive markers, such as F2-isoprostane and F4-neuroprostane, which are the products of peroxidation of AA and DHA, respectively, would be required for detection (Halliwell and Whiteman, 2004; Milatovic *et al*., 2006; Reich *et al*., 2001). For the purposes of this study, we have no definitive proof of oxidative stress manifested in the form of lipid peroxidation. However, differential gene expression results suggest that one of the early cellular responses to DFP was to ameliorate increases in ROS. Up-regulation of genes associated with vitamin C transport in the brainstem and response to oxidative stress and myeloperoxidase (mpo) in the cerebellum indicated that there was cellular detection of an imbalance of ROS that triggered an early gene response in these regions (differential gene expression data is available in Appendix III). It is probable that the gene expression changes are more sensitive markers of oxidative stress than MDA, and that a 1 mg/kg dose of DFP was enough to induce a level of oxidative stress that was low, yet significant enough to bring about a change in gene expression. However, induction of oxidative stress did not appear to be a major contributor to the overall mechanistic basis of low level toxicity of DFP.

4.5 Biological interactions in the cortex

The cortex had the most changes in gene expression, with the majority of genes being down-regulated. Three general processes were the focus of down-regulation in the cortex: apoptosis, synaptic functions and protein transport (Table 6). The down-regulation of two of these, apoptosis and synaptic functions, supported the concept of protection and repair. While the low dose of DFP likely caused a mild, yet sustained increase in postsynaptic stimulation, the level should not be enough to cause extensive excitotoxicity. Induction of apoptosis would be a gross overt response that would elicit more damage than the initial insult. The gene expression changes shown here are at 1 hr post-dose, representing an early response that enables the protection of survivable cells and allows for activation of mechanisms to repair damage.

Multiple processes involving synaptic functions were down-regulated, particularly those that regulate the levels and secretion of neurotransmitters. All brain regions were shown to have a maximum inhibition of AChE of approximately 50% with a slow trend toward recovery by 48 hr. As previously stated, losing function of up to half of the AChE would result in an increase in the available ACh in the synaptic space with a subsequent overstimulation of postsynaptic receptors. Although DFP, for the most part, does not age, the binding to AChE is essentially irreversible and reactivation would take longer than the formation of new protein, which is on the order of days to weeks. With diminished hydrolysis of ACh in the synaptic space, the two options for attenuating the postsynaptic stimulation are to: 1) reduce the number of postsynaptic ACh receptors and/or 2) reduce the amount of ACh being released into the synapse. In the cortex the differential gene expression data suggest that the synaptic structure is being modified to moderate the transmission of excitatory neurotransmitters. Using GeneSpring software, the biological interactions of down-regulated genes associated with synaptic functions in the cortex revealed the potential effect of DFP on the synapse (Fig. 24).

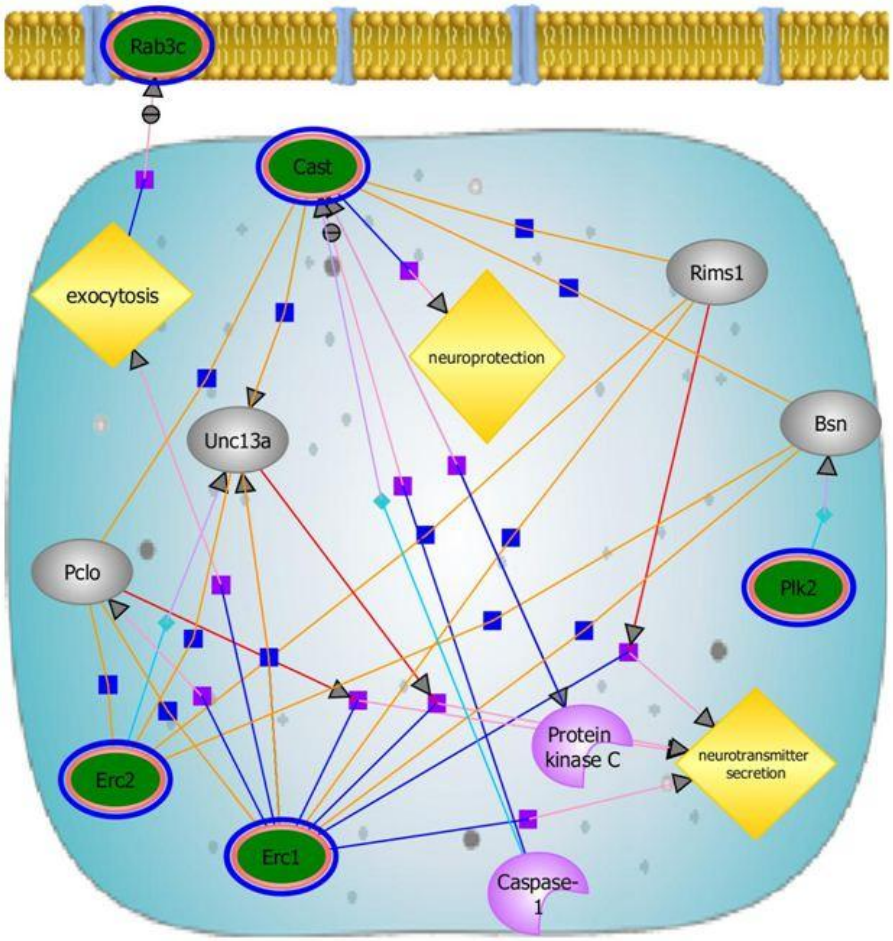

Figure 24. Biological interactions of synapse-related gene protein products and functions in the cortex (GeneSpring). Gene product legend: green – down-regulated; grey – unchanged. Interaction legend: blue square – binding; purple square – regulation; cyan diamond – metabolism. Rab3c is associated with the plasma membrane. All other genes/proteins are associated with cytosol.

The gene expression of the family of RIM-binding proteins, Erc1, Erc2, Rab3 and Cast were all down-regulated in the cortex. RIMs are proteins specific to the presynaptic active zone that serve to regulate neurotransmitter release and control membrane traffic (Wang *et al*., 2002). These proteins interact with Bsn, Rims1, Pclo and Unc13a, all of which are responsible for synaptic cytoskeleton organization, regulation of exocytosis, regulation of presynaptic cytomatrix proteins

and synaptic vesicle maturation with the ultimate outcome being the regulation of neurotransmitter secretion. A down-regulation in the expression of this protein family has the potential to induce further modulation of these genes and proteins to reduce the amount of excitatory neurotransmission, ultimately serving a neuroprotective role. Additionally, the expression of *grik2*, the gene coding for an ionotropic glutamate receptor specific to the synaptic membrane was also down-regulated. After acute doses of OPs, particularly nerve agents, severe AChE inhibition is quickly succeeded by activation of NMDA (N-methyl-D-aspartate) glutamate receptors, causing intracellular accumulation of Ca^{2+}. NMDA receptor activation is considered to be responsible for the induction of seizures and *status epilepticus* which cause the profound neuronal damage seen following acute exposure (McDonough and Shih, 1997). While the gene that codes specifically for subunits of the NMDA glutamate receptor, *grin*, did not have altered expression, the down-regulation of *grik2* is further evidence of neuroprotective changes in gene expression after a sub-acute dose. Finally, the inhibitory neurotransmitter GABA was increased at 48 hr post DFP, also promoting neuromodulation of excessive excitatory transmission. The release of GABA has been shown to be a neuronal defense mechanism in response to glutamate exposure (Sapolsky, 1998).

Expression of *Ptgds* was up-regulated and expression of *Nmur2* was not detectable in control cortical samples but was significantly up-regulated after DFP exposure. The search in DAVID linked these genes with the biological function termed 'disulfide bond', likely referring to three conserved cysteine residues in the prostaglandin D2 (PGD_2) protein, one of which, Cys^{65}, is critical for catalytic activity (Liu *et al*, 2008). Nmur2 is a G-protein coupled receptor that is expressed mainly in the CNS and, in particular, the hypothalamus (Zeng *et al*., 2006). The significance of Nmur2 is unclear, though it may be involved in adrenocorticotrophin-mediated stress response (Zeng *et al*., 2006). Interestingly, some studies have discovered that glucocorticoids impair neuronal defenses by inhibiting the release of extracellular adenosine

during an insult to the neurons (Sapolsky, 1998). Quantifying adenosine from the NMR spectrum is difficult because the best resolved signals arise from adenosine associated with ATP and not free adenosine. The protein product of Ptgds, however, catalyzes the synthesis of PGD_2 from PGH_2. PGD_2 is the most abundant prostaglandin in the brain (Saleem *et al*., 2009). Inflammation in the CNS is known to increase the synthesis of PGD_2. An up-regulation in *Ptgds* is a good indication of inflammatory processes in the cortex and correlates with the loss of membrane phospholipids and specifically n6 FA (AA) seen in the NMR lipid metabolite data.

The third down-regulated process, protein transport, is likely a result of injury and has the potential to be harmful to the cell. In a scenario where the cellular response is protection and repair, one of the means by which the cell accomplishes this task is to synthesize and localize proteins. As discussed earlier, the synthesis of new AChE is critical to re-establishing normal synaptic function and returning the cell to homeostasis. In the CNS, de novo synthesis of AChE occurs in the neuronal cell body and is then transported through the axon to the nerve terminal (Chippendale *et al*., 1974). If the mechanisms of protein transport are dysfunctional, then the localization of newly synthesized enzyme to the synapse will quite likely be delayed, prolonging the period of postsynaptic hyperstimulation. In fact, Chippendale *et al*. (1974) suggested that the delivery of new AChE after inhibition with 1 mg/kg DFP was via slow axoplasmic flow and not any rapid flow. However, it is possible that the protein transport mechanisms associated with rapid axoplasmic flow were disabled. Therefore, while cellular responses are focused on minimizing and repairing damage from the toxic insult, the secondary effects of the exposure are creating a roadblock for these mechanisms. Prolonging the repair process has the potential to lead to long-term neural dysfunction.

Finally, the molecular functions of nucleotide and ATP binding were significantly down-regulated, with the expression of a large number of genes being affected. The functions of nucleotide and ATP binding are broad, as they apply to nearly every process in the cell.

However, the overall message is that the energy status of the cell has been affected as a result of the DFP insult. An impairment of the ability to bind ATP impedes cellular progress toward homeostasis, just as down-regulation of protein transport does.

The signal representing NAA was significantly lower in the DFP-treated cortex samples as compared to control at 2 hr post-dose. NAA is specific to the nervous system and is considered to be a marker of neuronal health. Decreases in NAA have been shown to correlate to axonal degradation or dysfunctional metabolism, and nearly all brain diseases or disorders, with the exception of Canavan disease, have decreased levels of NAA (Moffett *et al*., 2007). It is important to note that neuronal dysfunction associated with decreases in NAA can be reversible and does not indicate a permanent loss of neurons (De Stephano *et al*., 1995; Moffett *et al*., 2007). The change in NAA seen at 2 hr was significant, yet returned to control levels by 48 hr. However, the decrease at 2 hr can be interpreted as a neuron-specific perturbation seen only in the cortex (Table 5).

Because of the changes seen in the cortex at 2 hr, we chose to look at the cortex at 48 hr post dose to determine if there was a progression of metabolic perturbation. At 48 hr post DFP exposure, the data reveal a perturbation in glycolysis (Figure 25).

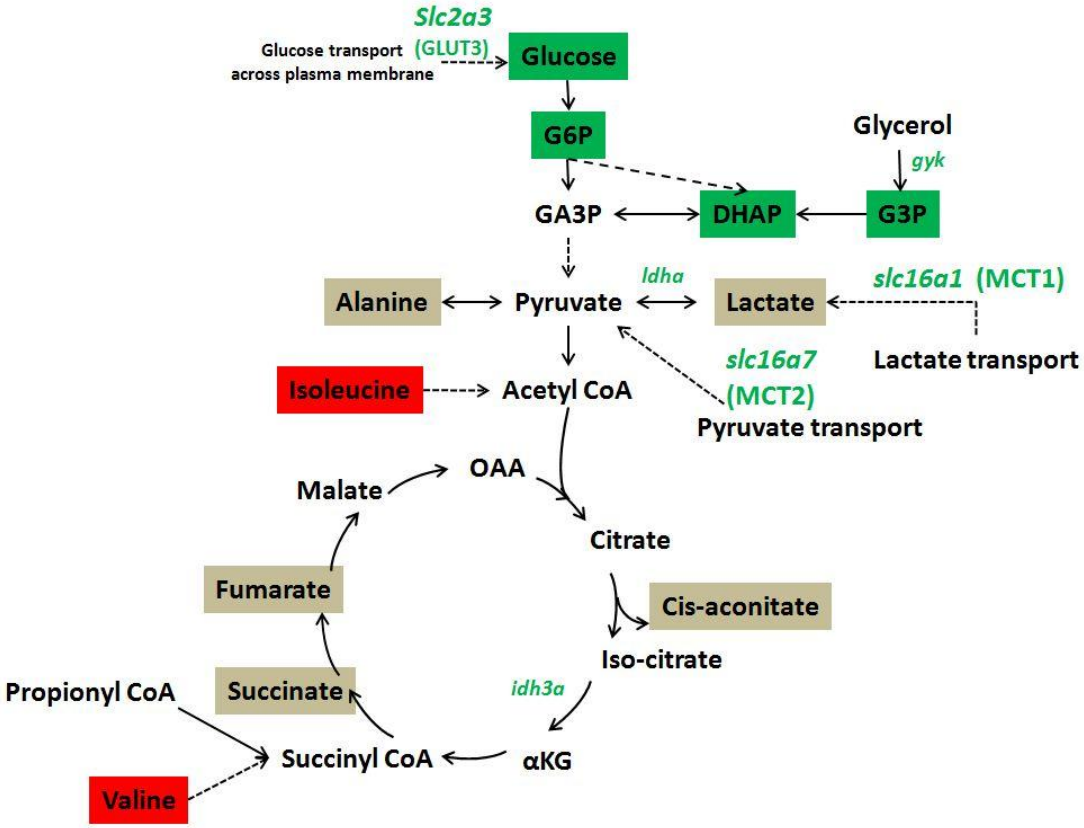

Figure 25. Schematic representation of glycolytic pathway and TCA cycle, showing changes in small molecule metabolites in the cortex at 48 hr post DFP exposure with associated gene expression changes at 1 hr post DFP exposure. Increases in measured metabolites are shaded red and decreases are shaded green. Metabolites that were measured from the NMR spectra but did not change after DFP exposure are shaded grey. Unshaded metabolites were not measured. Genes are denoted by lower case text in italics. Down-regulated genes are in green. Abbreviations: G6P – glucose-6-phosphate; GA3P – glyceraldehyde-3-phosphate; DHAP – dihydroxyacetone phosphate; G3P – glycerol-3-phosphate; OAA – oxaloacetate; αKG – α-ketoglutarate.

Differential gene expression data showed that expression of *slc2a3* was down-regulated at 1 hr with a subsequent decrease in glucose and G6P levels observed at 48 hr. *Slc2a3* codes for GLUT3, the primary neuronal glucose transporter, and is found predominantly in axons and dendrites of neurons (Vannucci *et al.*, 1998). The change in expression of the gene for GLUT3 but not GLUT1, the astrocytic glucose transporter, localized the site of injury to the neuron. Down-regulation for expression of *gyk* (glycerol kinase) at 1 hr was followed by a decrease in G3P and DHAP at 48 hr. The decreases in these metabolites are likely to alter the level of glyceraldehyde-3-phosphate (GA3P) and, ultimately, the amount of pyruvate available for the TCA cycle. Unfortunately, the signals for GA3P and pyruvate were not detectable in the NMR spectrum. The chemical shift for pyruvate in the spectrum was unobstructed by other signals; therefore, the levels of pyruvate are simply below the limit of detection. The decrease in DHAP was likely caused by decreases in both G6P and G3P, offsetting the equilibrium between DHAP and GA3P. Interestingly, gene expression for lactate dehydrogenase (*ldha*) was down-regulated at 1 hr, though no corresponding changes in levels of lactate were measured at either 2 or 48 hr. Lactate dehydrogenase is a tetrameric enzyme, containing either M and/or H subunits. *Ldha* codes for the M subunit, while *ldhb* codes for the H subunit. The LDH-1 isozyme, found mainly in neurons, is composed of 4 H subunits, while LDH-5, specific to astrocytes, contains M subunits only. Therefore, the down-regulation of *ldha*, which codes for the M subunit, localizes this change in gene expression to the astrocyte. Additionally, *slc16a1* and *slc16a7*, which code for MCT (monocarboxylate transporter) 1 and 2, respectively, were also down-regulated. MCT1 is the major lactate transporter of the BBB and is found in significant quantities in astrocytes. MCT2 is the major isoform for neurons and has high affinity for pyruvate. Taken together, these changes have the potential to impact energy production in the neuronal environment. Lactate as an alternative energy source for the neuron has been proposed (Pellerin and Magistretti, 1994); however, the astrocyte-neuron lactate shuttle hypothesis is quite controversial and is refuted by substantial data regarding the lactate dehydrogenase enzymes and lactate transporters. Glycolytic

enzymes are tightly regulated by cellular energy status. LDH, however, is not regulated by energy status; the rate and direction of the reaction catalyzed by LDH is controlled by the concentration of the substrates and products, lactate and pyruvate, as well as the NADH/NAD^+ ratio. Therefore, neuronal levels of pyruvate at rest or during increased neural activation drive the LDH reaction toward lactate. Also, both glycolysis and lactate dehydrogenation require NAD^+, which means that if lactate is used as an energy source, it is done at the expense of glucose. Finally, in order for the LDH reaction to shift towards pyruvate production, the levels of lactate must be excessively high. Lactate transport across the BBB, however, follows a concentration gradient facilitated by the MCTs. This process is relatively slow in the absence of a dramatic event such as seizure induced increases in brain lactate concentration. With the decrease in glucose, G6P, G3P and DHAP and the down-regulation of genes indicative of energy status, it is probable that the glycolytic rate was down, although the glycolytic metabolites may simply be depleted by increased energy demands. If the equilibrium reaction catalyzed by LDH normally favors the direction of lactate production, then the down-regulation of the astrocyte-specific LDH would reduce the conversion of pyruvate to lactate in the astrocyte, likely insuring that the available pyruvate from glucose is fully oxidized. It is interesting that this is localized to the astrocyte and not the neuron, where the conversion of energy substrate to ATP is critical. Gene array data do not show a change in the expression of GLUT1, only GLUT3. Based on this, glucose transport to the astrocyte is not compromised. This is compelling evidence to indicate that lactate from the astrocyte is not an alternative energy substrate. Because glycolytic ATPs are linked to ion transport (Dienel and Cruz, 2003; Roberts, 2007; Wu *et al*., 1997), the energy derived from glycolysis is essential, particularly for synaptic function as few to no mitochondria are found in the synaptic region. It is very unfortunate that pyruvate was not quantifiable from the NMR spectrum and future studies should include specific analysis of this metabolite. Additionally, time course measurement of lactate may reveal the temporal relationship between the gene expression change and any changes in lactate levels.

There was limited indication that the disruption in glycolysis translated to the TCA cycle at this time point. Only succinate and fumarate could be quantified from the NMR spectra, and the concentration of these two metabolites did not change after DFP exposure. Cis-aconitate was measured, and being in equilibrium with citrate, should be an indicator of citrate levels which were not quantifiable. Cis-aconitate levels were decreased at 48 hr, though this was not statistically significant. Expression of the gene coding for iso-citrate dehydrogenase (*idh3a*) was down-regulated at 1 hr with no apparent impact on the TCA cycle that is reflected later in the metabolites succinate and fumarate. What is known, though, is that the cell was responding to the DFP insult as early as 1 hr post dose, and glycolysis was impacted by 48 hr. These changes in the glycolytic pathway may mark the cellular attempt to return to homeostasis, which increases the demand for ATP. Based on gene expression data, the ability to use ATP has been compromised. In an environment where the demand for glucose and oxygen is already high, even a slight perturbation in glucose metabolism and energy usage can have deleterious effects for the neuron.

The increases in the BCAAs valine and isoleucine in cortex at 48 hr represent a potential impact on the TCA cycle. As essential amino acids, the sole source for BCAAs is dietary; therefore, the increase in these levels must be caused by decreased metabolism. Catabolism of valine in brain slices ultimately forms succinyl-CoA; this conversion has the potential to serve an anaplerotic function to the TCA cycle (Murin *et al*, 2009a). Glial metabolism of isoleucine yields acetyl-CoA and propionyl-CoA, the latter being catalyzed by propionyl-CoA carboxylase to succinyl-CoA for TCA cycle anaplerosis (Murin *et al*., 2009b). Gene array results showed no change in the expression of any genes associated with enzymes of these metabolic pathways. Impairment of valine and isoleucine metabolism potentially reduces this point of entry into the TCA cycle. At the 48 hr time point, however, there is no indication of any impact on metabolites within the TCA cycle. Future studies should investigate later time points to determine if the perturbation in BCAA metabolism translates to a change in TCA cycle metabolites.

The changes in these BCAAs may have broader implications than solely a connection to the TCA cycle. In addition to this function, BCAAs act as nutritional signals for cellular growth pathways through protein synthesis, specifically the mammalian Target of Rapamycin (mTOR) pathway. Increases in these amino acids stimulate the mTOR complex, triggering protein synthesis. If the neuronal response was to protect and repair, while returning to homeostasis, cellular growth in the form of increasing axon length and dendritic outgrowth would be counterproductive. Cell signaling cascades are complex and have many points of positive and negative feedback; however, the gene expression data showed down-regulation of several ephrin receptor tyrosine kinases (*epha6*, *epha7*, *ephb6*), as well as ephrin B2 ligand (*efnb2*). Ephrin receptors have been shown to inactivate mTOR by increasing upstream repressor activity (Nie *et al*, 2010). A down regulation of these receptors has the potential to stimulate mTOR activity further to the detriment of the neuron. Ephrin signaling is known to control growth cone dynamics such as axon branching and retraction and work through a variety of downstream effectors such as GTPases, phosphatases and guanine nucleotide exchange factors. There is no indication that the signaling pathway is linked to BCAA metabolism. As signaling molecules, BCAAs are specific to the mTOR complex itself, triggering the localization of the complex to a molecular scaffold of activating proteins. Therefore, it is unlikely that the down-regulation of ephrin gene expression is responsible for the increase in valine and isoleucine.

At 2 hr post dose, the cortex showed the greatest changes in the lipid profiles, with decreases in lipids and phospholipids associated with the plasma membrane. Cardiolipin, a phospholipid specific to the inner mitochondrial membrane, was not affected by DFP exposure. This seems to correlate with the lack of any observed impact on the TCA cycle at 48 hr that may have been caused by an earlier disruption in the mitochondrial membrane. The targeting of the plasma membrane may be related to the level of inhibition of AChE. Significant inhibition of enzyme was seen as early as 30 min after DFP dosing, reducing the amount of free choline from

ACh hydrolysis, and, therefore, the amount available for re-uptake by the presynaptic neuron. Under normal conditions, the presynaptic neuron uses the recycled choline as substrate for the synthesis of ACh (via choline acetyltransferase) and phosphocholine (via choline kinase) for phospholipid synthesis and incorporation into the membrane. The demand for this choline for ACh synthesis far exceeds that for PtdC synthesis, as very little dietary choline is used for ACh (Cansev *et al*., 2008; Zeisel, 2006). The impact on the membrane is two-fold: the incorporation of choline-containing phospholipids into the membrane decreases while the breakdown of choline-containing phospholipids increases. Choline deficiency has been shown to create a loss of PtdC from the membrane, although the levels of PtdE were reported to increase (Zeisel, 1997). However, PtdE-N-methyltransferase, the enzyme responsible for the synthesis of PtdC from PtdE using S-adenosylmethionine as a methyl donor, has been shown to have activity in the brain, particularly when PtdC breakdown increases during excessive neuronal firing (Blusztajn *et al*., 1986; Lakher and Wurtman, 1987; Zeisel, 1997). The majority of activity is located in the nerve terminal, corresponding to the region most immediately affected by excess neuronal stimulation (Blusztajn *et al*, 1986; Parducz *et al*., 1976; Zeisel, 1997). Therefore, lack of replenishment of the choline pool could explain the decreases in PtdC, PtdE and SM, which is another choline-containing phospholipid. The measured levels of choline did not change significantly from control at either 2 or 48 hr post dose, though this may be attributable to choline being both a breakdown product and synthetic precursor. However, phosphocholine, a precursor to PtdC synthesis, was decreased at 48 hr, suggesting that the rate of PtdC synthesis was being up-regulated in order to restore membrane phospholipids, and, therefore, membrane stability (Fig. 26). In fact, qualitative analysis of the phospholipid metabolites at 48 hr revealed that the levels of PtdC, PtdE and ChPl from control cortex were no longer significantly different than DFP-treated cortex, suggesting that the cellular environment in the cortex had recovered membrane phospholipids (Figs. 26, 27; data in Appendix IV). It should be noted that the expression of phospholipase C, which hydrolyzes PtdC to DAG and phosphocholine, and phospholipase D,

which hydrolyzes PtdC to PA and choline, was not changed. However, *smpd3* gene, which codes for sphingomyelinase, was down-regulated at 1 hr post dose. This could account for the decrease in phosphocholine since this enzyme catalyzes the hydrolysis of SM to phosphocholine and ceramide. However, it is also possible that this gene was down-regulated in order to prevent the hydrolysis of SM in order to preserve membrane integrity. Indeed, levels of SM from DFP-treated cortex were not significantly different than control at 48 hr post dose.

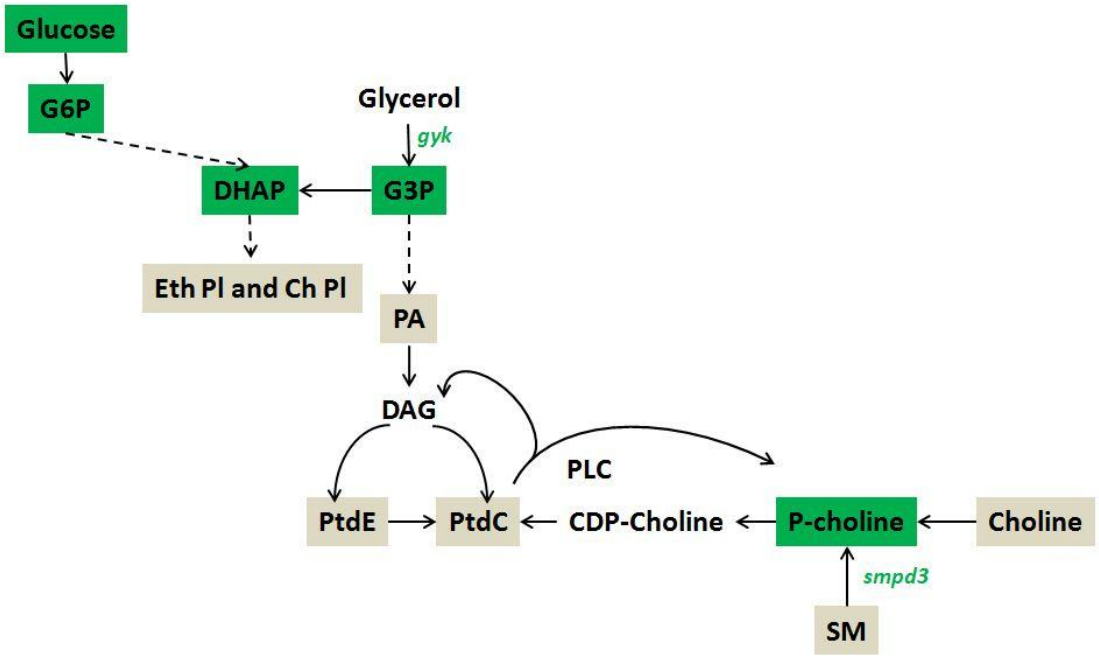

Figure 26. Schematic representation of interaction of glycolytic pathway and lipid metabolism, showing changes in small molecule metabolites in the cortex at 48 hr post DFP exposure with associated gene expression changes at 1 hr post DFP exposure. Decreases in measured metabolites are shaded green. Metabolites that were measured from the NMR spectra but did not change after DFP exposure are shaded grey. Unshaded metabolites were not measured. Genes are denoted by lower case text in italics. Down-regulated genes are in green. Abbreviations: G6P – glucose-6-phosphate; DHAP – dihydroxyacetone phosphate; G3P – glycerol-3-phosphate; Eth Pl – ethanolamine plasmalogen; Ch Pl – choline plasmalogen; PA – phosphatidic acid; DAG – diacylglycerol; PtdE – phosphatidylethanolamine; PtdC – phosphatidylcholine; CDP – cytidine diphosphate; PLC – phospholipase C; SM - sphingomyelin.

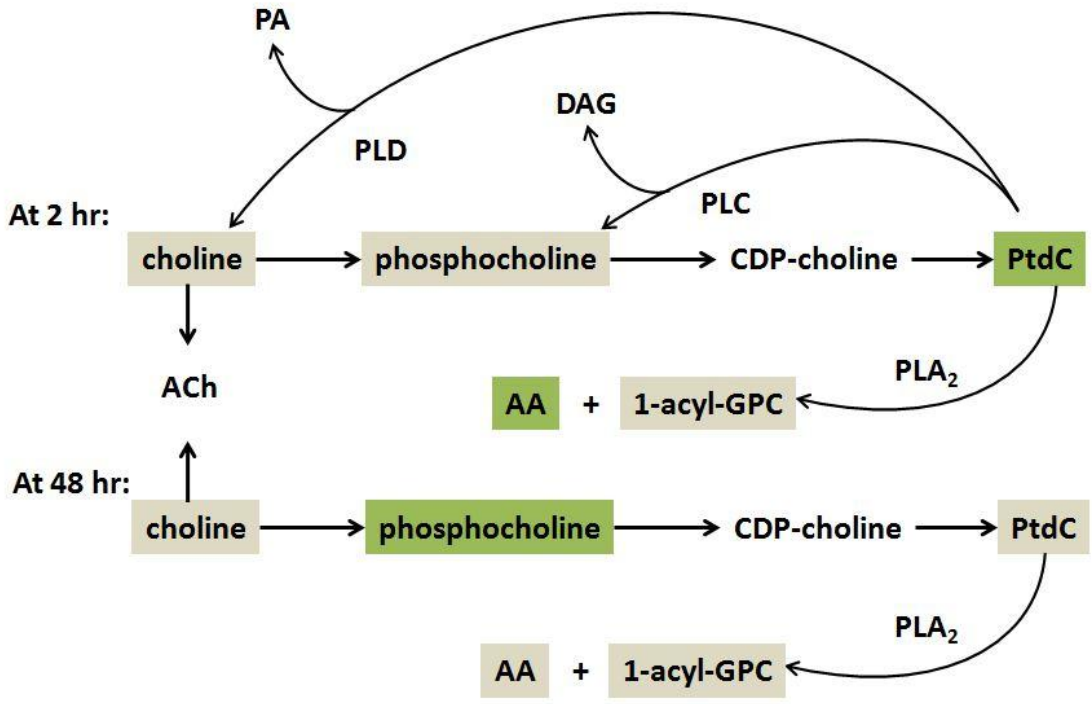

Figure 27. Temporal changes in phosphatidylcholine and related small molecule metabolites. Decreases in measured metabolites are shaded green. Metabolites that were measured from the NMR spectra but did not change after DFP exposure are shaded grey. Unshaded metabolites were not measured. Abbreviations: PA – phosphatidic acid; PLD – phospholipase D; DAG – diacylglycerol; PLC – phospholipase C; AA – arachidonic acid; GPC – glycerophosphocholine; CDP – cytidine diphosphate; PtdC – phosphatidylcholine; PLA_2 – phospholipase A_2.

The decrease in membrane phospholipids and n6 FA also provided additional evidence that the low level exposure to DFP induced an inflammatory response. Prostaglandin synthesis would require cleavage of membrane phospholipids to supply the required precursor, AA, leading to a loss of the phospholipids. Gene expression data do not show any change in phospholipase A_2. This does not explain, however, why the inflammatory response would be localized to just the cortex. Further evidence would be needed to determine if inflammation played a role in the mechanistic basis of effects caused by low level DFP exposure.

Because phospholipid metabolism, specifically fatty acid synthesis and turnover, in the brain consumes ATP at a high rate, restoring membrane integrity would also require a dramatic increase in ATP consumption (Purdon and Rapoport, 2007). Therefore, the loss of membrane phospholipids, either for replenishing the choline pool or for supplying AA, will generate an increased demand for energy in the neuronal environment. This may account for the perturbation in metabolites associated with the glycolytic pathway. Additionally, DHAP is the precursor for de novo synthesis of the ether-linked plasmalogens (Lee, 1998; Pollock *et al*., 1976; Purdon and Rapoport, 2007). The decrease in DHAP at 48 hr may be indicative of an up-regulation in synthesis of EthPl and ChPl, both of which had comparable levels in control and DFP-treated groups at 48 hr post dose (Fig. 26; data in Appendix IV).

Finally, the decrease in n3 FA cannot be overlooked and has unique significance to the CNS. As previously stated, the NMR signal for the n3 FA was a single peak and presumed to be DHA. This is consistent with reports that DHA is the most abundant long chain n3 PUFA in the CNS. Therefore, the decrease in the n3 FA signal in the cortex can be attributed to a loss of DHA. In addition to being a key component of membrane phospholipids (levels of unesterified DHA are negligible as free DHA is rapidly incorporated into the sn2 position of phospholipids), DHA may play a critical neuroprotective role in the CNS. A bioactive derivative of DHA, neuroprotection D1 (NPD1, 17S-docosatriene), has been shown to induce homeostasis and pro-survival signaling after insult by up-regulating anti-apoptotic proteins and down-regulating pro-apoptotic proteins (Bazan *et al*., 2011). NPD1 is considered to be anti-inflammatory. It is possible that the low level exposure to DFP induced the conversion of DHA to NPD1 for the promotion of cell survival. Gene array data do not show a change in the expression of 15-lipoxygenase-1, the enzyme responsible for conversion of DHA to NPD1, though this does not imply that the enzyme is not already active. However, the loss of DHA leads to potentially adverse implications for the cell. The phospholipid PtdS is rich in DHA and is a key player in Akt

signaling for promoting cell survival (Bazan *et al*., 2011). Because of the tight regulation between DHA and PtdS, a loss of DHA results in a preferential loss of PtdS. The data reported here show a significant decrease in PtdS, which could correlate to the decrease in n3 FA. This loss can translate to a deficit in Akt signaling, hampering the cellular attempt to return to homeostasis. DHA-rich membranes have also been linked to G protein coupled receptor (GPCR) signaling pathways, suggesting that GPCRs are located in DHA-rich regions of the cell membrane. Interestingly, muscarinic ACh receptors are GPCRs. Disruption in this region of the membrane can further challenge neuronal communication and function via impaired signaling pathways. It is obvious that future studies should further investigate the role of DHA in OP-mediated toxicity. Neuroprostane, the peroxidation product of DHA, and NPD1 levels are important markers for understanding the mechanisms of action within the CNS, and particularly, the cortex.

4.6 Biological interactions in the brainstem

The brainstem was the most unique of the four brain regions investigated, in terms of composition and response to the low level exposure to DFP. As previously stated, the brainstem was much higher in all measured phospholipids and cholesterol, relative to cortex, cerebellum and hippocampus, a finding that is not unusual considering the large degree of myelination in the brainstem. This lipid-rich environment makes the brainstem an attractive target site for lipophilic compounds such as OPs. DFP's large K_{ow} of 14.8 indicates that the compound will partition readily into the brainstem region. This was reflected in the AChE inhibition data. The maximum inhibition of AChE in the brainstem was at 40% of control activity, the greatest amount of inhibition of the four regions investigated. The basal level of enzyme activity in the brainstem was higher than cortex, cerebellum and hippocampus. Taken together, the brainstem received the largest dose of DFP. However, the lipid and small molecule metabolite profiles at 2 hr post DFP exposure were negligibly affected by the insult. Only the mitochondrial phospholipid cardiolipin

was decreased at 2 hr post dose. Of the small molecule metabolites that were identifiable from ^{1}H and ^{31}P NMR spectra, none were altered. PCA of the binned ^{1}H spectra revealed an overlap of control and DFP-treated groups, positive indication that no variables existed in the spectra, known or unknown, that contributed to separation of the two groups (Fig 28). Based on the metabolic data, it appeared that a 1 mg/kg DFP dose had no effect on the brainstem at 2 hr post dose.

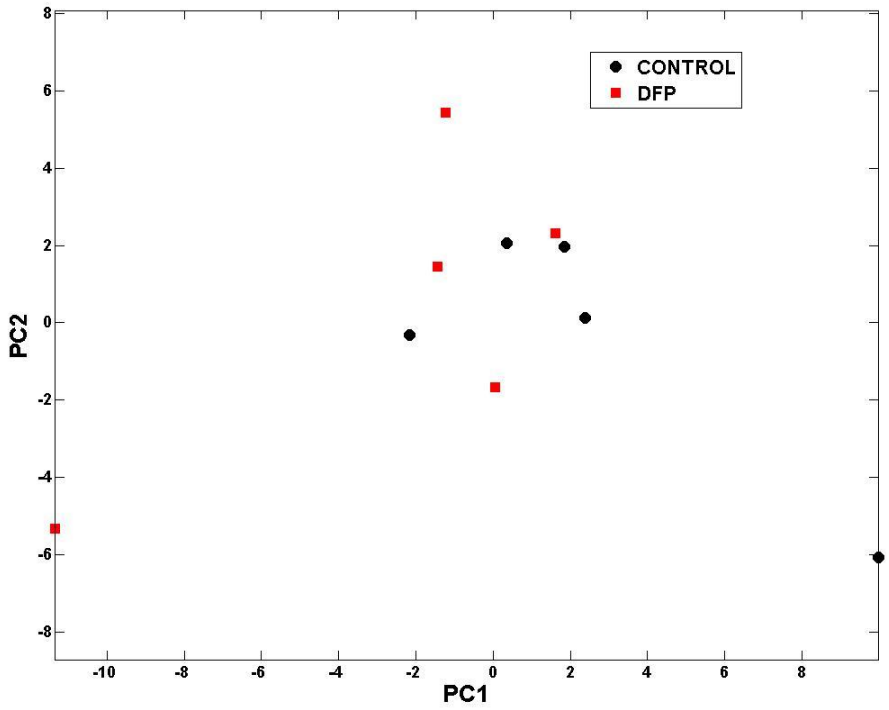

Figure 28. Principal components scores plot (PC1 vs. PC2) of ^{1}H-NMR spectra of aqueous metabolites from brainstem.

Gene expression data at 1 hr post dose did suggest that multiple processes could be occurring early on in the brainstem. As in the cortex, the expression of several genes encoding for proteins associated with synaptic function were down-regulated, including *Rab5a*, *Rab3b* and *stx1a*. Rab5a and Rab3b are specific to synaptic vesicles and synaptosomes and serve to regulate

vesicle transport and exocytosis at the synapse. *Stx1a* encodes for syntaxin, a protein which interacts with SNAP (soluble NSF-attachment proteins) and synaptobrevin proteins to form a macromolecule complex between the membrane of a synaptic vesicle and the synaptic membrane, allowing them to come together and fuse. Down-regulation of the expression of these genes allows the presynaptic neuron to modulate the amount of neurotransmitter being released into the synaptic space, attenuating the postsynaptic hyperstimulation caused by excess ACh.

The brainstem also showed gene expression up-regulation that indicated an early and immediate response to address the DFP insult and associated oxidative stress. The expression of *slc23a1* was up-regulated; in fact, *slc23a1* expression was only detectable after DFP exposure. The protein product of *Slc23a1* is an ascorbate/sodium symporter. Vitamin C, as ascorbate, provides antioxidant defense and reduces oxidized tocopherol (vitamin E), which is highly efficient at protecting against lipid peroxidation. Vitamin E, mainly as α-tocopherol, is critical to brain health, as long term deficiency induces neurological disease (Muller and Goss-Sampson, 1990). However, the concentration of α-tocopherol in the CNS is tightly regulated, and the levels do not change dramatically in short periods of time (Halliwell, 2001). Therefore, ascorbate is essential to reduce oxidized vitamin E. The CNS maintains high concentrations of ascorbate in grey and white matter and in cerebral spinal fluid (Halliwell, 2001). Ascorbate is actively transported by both neurons and glia to increase the intracellular concentration to millimolar levels (Siushansian and Wilson, 1995). Therefore, the up-regulation in the expression of the ascorbate transporter is good indication that the brainstem was responding to an increase in oxidative stress.

It is interesting to note that *aanat* was up-regulated and *arntl* was down-regulated. The protein product of *aanat* is arylalkylamine N-acetyltransferase (AANAT), which is the enzyme that catalyzes the conversion of serotonin to N-acetylserotonin in the synthetic pathway for melatonin. AANAT activity positively correlates to and is an important regulator of melatonin synthesis (Iuvone *et al*., 2005). Circadian clocks are set by melatonin, and Iuvone *et al* (2005)

reported that the rhythmicity of melatonin production is controlled by AANAT activity. The *arntl* gene codes for aryl hydrocarbon receptor nuclear translocator-like protein. The protein arntl forms a heterodimer complex with CLOCK, another circadian rhythm associated protein, to activate downstream genes that drive circadian cycles (Xu *et al*., 2010). The change in expression of these two genes in the brainstem provides the potential to disrupt circadian-controlled mechanisms. In a separate study, adult male rats that were subcutaneously dosed with 0.2 mg/kg/day of DFP showed disturbances in sleep/wake patterns (Deurveilher *et al*, 1999a). The contention of the authors was that changes in sleep patterns correlated directly to the inhibition of AChE. Indeed, as inhibition initially increased, the behavioral patterns worsened. However, while serum cholinesterase activity was inhibited by 70% of control 6 hr after the first dose, in the pontomesencephalic tegmentum, the region of interest for sleep behavior, cholinesterase activity was reduced only 40% after 3 days of DFP dosing, while differences in wakefulness and slow-wave sleep had reached a maximum (Deurveilher *et al*., 1999b). Cholinesterase activity in this region was reduced to as low as 25% of control with no corresponding increase in the changes in wakefulness and slow-wave sleep. This implies the possibility that the behavioral changes in the rats may have been caused by a mechanism other than AChE inhibition. It is possible that the exposure to DFP caused changes in the expression of genes associated with the regulation of circadian cycles within the brainstem, thus inducing a disruption in sleep patterns.

Just as was seen in the cortex, the processes and molecular functions of protein localization and ATP/ribonucleotide binding were down-regulated, potentially creating similar opportunities for neuronal dysfunction that may be manifested at later time points. Early gene expression changes associated with the disruption of protein localization implicate the axonal transport mechanisms. *Kif12*, encoding for a member of the kinesin superfamily of microtubule-based molecular motors, was up-regulated. Kinesin motors aid in the transport of vesicles along

microtubules by hydrolyzing ATP (Dagenbach and Endow, 2004). Increasing the transcription of mRNA for this protein would improve the ability to move vesicles containing newly synthesized proteins to the necessary regions, particularly the synapse. However, the down-regulation of ATP binding functions and utilization of ATP as an energy source would impede the motor function, and thus the ability to transport proteins effectively.

Finally, analysis of the lists of up- and down-regulated genes using GeneSpring software revealed a biological interaction pathway that suggests the exposure to DFP induced an inflammatory response in the brainstem (Fig. 29). Table 15 describes each gene/protein identified in the biological interaction pathway.

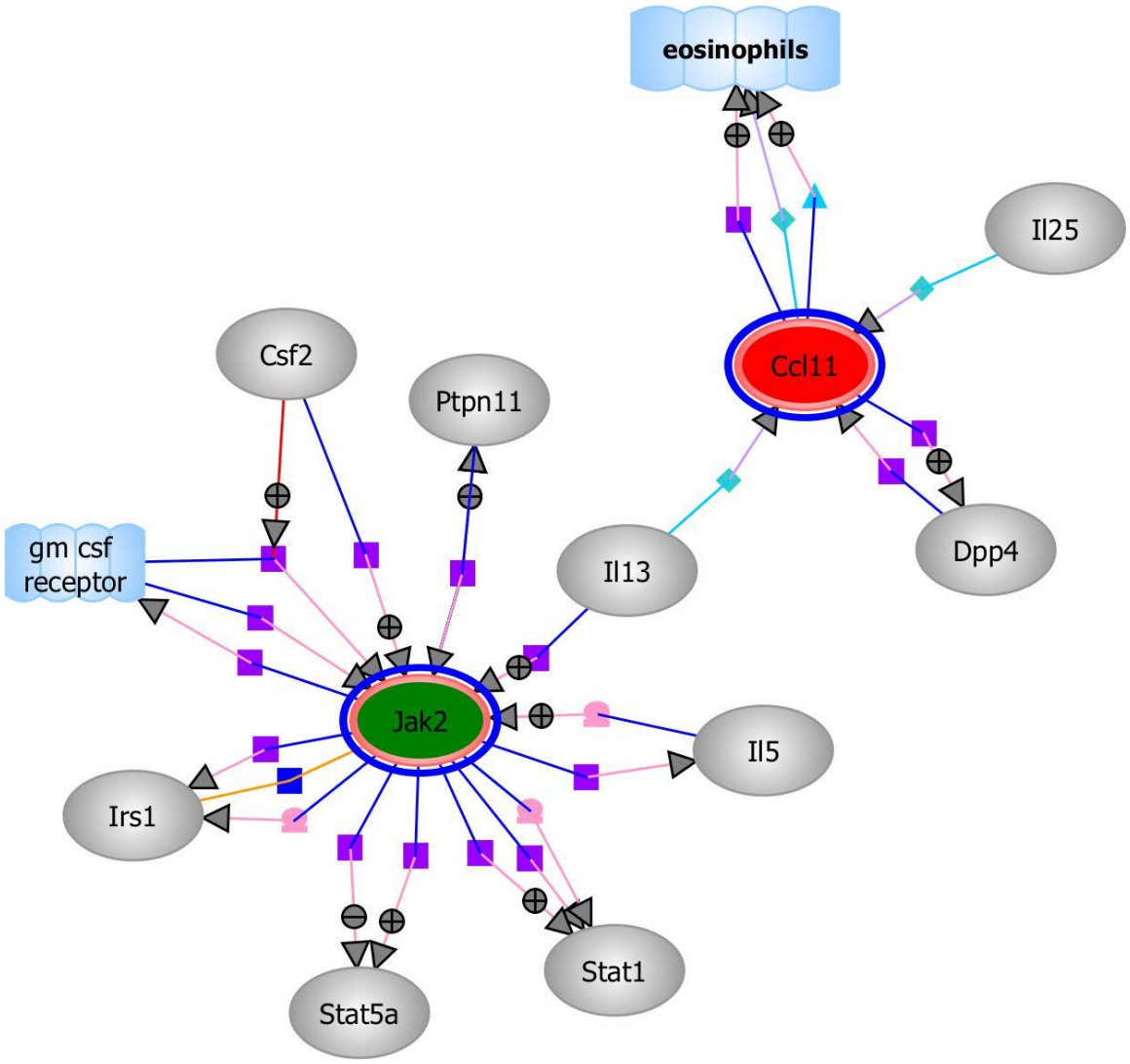

Figure 29. Biological interactions of inflammation pathway-associated gene protein products and functions in the brainstem (GeneSpring). Gene legend: red – up-regulated; green – down-regulated; grey – unchanged. Interaction legend: blue square – binding; purple square – regulation; cyan triangle – transport; cyan diamond – metabolism; pink symbol – protein modification. Connector legend: blue line – regulator; pink line – target; red line – catalyst/modulator; gold line – participant; cyan line – reactant. All genes/proteins are associated with cytosol.

Table 15. List of up- and down-regulated genes in the brainstem and associated protein products.

Gene	PMID #	Name	Description	Function
Ccl11	6356	Chemokine (C-C motif) ligand 11	Cytokine involved in immunoregulation and inflammation, eosinophil-specific	+ regulation/ transport of eosinophils, + regulation of *dpp4*
Jak2	3717	Janus kinase 2	Protein tyrosine kinase involved in cytokine receptor signaling pathways	multiple
Dpp4	1803	Dipeptidyl-peptidase 4	Regulation of T-cell mediated immunity	Regulates *ccl11*
Il25	64806	Interleukin 25	Induce NF-κB activation	Regulates *ccl11*
Il13	3596	Interleukin 13	B-cell maturation/ differentiation	+ regulation of *Jak2*
Il5	3567	Interleukin 5	Colony stimulating factor, eosinophils	+ regulation of *Jak2*, regulated by *Jak2*
Stat1	6772	Signal transducer and activator of transcription 1	Transcription factor, cell viability in response to stimuli and pathogens	Regulated and modified by *Jak2*
Stat5a	6776	Signal transducer and activator of transcription 5a	Response to cytokines, transcription activator, anti-apoptosis	+ and – regulated by *Jak2*
Ptpn11	5781	Protein tyrosine phosphatase, non-receptor type 11	Signaling molecule regulating cell growth and differentiation	Regulates *Jak2*, + and – regulated by *Jak2*
Csf2	1437	Colony stimulating factor 2 (granulocyte-macrophage)	Cytokine that control production, differentiation and function of granulocytes and macrophages	+ regulates *Jak2*
Irs1	3667	Insulin receptor substrate 1	Protein phosphorylated by insulin receptor tyrosine kinase	Binds with *Jak2*

The up-regulated gene, *ccl11*, encodes for C-C motif chemotactic chemokine ligand and is involved in inflammatory and immune responses. This chemokine has chemotactic activity specifically for eosinophils, efficiently recruiting the inflammatory cells to sites of acute inflammation, often leading to a hyper-response (Ishii *et al*, 1998). Up-regulation of *ccl11* was a positive indication of an inflammatory response. The down-regulation of *jak2*, however, suggests a modulatory effect for the immune response. Both *jak2* and *ccl11* either regulate or are regulated by many proteins associated with immune responses involving T-cells, B-cells,

eosinophils, macrophages and cytokine signaling pathways. Changes in the expression of these two genes have the potential to impact a dynamic range of immunological mediators and effectors. A full time course metabolomic study would be an effective way to determine if the gene expression changes translated to a perturbation in the metabolome at a later time point.

4.7 Biological interactions in the cerebellum

The cerebellum had the lowest amount of basal activity of AChE as compared to the other three regions measured. This corresponded to reports that while levels of choline acetyltransferase (ChAT) and expression of nicotinic ACh receptor subunits are high during postnatal cerebellar ontogenesis, immunoreactivity and levels of transcripts for the receptor subunits are much lower in adulthood (De Filippi *et al*., 2005). The conclusion is that the cholinergic system is critical for development of the cerebellum, particularly for neuronal differentiation and migration. However, in adult rats, nearly all lobules of the cerebellum receive cholinergic afferents with higher density of labeling in the vestibulo-cerebellum in the vermis (De Filippi *et al*., 2005). The primary function of nicotinic ACh receptor activation in the cerebellum is to modulate neurotransmitter release, indicating that the cholinergic system has a unique function in the cerebellum beyond simple neuronal communication. The diffuse distribution of cholinergic synapses coupled with a neuromodulatory function could have implications for the cerebellar response to a low level exposure of a cholinergic inhibitor. While the metabolic response at 2 hr post dose was minimal, the transcriptomic response was diverse and unique from the other brain regions investigated.

Few correlative changes were seen in the lipid or small molecule metabolites in the cerebellum. The loss of n3 fatty acids in the cerebellum, however, may mark an oxidative attack on DHA. This may become more evident at later time points, which should be considered for future studies. Gene expression changes seen at 1 hr post dose indicated that there was an early cellular response to oxidative stress. It is worth noting that NAA levels were stable at 2 hr post

dose, indicating that neuronal integrity had not been significantly affected. The increases in alanine and succinate may mark an initial adjustment in glycolysis or the TCA cycle that could be elucidated by investigation of later time points. As seen in the cortex, slight changes in small molecule metabolites at 2 hr were followed by a progression of increased glycolytic perturbation at 48 hr.

The cerebellum had the second most changes in gene expression after the cortex. DFP exposure had an effect on diverse biological processes in the cerebellum. Similar to the cortex, apoptotic pathways were down-regulated, while anti-apoptotic pathways were up-regulated. As anticipated, the cellular response was protection and repair, not self-destruction, as the injury induced by the low level exposure should have been survivable. The neuromodulatory nature of cholinergic transmission in the cerebellum may have further attenuated the extent of injury caused by AChE inhibition. Indeed, the extent of depression of gene expression associated with synaptic transmission was not seen in the cerebellum, unlike the cortex and the brainstem. This mode of protection and repair was also reflected in the down-regulation of processes associated with protein degradation, minimizing catabolic pathways and preserving cellular integrity.

In spite of protein catabolic processes being down-regulated, it appeared that protein synthesis was negatively impacted. Several transcription-related processes were up-regulated but translation was down-regulated, particularly ribosomal biogenesis. Impairment of the protein synthetic machinery would impede the cell's ability to repair cellular damage, as well as restore functional AChE to the synapse, delaying the return to homeostasis.

It is unclear if the down-regulation of DNA repair processes was a result of cellular injury or a cellular response of protection. No conclusive evidence exists that definitively supports OP-induced DNA damage, although the OP pesticide phorate was shown to cause DNA breaks in the sentinel fish species rohu (Mohanty *et al*, 2011). DFP has not been reported to

cause DNA damage. It seems possible that down-regulation of DNA repair was a cellular response of protection, possibly to conserve sources of energy for the restoration of cellular homeostasis. A low level exposure of the nerve agent GB (similar in structure to DFP) in rat hepatocytes also caused a down-regulation of DNA repair that was unrelated to cell death (Klein *et al*, 1987). However, in a study with the same agent, the hippocampus showed up-regulation of DNA repair processes 6 hr post low level treatment (Dr. Victor Chan, personal communication). Therefore, it is unclear if these OPs, at low level, are either inhibiting DNA repair or, possibly, protecting DNA from damage. It is also impossible to determine if the DNA repair is for nuclear DNA, mitochondrial DNA or both. Most DNA repair processes are shared by both mitochondrial and nuclear DNA, with the exception of nucleotide excision repair which is specific to nuclear DNA (Larsen et al, 2005). Differential gene expression data do not indicate the exact pathways of DNA repair that were down-regulated. What is clear, however, is that the expression of processes that are both pro and anti-cell survival have been altered, and these processes are likely competing with each other, prolonging the disruption in the neuronal environment and hindering the return to homeostasis. Additional metabolomic studies should include later time points to determine if the cellular phenotype continues to reflect a progression of metabolic disruption.

Despite the lack of any measureable increases in the lipid peroxidation marker MDA, gene expression data suggested that the cerebellum was responding to an early detection of oxidative stress. From the DAVID database search, response to reactive oxygen species was an up-regulated process and included the genes *dusp*, *fos*, and *hdac6* (dual specificity phosphatase, FBJ osteosarcoma oncogene and histone deacetylase 6). Response to oxidative stress was also up-regulated and included the same genes, as well as *mpo* (myeloperoxidase), which is located in the mitochondrion. Interestingly, the mitochondrion was identified as a down-regulated cellular component with some specificity for the inner membrane. Changes in expression of genes associated with the inner mitochondrial membrane include key components of the mitochondrial

electron transport chain (Table 16). A*tp5f1* and *atp5c1* encode for the membrane proton channel linked to the F1 complex by central and peripheral stalks and the extramembranous catalytic core (F1 complex) of the ATP synthase complex, respectively. The protein product of *cox4i2* (cytochrome c oxidase) is the terminal oxidase in the electron transport chain, while *surf1* proteins are involved in the biogenesis of the cytochrome c oxidase complex. The gene for the acylcarnitine transporter (*slc25a20*) was also down-regulated. Acylcarnitines of various lengths are transported across the inner mitochondrial membrane from the cytosol to the mitochondrial matrix via this transporter for fatty acid oxidation. A down-regulation in the expression of these genes indicates a loss of critical energy-producing capabilities. The up-regulation of myeloperoxidase and the down-regulation of energy producing pathways make the cerebellar mitochondria a clear target of the exposure to DFP. Future studies should include a temporal investigation of the metabolic profiles of this region, particularly those metabolites associated with mitochondrial function, including TCA cycle metabolites and the phospholipid cardiolipin. Future studies should also include *in vitro* metabolic measurements of basal oxygen consumption and glycolytic rates, as well as metabolic respiration and ATP usage in order to assess any mitochondrial damage.

Table 16. Functional annotation clustering of inner mitochondrial membrane associated genes down-regulated in the cerebellum.

Affymetrix Exon Gene ID	Entrez Gene ID	Official Gene Symbol	ID	GENE NAME
7212517	171375	Atp5f1	ATP synthase, H+ transporting, mitochondrial F0 complex, subunit B1	ATP synthase, H+ transporting, mitochondrial F0 complex, subunit B1
7159732	116550	Atp5c1	ATP synthase, H+ transporting, mitochondrial F1 complex, gamma polypeptide 1	ATP synthase, H+ transporting, mitochondrial F1 complex, gamma polypeptide 1
7233997	84683	Cox4i2	cytochrome c oxidase subunit IV isoform 2	cytochrome c oxidase subunit IV isoform 2
7340393	117035	Slc25a20	solute carrier family 25 (carnitine/acylcarnitine translocase), member 20	solute carrier family 25 (carnitine/acylcarnitine translocase), member 20
7237053	619346	Surf1	surfeit 1; surfeit 4	surfeit 1; surfeit 4

Finally, it is worth noting the increase in expression of two specific genes that may have significance in the cerebellum: *tnfrsf4* and *npas4*. The protein encoded by t*nfrsf4* is a member of the superfamily of tumor necrosis factor receptors, integral to the plasma membrane. The receptor ligand, TNF-α, is a pro-inflammatory cytokine that is released by microglia primarily in response to brain injury such as ischemia, trauma and excitotoxicity (Raivich *et al*., 1999). Injured neurons have been shown to up-regulate receptors for TNF-α (Knott *et al*, 2000). However, TNF-α may be a driver of neuroinflammation and contribute to the pathology of neurological diseases. TNF-α alone was able to promote motor neuron death *in vitro* (He *et al*., 2002), and induction of apoptosis by TNF-α related ligands has been shown to be involved in both HIV-1 dementia and Alzheimer's disease (Huang *et al*., 2005). Up-regulation of receptors for TNF-α at 1 hr post exposure was a neuroprotective response that has the potential to contribute to long term neuronal dysfunction.

Npas4 (neuronal PAS domain protein 4) is a brain-specific transcription factor complex localized in the nucleus. It has been hypothesized that this protein serves as an "on demand" neuroprotectant in response to neurodegenerative stimuli (Ooe *et al*., 2009). These authors describe the effects of multiple neuronal stress inducers and have shown that kainate-induced glutamate excitotoxicity was fatal for npas4 knockout mice but not for wild type littermates. As previously stated, activation of NMDA glutamate receptors plays a key role in the neuropathology associated with acute OP exposure (McDonough and Shih, 1997). Additionally, expression of npas4 was up-regulated in mouse hippocampal cells that survived transient global ischemia (as a stroke model), while the nearby dying cells had little expression of the protein. Npas4 has also been reported to regulate the expression of genes that control the quantity of GABAergic synapses in order to modulate the activity of excitatory neurons (Lin *et al*, 2008). Up-regulation of this gene in the cerebellum was good indication that neuroprotective pathways were being activated. Ooe *et al* (2009) proposed a hypothetical model of the neuroprotective response of npas4 that included downstream regulation of expression of stress-inducible enzymes, including glutathione peroxidase, X-box binding protein and heat shock protein 5 as potential target genes. While none of these genes showed a change in expression at 1 hr, these are notable targets for investigation at later time points.

4.8 Biological interactions in the hippocampus

The hippocampus is a subcortical structure that is associated with mechanisms of learning and memory, specifically spatial memory and the consolidation of short to long term memory. Numerous studies have reported that OP exposure creates deficits in behavior and cognition, indicating that the hippocampus is affected by OPs. Cholinergic projections to the hippocampus come primarily from the medial septum by way of the fimbria-fornix (Alonso and Amaral, 1995; Placzek *et al*., 2009; Yoshida and Oka, 1995), and both nicotinic and muscarinic receptors are expressed throughout the hippocampus (Grybko *et al*., 2010; Jerusalinsky *et al*., 1997; Placzek *et*

al, 2009). ACh is considered to be involved in a variety of cognitive functions, and antagonists for both receptors diminish long term potentiation and cause deficits in learning and memory (Jerusalinsky *et al*., 1997; Tai and Leung, 2012). Given the wide distribution of ACh receptors and importance of cholinergic innervation in the hippocampus, it is not surprising that exposure to an OP, a cholinergic disruptor, would cause a deficit in the cognitive functions of this brain region.

In terms of AChE, the hippocampus had levels of basal enzyme activity similar to the cortex, being significantly greater than the cerebellum and less than the brainstem (Fig. 12). This level of activity corresponds to literature reports of the distribution of cholinergic synapses in the hippocampus. AChE activity reached a maximum inhibition of 55% of control at 2 hr post exposure, a moderate loss of enzyme function that would not be cholinergically toxic but certainly cause sustainment of ACh in the synaptic space and hyperexcitation of postsynaptic receptors. However, unlike the cortex and brainstem, gene expression data demonstrated little to no down-regulation of synaptic functions as a means to attenuate excess postsynaptic stimulation. Because ACh receptor activity is linked to cognitive functions in the hippocampus, excess receptor binding may not cause an immediate neuromodulatory response. In fact, pharmaceuticals used for the treatment of Alzheimer's disease and dementia are often anticholinergic compounds (Howard *et al*., 2012). However, persistent ACh in the synapse will eventually upset the homeostatic regulation of the neuronal environment. It is possible that synaptic functions would be altered at a later time point. The expression of *rab3b* was down-regulated at 1 hr, indicating that a cellular response to decrease the synaptic docking function may have been initiated, and further transcriptomic changes associated with the synapse could occur after the 1 hr time point.

An unexpected gene expression change was the down-regulation of the Wnt signaling pathway (Fig. 30). This pathway has long been known to play a key role in neuronal development in the CNS. However, Wnt has been shown to be active in adult hippocampal

dentate gyrus (Garbe and Ring, 2012; Lie *et al*., 2005), possibly playing a role in cognitive functions associated with the hippocampus. Considering the number of reports of cognitive deficits occurring after exposure to OPs, it is quite conceivable that down-regulation of neurogenesis is part of the mechanistic basis of the deficits. Five genes associated with the Wnt signaling pathway were down-regulated. *Sfrp4* encodes for a cysteine-rich domain that is the putative binding site of Frizzled proteins and is considered to be a modulator of Wnt signaling. The protein product of *dvl1* is a cytoplasmic phosphoprotein that is directly downstream of frizzled receptors. *Ctnnbip1* is encoded to a protein that binds catenin and prevents interaction with a specific family of transcription factors, negatively regulating the Wnt signaling pathway (Daniels and Weis, 2002). The protein product of *ctbp1* is a transcriptional repressor (PubMed Gene ID 1488). Finally, *camk2d* is part of the Wnt/Ca^{2+} signaling pathway. Down-regulation of the expression of these genes hints at a modulatory effect on the pathway. Just as with the potential involvement of the mTOR pathway in the cortex, neurogenesis would be an energy-demanding process at a time when cellular functions are focused on returning to homeostasis. Therefore, down-regulation of the Wnt pathway appears to promote this goal. Future studies should include time course investigation of components of this pathway to determine if the perturbation in the signaling cascade progresses or subsides.

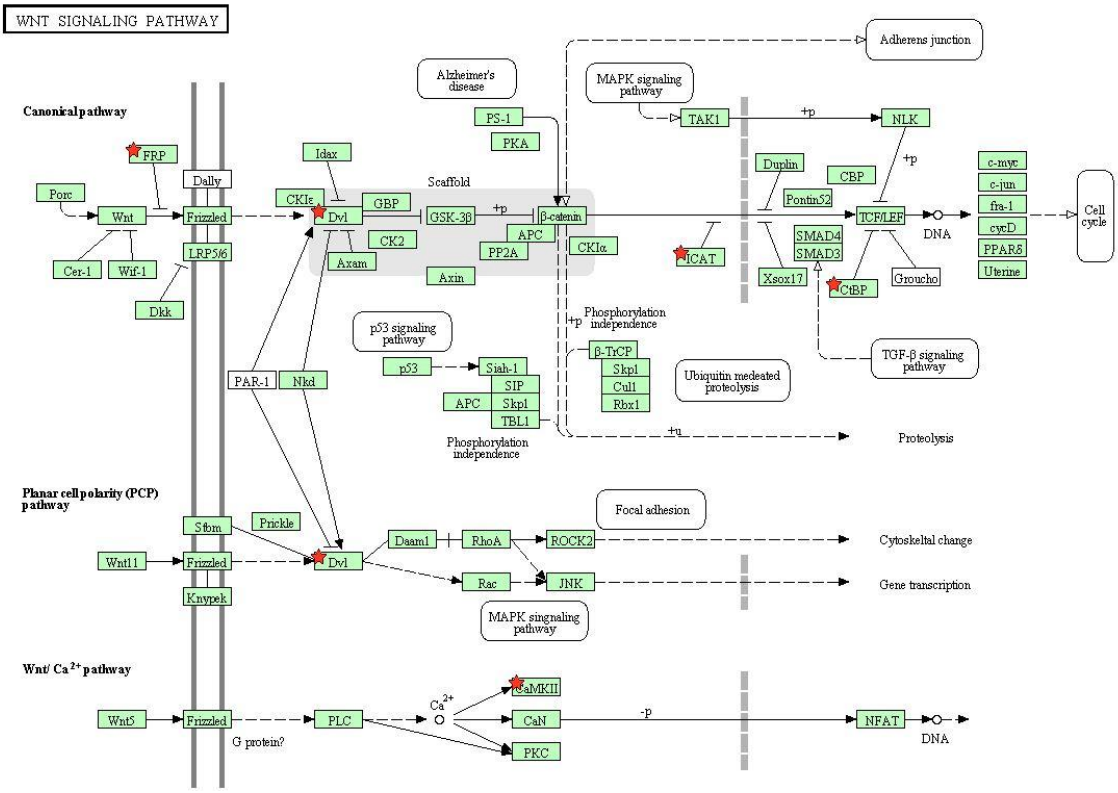

Figure 30. KEGG schematic for the Wnt Signaling pathway. Red stars mark genes that were down-regulated 1 hr after 1 mg/kg DFP exposure. Gene symbol identifications: *sfrp4* (FRP) – secreted frizzled-related protein 4; *dvl1* – disheveled, dsh homolog 1; *ctnnbip1* (ICAT) – catenin, beta interacting protein 1; *camk2d* (CAMKII) – calcium/calmodulin-dependent protein kinase II delta; *ctbp2* (loc685847, CtBP) – c-terminal binding protein 2.

The I-kappaB kinase/NF-kappaB cascade was also down-regulated in the hippocampus. Activation of the I-kappaB kinase (interferon-kappaB kinase, IKK) complex triggers phosphorylation events that release an inhibitory protein that complexes with NF-κB (nuclear factor kappa light chain enhancer of activated B cells) and localizes it in the cytosol. Release of the protein allows the NF-κB dimer to translocate to the nucleus where it binds DNA response elements to induce expression of proteins associated with immune and pro-inflammatory responses. Inducers of NF-κB include ROS and TNF-α (Chandel *et al*., 2000). Activation of NF-κB transcription factors is caused by nearly all receptors of the innate and adaptive immune system (Ruland, 2011). Because it is important for the effects of this cascade to be transient, modulation and termination of the cascade are as important for the cell as the initial activation. Uncontrolled activity of NF-κB can lead to inflammation and tumor development (Ruland, 2011). Therefore, negative regulation of the pathway is essential for normal cell maintenance. The expression of three genes from this cascade was affected: *traf2*, *irak1bp1* and *nfkbib*. The Traf2 protein is part of the canonical NF-κB pathway activated by TNF. Upon TNF receptor activation, traf2, among other proteins, is recruited to the receptor in order to induce recruitment of IKK. *Irak1bp1* encodes for a protein within the cascade initiated by activation of toll-like receptor 4. Irak proteins act as IKK complex stabilizers. Finally, the protein product of *nfkbib* inhibits NF-κB and traps it in the cytoplasm. So, interestingly, down-regulation of nfkbib would actually increase the activity of transcription factors in the nucleus. It seems evident that down-regulation of the expression of these genes serves to modulate the activity of the entire cascade in order to attenuate the effect, address the low level insult that certainly would have activated the pathway and still return to homeostasis.

The hippocampus showed a number of changes in metabolites linked to glycolysis and the TCA cycle at 2 hr post dose (Fig. 31). The decrease in succinate and increase in fumarate may indicate a shift in the equilibrium between the two metabolites towards fumarate. Cis-aconitate, the intermediate formed from the 2-step conversion of citrate to isocitrate was also

increased. Unfortunately, it was not possible to detect citrate or iso-citrate in the NMR spectra. However, cis-aconitate is in equilibrium with citrate and should reflect levels of this metabolite. Similar to the cortex, the two BCAAs, valine and isoleucine, were increased after DFP exposure. As essential amino acids, the increase in valine and isoleucine must be caused by decreased metabolism. As previously stated, both valine and isoleucine can serve an anaplerotic function to the TCA cycle at the point of succinyl-CoA (Murin *et al*., 2009a,b). Impairment of BCAA metabolism potentially reduces this point of entry into the TCA cycle. If decreased metabolism of valine and isoleucine was reducing a source of succinyl CoA, this may explain the decrease in succinate. However, it seems unlikely that fumarate would be increased following a decrease in succinate caused by loss of anaplerotic functions. Finally, the amino acid alanine is in equilibrium with pyruvate, catalyzed by aminotransferase. An increase in alanine, which is an important glucogenic amino acid, would disrupt the equilibrium with pyruvate which, unfortunately, we were unable to measure from the NMR spectrum. However, if the increase in alanine was independent of any change in pyruvate, the equilibrium reaction could be shifted towards pyruvate, once again disrupting the TCA cycle and the glycolytic energy production pathway in the hippocampus. Overall, it appears that the hippocampal cells were increasing glucose metabolism in order to meet higher energy demands. Just as with the brainstem and cerebellum, future studies should investigate later time points to determine if the metabolic perturbation persists or even progresses, as seen in the cortex. Indeed, several studies with individuals exposed to low levels of nerve agents have reported deficits in learning and memory that still manifest long after the initial exposure (Proctor *et al*., 2006; Yanagisawa *et al*., 2006; Yokoyama *et al*., 1998), suggesting that long term disruption in the hippocampus has occurred. It is important to note that the lipid profile did not change at 2 hr post DFP exposure. At later time points, the lipid metabolites may provide additional information to determine the mechanistic basis of neuronal dysfunction in the hippocampus.

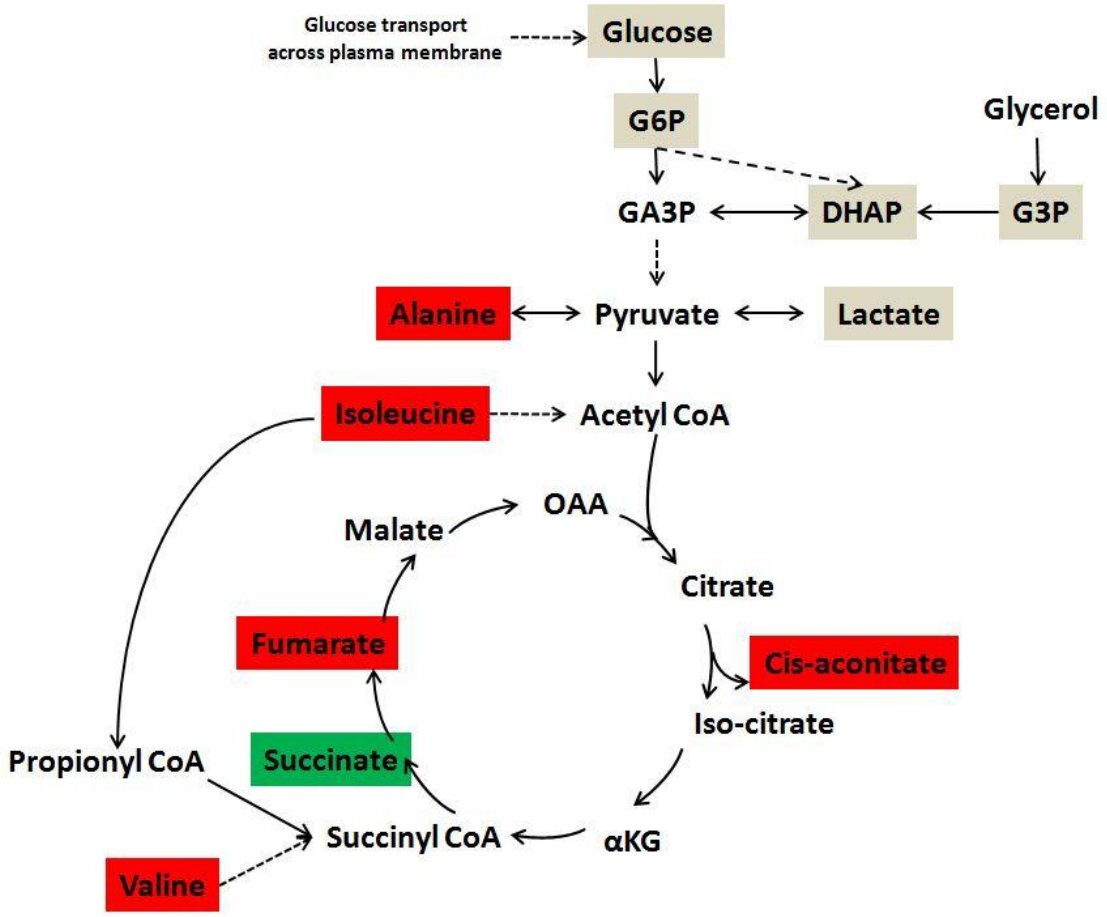

Figure 31. Schematic representation of glycolytic pathway and TCA cycle, showing changes in small molecule metabolites in the hippocampus at 2 hr post DFP exposure. Increases in measured metabolites are shaded red and decreases are shaded green. Metabolites that were measured from the NMR spectra but did not change after DFP exposure are shaded grey. Unshaded metabolites were not measured. Abbreviations: G6P – glucose-6-phosphate; GA3P – glyceraldehyde-3-phosphate; DHAP – dihydroxyacetone phosphate; G3P – glycerol-3-phosphate; OAA – oxaloacetate; αKG – α-ketoglutarate.

4.9 Summary

While many studies have shown diverse effects of low level exposure to OPs, little is understood about the mechanistic basis of the off-target toxicity of this class of compounds. This study was an initial attempt to characterize the effects of non-cholinergic toxicity of a model OP, DFP. The –omic approach was selected in order to provide a global view of the changes occurring in each brain region investigated, giving a snapshot in time of the early metabolic and gene expression changes. Integration of transcriptomic and metabolomic data is challenging, at

best, and a full time-course study would improve the ability to link differential gene expression with altered metabolic phenotypes. However, by focusing on initial cellular responses to insult we have shown that a low dose of DFP induced early changes in metabolite and gene expression profiles that indicated a response of protection and repair of the neuronal environment.

One of the most interesting findings of this research effort was the uniqueness of response from each of the four brain regions investigated. Table 17 summarizes the significant effects for both gene expression and metabolite results. Some of the regions showed similarities in the biological interactions, such as the down-regulation of apoptotic pathways in both the cortex and cerebellum and the decrease in gene expression associated with synaptic function in the cortex and brainstem. Additionally, a depression in gene expression related to protein movement, folding and synthesis was seen in the cortex, brainstem and the cerebellum. The cortex and hippocampus had metabolic phenotypes that suggested a perturbation in energy metabolism. However, each region had many differences in gene expression and metabolic profile changes that reflected the distinct structure, chemistry and function of each region. Indeed, PCA of the ^{1}H spectra, the full profile of the very compounds carrying out the biochemical reactions of the cell, revealed complete separation of each region in PC space. This was compelling evidence regarding the importance of examining the brain as many subsystems, rather than as a whole. In the search for better neuroprotectants, it is vital to consider the unique sensitivity of each brain region to OP insult.

While the apparent response of each brain region was to protect and repair the neuronal environment from the low level DFP exposure, evidence also exists for the potential for dysregulation. In particular, the cortex showed down-regulation of processes to minimize damage and reduce excitotoxicity. In spite of this there was some indication of neuronal distress at 2 hr manifested by changes in the lipid and phospholipid profile, followed by a perturbation in glycolysis at a later time point. In the CNS, where the demand for energy is high, a disruption in

energy producing pathways has the potential to prolong recovery efforts and lead to sustained damage. Increases in gene expression of prostaglandin synthesis linked with loss of phospholipid metabolites also suggests a response that may go from neuroprotective to neurotoxic, with the possibility of leading to long term dysfunction. These metabolomic and transcriptomic approaches can increase the knowledge base and improve understanding of the mechanistic basis of adverse effects of low level DFP exposure, providing targets for novel therapeutics for neuroprotection.

Table 17. Summary of gene expression and metabolic effects in cortex, brainstem, cerebellum and hippocampus after 1 mg/kg DFP exposure.

Brain region	Gene Effects	Metabolite Effects[a]
CX	Apoptosis ↓ Synaptic function ↓ RIM binding proteins ↓ Glutamate receptor ↓ Protein transport ↓ ATP binding ↓ GLUT3 (neuronal)↓ LDH (astrocyte) ↓ MCT1 (astrocyte, BBB) ↓ MCT2 (neuronal) ↓ Ptgds ↑	NAA: 2 hr ↓ 48 hr normal All lipids except PA, CL ↓ Phosphocholine ↓ Glucose, G6P, G3P, DHAP ↓ BCAA ↑
BS	Ascorbate transport ↑ Protein localization ↓ Exocytosis ↓ ATP binding ↓	CL ↓
CB	Phosphatase activity ↓ ATPase activity ↓ DNA repair ↓ Ribosome synthesis ↓ Anti-apoptosis ↑ Response to oxidative stress ↑ Myeloperoxidase ↑ Mitochondrial function ↓ Npas4 (neuroprotection) ↑	PtdI ↓ n3 FA ↓ Alanine ↑ Succinate ↑
HP	Wnt signaling pathway ↓ I-κB kinase/NF-κB pathway ↓	BCAA ↑ Alanine ↑ Cis-aconitate ↑ Fumarate ↑ Nicotinate ↑ Succinate ↓ GABA ↓

[a]Metabolite effects are at 2 hr unless otherwise noted.

V. REFERENCES

Alonso, JR, Amaral, DG. Cholinergic innervation of the primate hippocampal formation. I. Distribution of choline acetyltransferase immunoreactivity in the Macaca fascicularis and Macaca mulatta monkeys. J Compar Neurol 1995;355:135-70.

Anderson, P.E., Mahle, D.A., Doom, T.E., Reo, N.V., DelRaso, N.J. and Raymer, M.L. Dynamic adaptive binning: an improved quantification technique for NMR spectroscopic data. Metabolomics 2010;7(2):179-90.

Anthony, ML, Sweatman, BC, Beddell, CR, Lindon, JC, Nicholson, JK. Pattern recognition classification of the site of nephrotoxicity based on metabolic data derived from proton nuclear magnetic resonance spectra of urine. Mol Pharmacol 1994;46:199-211.

Bagchi, D., Bagchi, M., Hassou, E.A. and Stohs, S.J. In vitro and in vivo generation of reactive oxygen species, DNA damage and lactate dehydrogenase by selected pesticides. Toxicology 1995;104:129-40.

Bazan, NG, Molina, MF, Gordon, WC. Docosahexaenoic acid signalolipidomics in nutrition: Significance in aging, neuroinflammation, macular degeneration, Alzheimer's, and other neurodegenerative diseases. Anuu Rev Nutr 2011;31:321-351.

Betancourt, A.M., Burgess, S.C. and Carr, R.L. Effect of developmental exposure to chlorpyrifos on the expression of neurotrophin growth factors and cell-specific markers in neonatal rat brain. Toxicol Sci 2006;92(2):500-6.

Bevilacqua, VLH, D'Onofrio, TG, Jakubowski, EM, Hulet, SW, Maguire, KJ, Edwards, JL, Laramee, JA, Brickhouse, MD. Metabonomics of pig blood plasma following whole body exposure to low levels of GB vapor. 2005. Edgewood Chemical Biological Center, Aberdeen Proving Ground, MD. ADA448901.

Blusztajn, JK, Hollbrook, PG, Lakher, M, Liscovitch, M, Maire, JC, Mauron, C, Richardson, UI, Tacconi, M, Wurtman, RJ. "Autocannibalism" of membrane choline-phospholipids: physiology and pathology. Psychopharmacology Bull 1986;22(3):781-6.

Brosche, T, Platt, D. The biological significance of plasmalogens in defense against oxidative damage. Exp Gerontol 1998;33(5):363-369.

Cansev, M, Wurtman, RJ, Sakamoto, T, Ulus, IH. Oral administration of circulating precursors for membrane phosphatides can promote the synthesis of new brain synapses. Alzheimers Dement 2008;4(1):s153-s168.

Chambers, J.E. and Oppenheimer, S.F. Organophosphates, serine esterase inhibition, and modeling of organophosphate toxicity. Toxicol Sci 2004;77(2):185-7.

Chandel, NS, Trzyna, WC, McClintock, DS, Schumacker, PT. Role of oxidants in NF-kappa B activation and TNF-alpha gene transcription induced by hypoxia and endotoxin. J Immunol 2000;165(2):1013-1021.

Chapman, S, Kadar, T, Gilat, E. Seizure duration following sarin exposure affects neuro-inflammatory markers in the rat brain. Neurotoxicology 2006;27:277-83.

Chippendale, TJ, Cotman, CW, Kozar, MD, Lynch, GS. Analysis of acetylcholinesterase and transport in the rat hippocampus: recovery of acethylcholinesterase activity in the septum and hippocampus after administration of diisopropylfluorophosphate. Brain Res 1974;81:485-96.

Dagenbach, EM, Endow, SA. A new kinesin tree. J Cell Sci 2004;117(1):3-7.

Damodaran, TV, Patel, A, Greenfield, ST, Dressman, HK, Lin, SK, Abou-Donia, MB. Gene expression profiles of the rat brain both immediately and 3 months following acute sarin exposure. Biochem Pharmacol 2006a;71:497-520

Damodaran, TV, Greenfield, ST, Patel, A, Dressman, HK, Lin, SK, Abou-Donia, MB. Toxicogenomic studies of the rat brain at an early time point following acute sarin exposure. Neurochem Res 2006b;31:367-81.

Daniels, DL, Weis, WI. ICAT inhibits beta-catenin binding to Tcf/Lef-family transcription factors and the general coactivator p300 using independent structural modules. Mol Cell 2002;10(3):573-84.

De Filippi, G, Baldwinson, T, Sher, E. Nicotininc receptor modulation of neurotransmitter release in the cerebellum. Prog Brain Res 2005;148:307-20.

De Stephano, N, Matthews, PM, Arnold, DL. Reversible decreases in N-acetylaspartate after acute brain injury. Magn Reson Med 1995;34(5):721-7.

Dennis Jr, G, Sherman, BT, Hosack, DA, Yang, J, Gao, W, Lane, HC, Lempicki, RA. DAVID: Database for Annotation, Visualization, and Integrated Discovery. Genome Biol 2003;4(5):3.

Deurveilher, S, Hars, B, Hennevin, E. Chronic, low-level exposure to the cholinesterase inhibitor DFP. II. Time course of behavioral state changes in rats. Pharm Biochem Behav 1999a;64(1):105-14.

Deurveilher, S, Delamanche, IS, Hars, B, Breton, P, Hennevin, E. Chronic, low-level exposure to the cholinesterase inhibitor DFP. I. Time course of neurochemical changes in the rat pontomesencephalic tegmentum. Pharm Biochem Behav 1999b;64(1):95-103.

Dhote, F, Peinnequin, A, Carpentier, P, Baille, V, Delacour, C, Foquin, A, Lallement, G, Dorandeu, F. Prolonged inflammatory gene response following soman-induced seizures in mice. Toxicology 2007;238:166-76.

Dienel, GA, Cruz, NF. Neighborly interactions of metabolically-actived astrocytes in vivo. Neurochem Int 2003;43(4-5):339-54.

Ellman, GL, Courtney, KD, Andres Jr, V, Feather-Stone, RM. A new and rapid colorimetric determination of acetylcholinesterase activity. Biochem Pharmacol 1961;7:88-95.

Emerit, J, Edeas, M, Bricaire, F. Neurodegenerative diseases and oxidative stress. Biomed Pharmacother 2004;58:39-46.

Engelmann, B, Brautigam, C, Thiery, J. Plasmalogen phospholipids as potential protectors against lipid peroxidation of low density lipoproteins. Biochem Biophys Res Commun 1994;204(3):1235-1242.

Forgacs, AL, Kent, MN, Makley, MK, Mets, B, DelRaso, N, Jahns, GL, Burgoon, LD, Zacharewski, TR, Reo, NV. Comparative metabolomic and genomic analyses of TCDD-elicited metabolic disruption in mouse and rat liver. Toxicol Sci 2012;125(1):41-55.

Garbe, DS, Ring, RH. Investigating tonic Wnt signaling throughout the adult CNS and in the hippocampal neurogenic niche of BatGal and Ins-TopGal mice. Cell Mol Neurobiol epub ahead of print 2012; DOI 10.1007/s10571-012-9841-3.

Garcia, GE, Campbell, AJ, Olson, J, Moorad-Doctor, D, Morthole, VI. Novel oximes as blood-brain barrier penetrating cholinesterase reactivators. Chem-Biol Interact 2010;187:199-206.

Gearhart, JM, Jepson, GW, Clewell III, HJ, Andersen, ME, Conolly, RB. Physiologically based pharmacokinetic and pharmacodynamic model for the inhibition of acetylcholinesterase by diisopropylfluorophosphate. Toxicol Appl Pharmacol 1990;106:295-310.

Genovese, RF, Benton, BJ, Shippee, SJ, Jakubowski, EM, Bonnell, JC. Effects of low-level inhalation exposure to cyclosarin on learned behaviors in Sprague-Dawley rats. J. Toxicol Enviro Health, Part A 2006;69: 2167-80.

Gentleman, R, Carey, V, Huber, W, Irizarry, R, Dudoit, S. Bioinformatics and Computational Biology Solutions Using R and Bioconductor. 1st ed. New York: Springer-Verlag; 2005.

Glantz, S. Primer of Bio-Statistics. 4th ed. New York: McGraw Hill, Inc; 1996.

Grybko, M, Sharma, G, Vijayaraghavan, S. Functional distribution of nicotinic receptors in CA3 regions of the hippocampus. J Mol Neurosci 2010;40(1-2):114-20.

Hahnel, D, Beyer, K, Engelmann, B. Inhibition of peroxyl radical-mediated lipid oxidation by plasmalogen phospholipids and α-tocopherol. Free Radical Biol Med 1999;27(9-10):1087-1094.

Haley, RW. Excess incidence of ALS in young Gulf War veterans. Neurology 2003;61:750-6.

Halliday, KR, Fenoglio-Preiser, C, Sillerud, LO. Differentiation of human tumors from nonmalignant tissue by natural-abundance 13C NMR spectroscopy. Magn Reson Med 1988;7:384-411.

Halliwell, B. Oxidative stress and neurodegeneration: Where are we now? J Neurochem 2006;97:1634-58.

Halliwell, B. Role of free radicals in the neurodegenerative diseases: therapeutic implications for antioxidant treatment. Drugs Aging 2001;18(9):685-716.

Halliwell, B, Whiteman, M. Measuring reactive species and oxidative damage *in vivo* and in cell culture: how should you do it and what do the results mean? Br J Pharm 2004;142:231-55.

He, BP, Wen, W, Strong, MJ. Activated microglia (BV-2) facilitation of TNF-α-mediated motor neuron death in vitro. J Neuroimmunol 2002;128:31-8.

Holm, S. A simple sequentially rejective bonferroni test procedure. Scand J Stat 1979;6:65-70.

Holmes, E, Nicholl, AW, Lindon, JC, Ramos, S, Spraul, M, Neidig, P, Connor, SC, Connelly, J, Damment, SJ, Haselden, J, Nicholson, JK. Development of a model for classification of toxin-induced lesions using 1H NMR spectroscopy of urine combined with pattern recognition. NMR in Biomed 1998a;11:235-244.

Holmes, E, Nicholson, JK, Bonner, FW, Sweatman, BC, Beddell, CR, Lindon, JC. Mapping the biochemical trajectory of nephrotoxicity by pattern recognition of NMR urinalysis. NMR in Biomed 1992;5:372-386.

Holmes, E, Nicholson, JK, Nicholl, AW, Lindon, JC, Connor, SC, Polley, S, Connelly, J. The identification of novel biomarkers of renal toxicity using automatic data reduction techniques and PCA of proton NMR spectra of urine. Chemometrics and Intelligent Laboratory Systems 1998b;44(1-2):245-255.

Horner, RD, Kamins, KG, Feussner, JR, Grambow, SC, Hoff-Lindquist, J, Harati, Y, Mitsumoto, H, Pascuzzi, R, Spencer, PS, Tim, R, Howard, D, Smith, TC, Ryan, MAK, Coffman, CJ, Kasarskis, EJ. Occurrence of amyotrophic lateral sclerosis among Gulf War veterans. Neurology 2003;61:742-9.

Howard, R, McShane, R, Lindesay, J, Ritchie, C, Baldwin, A, Barber, R, Burns, A, Dening, T, Findlay, D, Holmes, C, Hughes, A, Jacoby, R, Jones, R, Jones, R, McKeith, I, Macharouthu, A, O'Brien, J, Passmore, P, Sheehan, B, Juszczak, E, Katona, C, Hills, R, Knapp, M, Ballard, C, Brown, R, Banerjee, S, Onions, C, Griffin, M, Adams, J, Gray, R, Johnson, T, Bentham, P, Phillips, P. Donepezil and memantine for moderate-to-severe Alzheimer's disease. N Engl J Med 2012;366(10):893-903.

Huang, DW, Sherman, BT, Lempicki, RA. Systematic and integrative analysis of large gene lists using DAVID Bioinformatics Resources. Nature Protoc 2009a;4(1):44-57.

Huang, DW, Sherman, BT, Lempicki, RA. Bioinformatic enrichment tools: paths toward the comprehensive functional analysis of large gene lists. Nucleic Acids Res 2009b;37(1):1-13.

Huang, Y, Erdmann, N, Peng, H, Zhao, Y, Zheng, J. The role of TNF related apoptsis-inducing ligand in neurodegenerative diseases. Cell Mol Immunol 2005;2(2):113-22.

Irizarry, RA, Hobbs, B, Collin, F, Beazer-Barclay, YD, Antonellis, KJ, Scherf, U, Speed, TP. Exploration, normalization and summaries of high density oligonucleotide array probe level data. Biostatistics 2003a;4:249-64.

Irizarry, RA, Bolstad, BM, Collin, F, Cope, LM, Hobbs, B, Speed, TP. Summaries of Affymetrix GeneChip probe level data. Nucleic Acids Research 2003b;31: e15.

Ishii, Y, Shirato, M, Nomura, A, Sakamoto, T, Uchida, Y, Ohtsuka, M, Sagai, M, Hasegawa, S. Cloning of rat eotaxin: ozone inhalation increases mRNA and protein expression in lungs of Brown Norway rats. Am J Physiol Lung Cell Mol Physiol 1998;274:171-6.

Iuvone, PM, Tosinin, G, Pozdeyev, N, Haque, R, Klein, DC, Chaurasia, SS. Circadian clocks, clock networks, arylalkylamine N-acetyltransferase, and melatonin in the retina. Prog Ret Eye Res 2005;24:433-56.

Jerusalinsky, D, Kornisiuk, E, Izquierdo, I. Cholinergic neurotransmission and synaptic plasticity concerning memory processing. Neurochem Res 1997;22(4):507-15.

Jolliffe, IT. Principal component analysis. New York: Springer; 1986.

Kaddurah-Daouk, R, Krishnan, KRR. Metabolomics: A global biochemical approach to the study of central nervous system diseases. Neuropsychopharm 2009;34:173-86.

Kassa, J, Koupilova, M, Vachek, J. The influence of low-level sarin inhalation exposure on spatial memory in rats. Pharm Biochem Behav 2001;70:175-9.

Klein, AK, Nasr, ML, Goldman, M. The effects of in vitro exposure to the neurotoxins sarin (GB) and soman (GD) on unscheduled DNA synthesis by rat hepatocytes. Tox Lett 1987;38(3):239-49.

Knott, C, Stern, G, Wilkin, GP. Inflammatory regulators in Parkinson's disease: iNos, lipocortin-1 and cyclooxygenases-1 and -2. Mol Cell Neurosci 2000;16:724-39.

Kuczynski, B, Reo, NV. Evidence that plasmalogen is protective against oxidative stress in the rat brain. Neurochem Res 2006;31(5):639-56.

Lakher, M, Wurtman, RJ. In vivo synthesis of phosphatidylcholine in rat brain via the phospholipid methylation pathway. Brain Res 1987;419(1-2):131-40.

Lanks, KW, Dorwin, JM, Papirmeister, B. Increased rate of acetylcholinesterase synthesis in differentiating neuroblastoma cells. J Cell Biol 1974;63:824-30.

Larsen, NB, Rasmussen, M, Rasmussen, LJ. Nuclear and mitochondrial DNA repair: similar pathways? Mitochondrion 2005;5:89-108.

Lee, TC. Biosynthesis and possible biological functions of plasmalogens. Biochim Biophys Acta 1998;1394:129-45.

Lie, D-C, Colamarino, SA, Song, H-J, Desire, L, Mira, H, Consiglio, A, Lein, ES, Jessberger, S, Lansford, H, Dearie, AR, Gage, FH. Wnt signaling regulates adult hippocampal neurogenesis. Nature 2005;437:1370-1375.

Lin, Y, Bloodgood, BL, Hauser, JL, Lapan, AD, Koon, AC, Kim, T-K, Hu, LS, Malik, AN, Greenberg, ME. Activity-dependent regulation of inhibitory synapse development by Npas4. Nature 2008;455:1198-204.

Liu, J, Guo, C, Yao, Y, Lin, D. Effects of removing a conserved disulfide bond on the biological characteristics of rat lipocalin-type prostaglandin D synthase. Biochimie 2008;90:1637-46.

Mahle, DA, Anderson, PE, DelRaso, NJ, Raymer, ML, Neuforth, AE, Reo, NV. A generalized model for metabolomic analyses: application to dose and time dependent toxicity. Metabolomics 2010;7(2):206-216.

Martin, BR. Biodisposition of [^{3}H]diisopropylfluorophosphate in mice. Toxicol Appl Pharmacol 1985;77:275-84.

McCombie, H, Saunders, BB. Alkyl fluorophosphonates: Preparations and physiological properties. Nature 1946;157:287-9.

McDonough, JH, Shih, T-M. Neuropharmacological mechanisms of nerve agent-induced seizure and neuropathology. Neurosci Biobehav Rev 1997;21(5):559-579.

Meneses, P, Glonck, T. High resolution ^{31}P NMR of extracted phospholipids. J Lipid Res 1988;29:679-89.

Milatovic, D, Gupta, RC, Aschner, M. Anticholinesterase toxicity and oxidative stress. The Scientific World Journal 2006;6:295-310.

Moffett, JR, Ross, B, Arun, P, Madhavarao, CN, Namboodiri, AA. N-acetylaspartate in the CNS: From neurodiagnostics to neurobiology. Prog Neurobiol 2007;81(2):89-131.

Mohanty, G, Mohanty, J, Nayak, AK, Mohanty, S, Dutta, SK. Application of comet assay in the study of DNA damage and recovery in rohu (*Labeo rohita*) fingerlings after an exposure to phorate, an organophosphate pesticide. Ecotoxicology 2011;20:283-92.

Montgomery, DC. Design and Analysis of Experiments. 5th ed. New York: Wiley and Sons; 2006.

Muakkassa, FF, Koruda, MJ, Ramadan, FM, Kawakami, M, Meyer, AA. Effect of dietary fish oil on plasma thromboxane B_2 and 6-keto-prostaglandin $F_{1\alpha}$ levels in septic rats. Arch Surg 1991;126:179-182.

Muller, DP, Goss-Sampson, MA. Neurochemical, neurophysiological and neuropathological studies in vitamin E deficiency. Crit Rev Neurobiol 1990;5:239-63.

Murin, R, Mohammadi, G, Leibfritz, D, Hamprecht, B. Glial metabolism of valine. Neurochem Res 2009a;34(7):1195-203.

Murin, R, Mohammadi, G, Leibfritz, D, Hamprecht, B. Glial metabolism of isoleucine. Neurochem Res 2009b;34(1):194-204.

Nicholson, JK, Connelly, J, Lindon, JC, Holmes, E. Metabonomics: a platform for studying drug toxicity and gene function. Nat Rev Drug Discov 2002;1:153-61.

Nicholson, JK, Lindon, JC, Holmes, E. 'Metabonomics': understanding the metabolic response of living systems to pathophysiological stimuli via multivariate statistical analysis of biological NMR spectroscopic data. Xenobiotica 1999;29:1181-9.

Nie, D, Di Nardo, A, Han, JM, Baharanyi, Kramvis, I, Huynh, T, Dabora, S, Codeluppi, S, Pandolfi, PP, Pasquale, EB, Sahin, M. Tsc2-Rheb signaling regulates EphA-mediated axon guidance. Nat Neuroscience 2010;13(2):163-72.

Ooe, N, Motonaga, K, Kobayashi, K, Saito, K, Kaneko, H. Functional characterization of basic helix-loop-helix-PAS type transcription factor NXF in vivo: putative involvement in an "on demand" neuroprotection system. J Bio Chem 2009;284(2):1057-63.

Parducz, A, Kiss, Z, Joo, F. Changes of the phosphatidylcholine content and the number of synaptic vesicles in relation to the neurohumoral transmission in sympathetic ganglia. Experienta 1976;32(12):1520-1.

Pellerin, L, Magistretti, PJ. Glutamate uptake into the astrocytes stimulates aerobic glycolysis: A mechanism coupling neuronal activity to glucose utilization. Proc Natl Acad Sci USA 1994;91(22):10625-9

Peña-Philippides, JC, Razani-Boroujerdi, S, Singh, SP, Langley, RJ, Mishra, NC, Henderson, RF, Sopori, ML. Long- and short-term changes in the neuroimmune-endocrine parameters following inhalation exposures of F344 rats to low-dose sarin. Toxicol Sci 2007;97(1):181-8.

Placzek, AN, Zhang, TA, Dani, JA. Nicotinic mechanisms influencing synaptic plasticity in the hippocampus. Acta Pharmacol Sin 2009;30(6):752-60.

Pollock, RJ, Hajra, AK, Agranoff, BW. Incorporation of D-[3-3H, U-14C] glucose into glycerolipid via acyl dihydroxyacetone phosphate untransformed and viral-transformed BHK-21-c13 fibroblasts. J Biol Chem 1976;251:5149-54.

Pope, CN. Organophosphorous pesticides: Do they all have the same mechanism of toxicity? J Toxicol Env Health 1999;2:161-81.

Proctor, SP, Heaton, KJ, Heeren, T, White, RF. Effects of sarin and cyclosarin exposure during the 1991 Gulf War on neurobehavioral functioning in US army veterans. Neurotox 2006;27:931-9.

Purdon, AD, Rapoport, SI. Energy consumption by phospholipid metabolism in mammalian brain. In: Lajtha, A, Gibson, GE, Dienel, GA, editors. Handbook of neurochemistry and

molecular neurobiology. 3rd ed. Brain energetics: integration of molecular and cellular processes. Heidelberg: Springer-Verlag; 2007. p. 401-427.

Raivich, G, Bohatschek, M, Kloss, CUA, Werner, A, Jones, LL, Kreutzberg, GW. Neuroglial activation repertoire in the injured brain: graded response, molecular mechanisms and cues to physiological function. Brain Res Rev 1999;30:77-105.

Reich, EE, Markesbery, WR, Roberts, LJ, Swift, LL, Morrow, JD, Montine, TJ. Brain regional quantification of F-ring and D-/E-ring isoprostanes and neuroprostanes in Alzheimer's disease. Am J Pathol 2001;158(1):293-7.

Reid, MN, Shoji, T, Moody, MR, Entman, M.L. Reactive oxygen in skeletal muscle. II. Extracellular release of free radicals. J Appl Physiol 1992;73:1805-9.

Richardson, RJ. Interactions of organophosphorous compounds with neurotoxic esterase. In: Chambers, JE, Levi, PE. Organophosphates - Chemistry, fate and effects, San Diego: Academic Press; 1992. p. 299-323.

Roberts Jr, EL. The support of energy metabolism in the central nervous system with substrates other than glucose. In: Lajtha, A, Gibson, GE, Dienel, GA, editors. Handbook of neurochemistry and molecular neurobiology. 3rd ed. Brain energetics: integration of molecular and cellular processes. Heidelberg: Springer-Verlag; 2007. p. 139-168.

Rocha, ES, Santos, MD, Chebabo, SR, Aracava, Y, Albuquerque, EX. Low concentrations of the organophosphate VX affect spontaneous and evoked transmitter release from hippocampal neurons: Toxicological relevance of cholinesterase-independent actions. Toxicol Appl Pharmacol 1999;159:31-40.

Rosen, DR, Siddique, T, Patterson, D, Figlewicz, DA, Sapp, P, Hentati, A, Donaldson, D, Goto, J, O'Regan, JP, Deng, HX, *et al*. Mutations in Cu/Zn superoxide dismutase gene are associated with familial amyotrophic lateral sclerosis. Nature 1993;362(6415):59-62.

Rozen, S, Cudkowicz, ME, Bogdanov, M, Matson, WR, Kristal, BS, Beecher, C, Harrison, S, Vouros, P, Flarakas, J, Vigneau-Callahan, K, Matson, TD, Newhall, KM, Beal, MF, Brown Jr, RH, Kaddurah-Douk, R. Metabolomic analysis and signatures in motor neuron disease. Metabolomics 2005;1:101-8.

Ruland, J. Return to homeostasis: downregulation of NF-κB responses. Nature Immunol 2011;12(8):709-714.

Saleem, S, Shah, ZA, Urade, Y, Doré, S. Lipocalin-prostaglandin D synthase is a critical beneficial factor in transient and permanent focal cerebral ischemia. Neuroscience 2009;160:248-54.

Sapolsky, RM. Deleterious and salutary effects of steroid hormones in the nervous system. In: Mattson, MP, editor. Neuroprotective signal transduction. Totowa, New Jersey: Humana Press;1998. p. 259-283.

Schena, M, Shalon, D, Davis, RW, Brown, PO. Quantitative monitoring of gene expression patterns with a complementary DNA microarray. Science 1995;270(5235):467-70.

Sillerud, LO, Han, CH, Bitensky, MW, Francendese, AA. Metabolism and structure of triacylglycerols in rat epididymal fat pad adipocytes determined by 13C nuclear magnetic resonance. J Biol Chem 1986;261:4380-8.

Siushansian, R, Wilson, JX. Ascorbate transport and intracellular concentration in cerebral astrocytes. J Neurochem 1995;65:41-9.

Slotkin, TA, Levin, ED, Seidler, FJ. Comparative developmental neurotoxicity of organophosphate insecticides: Effects on brain development are separable from systemic toxicity. Environ Health Persp 2006;114(5);746-51.

Smith, IC, Baert, R. Medical diagnosis by high resolution NMR of human specimens. IUBMB 2003;55:273-7

Song, X, Seidler, FJ, Saleh, JL, Zhang, J, Padilla, S, Slotkin, T.A. Cellular mechanisms for developmental toxicity of chlorpyrifos: Targeting the adenylyl cyclase signaling cascade. Toxicol Appl Pharmacol 1997;145:158-74.

Song, X, Violin, JD, Seidler, FJ, Slotkin, T.A. Modeling the developmental neurotoxicity of chlorpyrifos *in vitro*: Macromolecule synthesis in PC12 cells. Toxicol Appl Pharmacol 1998;151:182-91.

Soreq, H, Seidman, S. Acetylcholinesterase – new roles for an old actor. Nature 2001;2:294-302.

Spradling, KD, Lumley, LA, Robison, CL, Meyerhoff, JL, Dillman III, JF. Transcriptional responses of the nerve agent-sensitive brain regions amygdale, hippocampus, piriform cortex, septum, and thalamus following exposure to the organophosphate anticholinesterase sarin. J Neuroinflammation 2011;8:84-105.

Sweeley, CC, Young, ND, Holland, JF, Gates, SC. Rapid computerized identification of compounds in complex biological mixtures by gas chromatography-mass spectrometry. J Chromatogr 1974;99:507-17.

Tai, SK, Leung, LS. Vestibular stimulation enhances hippocampal long-term potentiation via activation of cholinergic septohippocampal cells. Behav Brain Res 2012;232:174-82.

Taylor, P. Anticholinesterase agents. In: The pharmacological basis for therapeutics, 6th ed. Goodman, LS, Gilman, AG. New York: MacMillan Pub. Co; 1980. p. 100-116.

Tyagi, RK, Azrad, A, Degani, H, Salomon, Y. Simultaneous extraction of cellular lipids and water-soluble metabolites: evaluation by NMR spectroscopy. Magnet Reson Med 1996;35:194-200.

Van den Berg, HC, Hoefsloot, JA, Westerhuis, JA, Smilde, AK, Van der Werf, MJ. Centering, scaling, and transformations: Improving the biological information content of metabolomics data. BMC Genomics 2006;7:142-167.

Vannucci, SJ, Clark, RR, Koehler-Stec, E, Li, K, Smith, CB, Davies, P, Maher, F, Simpson, IA. Glucose transporter expression in brain: relationship to cerebral glucose utilization. Dev Neurosci 1998;20(4-5):369-79.

Wang, Y, Liu, X, Biederer, T, Südhof, TC. A family of RIM-binding proteins regulated by alternative splicing: implications for the genesis of synaptic active zones. PNAS 2002;99(22):14464-9.

Weisskopf, MG, O'Reilly, EJ, McCullough, ML, Calle, EE, Thun, MJ, Cudkowicz, M, Ascherio, A. Prospective study of military service and mortality from ALS. Neurology 2005;64:32-7.

Williams, AJ, Berti, R, Yao, C, Price, RA, Velarde, LC, Koplovitz, I, Schultz, SM, Tortella, FC, Dave, JR. Central neuro-inflammatory gene response following soman exposure in the rat. Neurosci Lett 2003a;349:147-50.

Williams, RE, Cottrell, L, Jacobson, M, Bandara, LR, Kelly, MD, Kennedy, S. 1H-Nuclear magnetic resonance pattern recognition studies with N-phenylanthranilic acid in the rat: Time- and dose-related metabolic effects. Biomarkers 2003b;8:472-490.

Wishart, D. Metabolomics in humans and other mammals. In: Villas-Boas SG, Nielsen J, Smedsgaard J, Hansen MAE, Roessner-Tunali U. Metabolome analysis: an introduction. Hoboken, NJ: Wiley-Interscience; 2007. p. 253-288.

Wu, K, Aoki, C, Elste, A, Rogalski-Wilk, AA, Siekevitz, P. the synthesis of ATP by glycolytic enzymes in the postsynaptic density and the effect of endogenously generated nitric oxide. PNAS 1997;94(24):13273-8.

Xu, C-X, Krager, SL., Liao, D-F, Tischkau, SA. Disruption of CLOCK-BMAL1 transcriptional activity is responsible for aryl hydrocarbon receptor-mediated regulation of period1 gene. Toxicol Sci 2010;115(1):98-108.

Yanagisawa, N, Morita, H, Nakajima, T. Sarin experiences in Japan: acute toxicity and long-term effects. J Neurol Sci 2006;249:76-85.

Yang, ZP, Dettbarn, WD. Diisopropylphosphorofluoridate-induced cholinergic hyperactivity and lipid peroxidation. Toxicol Appl Pharmacol 1996;138:48-53.

Yao, JK, Wengenack, TM, Curran, GL and Poduslo, JF. Reduced membrane lipids in the cortex of Alzheimer's Disease transgenic mice. Neurochem Res 2009;34:102-8.

Yokoyama, K, Araki, S, Murata, K, Nishikitani, M, Okumura, T, Ishimatsu, S, Takasu, N. Chronic neurobehavioral effects of Tokyo subway sarin poisoning in relation to posttraumatic stress disorder. Arch Environ Health 1998;53(4):249-56.

Yoshida, K, Oka, H. Topographical projections from the medial septum-diagonal band complex to the hippocampus: a retrograde tracing study with multiple fluorescent dyes in rats. Neurosci Res 1995;21:199-209.

Zaja-Milatovic, S, Gupta, RC, Aschner, M, Milatovic, D. Protection of DFP-induced oxidative damage and neurodegeneration by antioxidants and NMDA receptor antagonist. Toxicol Appl Pharmacol 2009;240:124-31.

Zeisel, SH. Choline: Critical role during fetal development and dietary requirements in adults. Annu Rev Nutr 2006;26:229-50.

Zeisel, SH. Choline: Essential for brain development and function. Adv Pediatr 1997;44:263-95.

Zeng, H, Gragerov, A, Hohmann, JG, Pavlova, MN, Schimpf, BA, Xu, H, Wu, L-J, Toyoda, H, Zhao, M-G, Rohde, AD, Gragerova, G, Onrust, R, Bergmann, JE, Zhuo, M, Gaitanaris, GA. Neuromedin U receptor 2-deficient mice display differential responses to sensory perception, stress and feeding. Mol Cell Biol 2006;26(24):9352-63.

VI. APPENDIX I

6.1 RNA isolation gel electrophoresis images

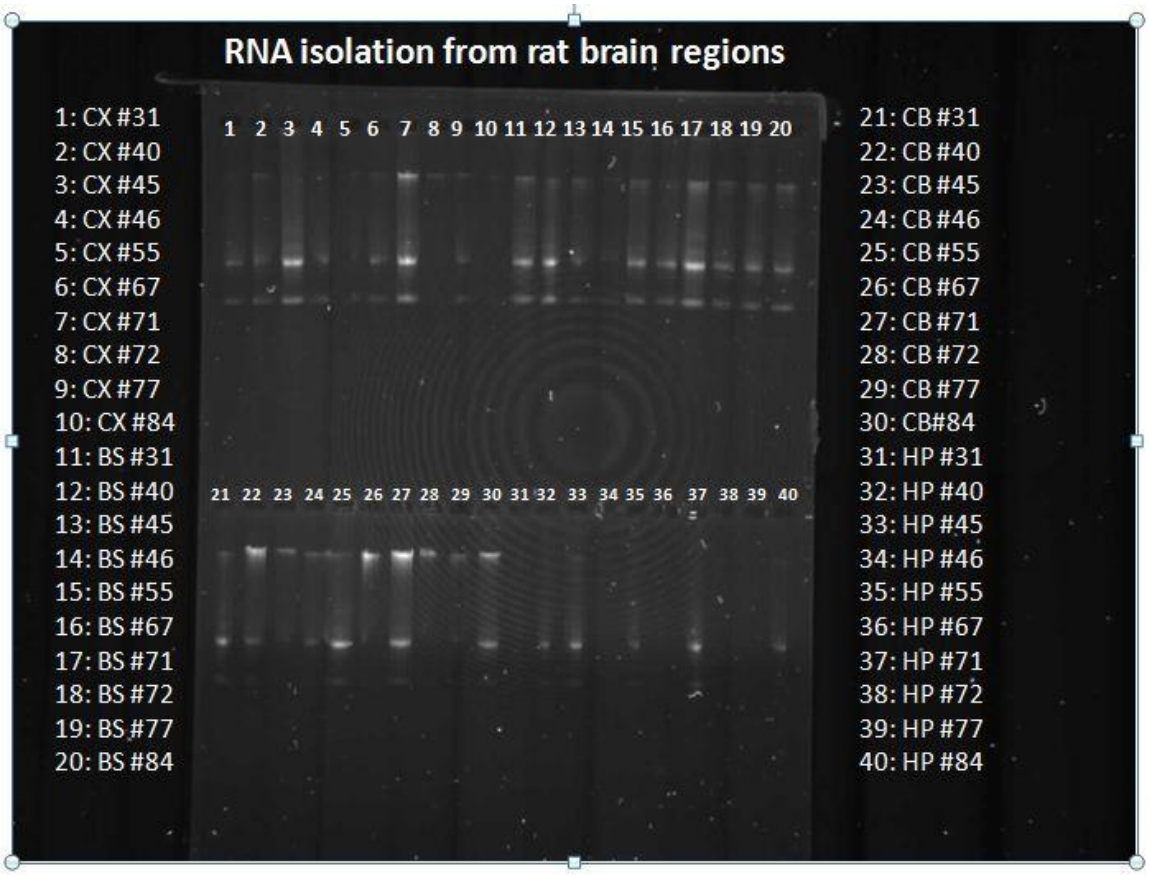

Figure 32. Agarose gel images of RNA isolation quality check. Top band is the 28S fragment and the bottom band is the 18S fragment. Abbreviations: CX – cortex; BS – brainstem; CB – cerebellum; HP – hippocampus.

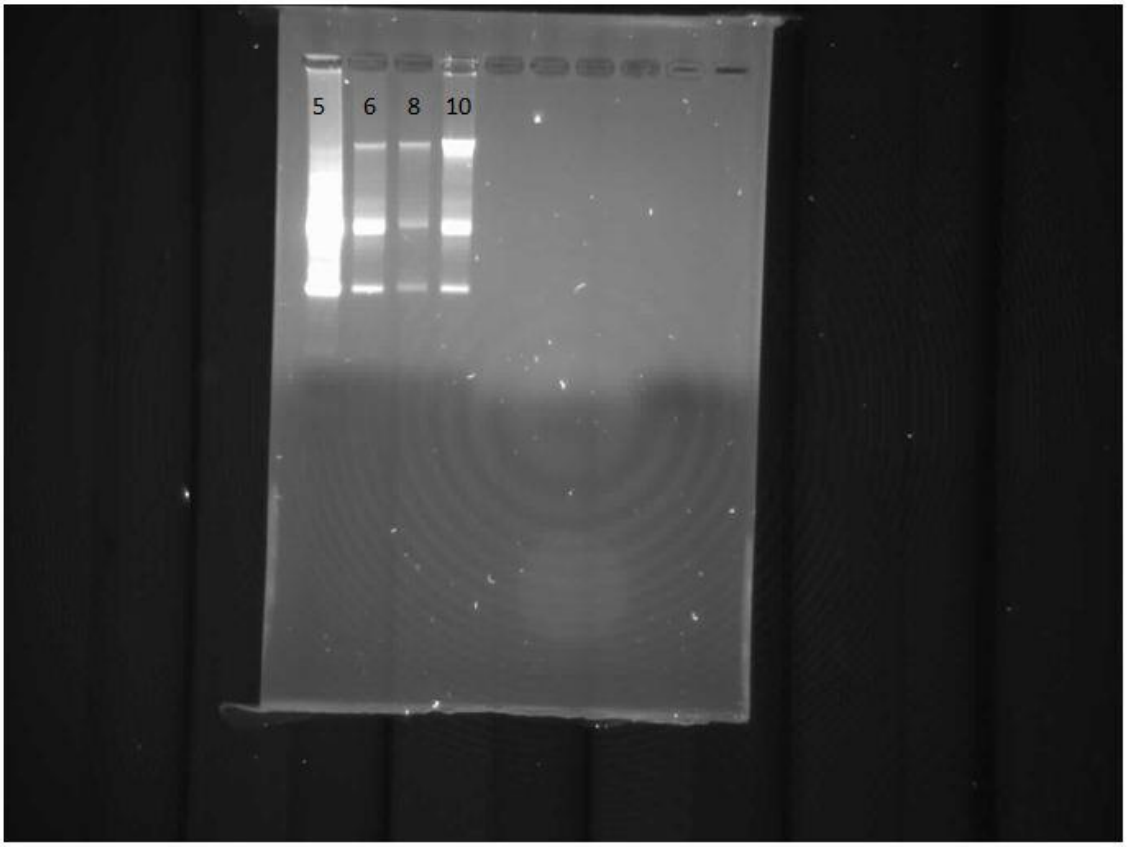

Figure 33. Agarose gel images of RNA isolation quality check for cortex sample re-isolated.

6.2 Quantification of total RNA

Table 18. RNA isolation log with $A_{260/280}$ and $A_{260/230}$ ratios to detect degradation.

Tube #	Sample ID	Brain region	260/280	260/230	ng/µL
1	31	CX	2.06	.64	152.8
2	40	CX	2.07	.24	82.4
3	45	CX	2.05	1.29	182.5
4	46	CX	2.07	0.3	101.3
5	55	CX	2.09	1.95	740.8
6	67	CX	2.07	0.20	50.7
7	71	CX	2.07	0.42	182.0
8	72	CX	2.18	1.30	35.8
9	77	CX	2.04	0.29	147.8
10	84	CX	2.03	0.27	104.2
11	31	BS	2.06	1.67	225.3
12	40	BS	2.03	2.02	393.3
13	45	BS	2.13	0.15	75.4
14	46	BS	2.17	0.09	42.5
15	55	BS	2.05	1.26	208.3
16	67	BS	2.05	0.91	180.8
17	71	BS	2.05	1.51	276.1
18	72	BS	2.06	1.19	131.0
19	77	BS	2.04	1.61	154.1
20	84	BS	2.02	0.68	81.6
21	31	CB	2.06	2.02	744.5
22	40	CB	2.01	1.34	205.7
23	45	CB	1.99	1.24	114
24	46	CB	2.06	1.71	320.6
25	55	CB	2.15	0.36	185.2
26	67	CB	1.99	0.41	216.3
27	71	CB	2.03	1.63	283.9
28	72	CB	1.99	0.29	147.3
29	77	CB	2.05	0.33	107.1
30	84	CB	2.11	0.28	152.0
31	31	HP	2.05	1.08	111.4
32	40	HP	2.11	1.68	129.3
33	45	HP	2.03	1.25	451.3
34	46	HP	2.1	1.67	87.2
35	55	HP	2.06	2.00	324.0
36	67	HP	2.06	1.83	228.0
37	71	HP	2.02	1.99	461.9
38	72	HP	2.02	1.29	101.9
39	77	HP	2.14	0.06	26.3
40	84	HP	2.02	1.68	444.2

6.3 cDNA fragmentation gel electrophoresis images

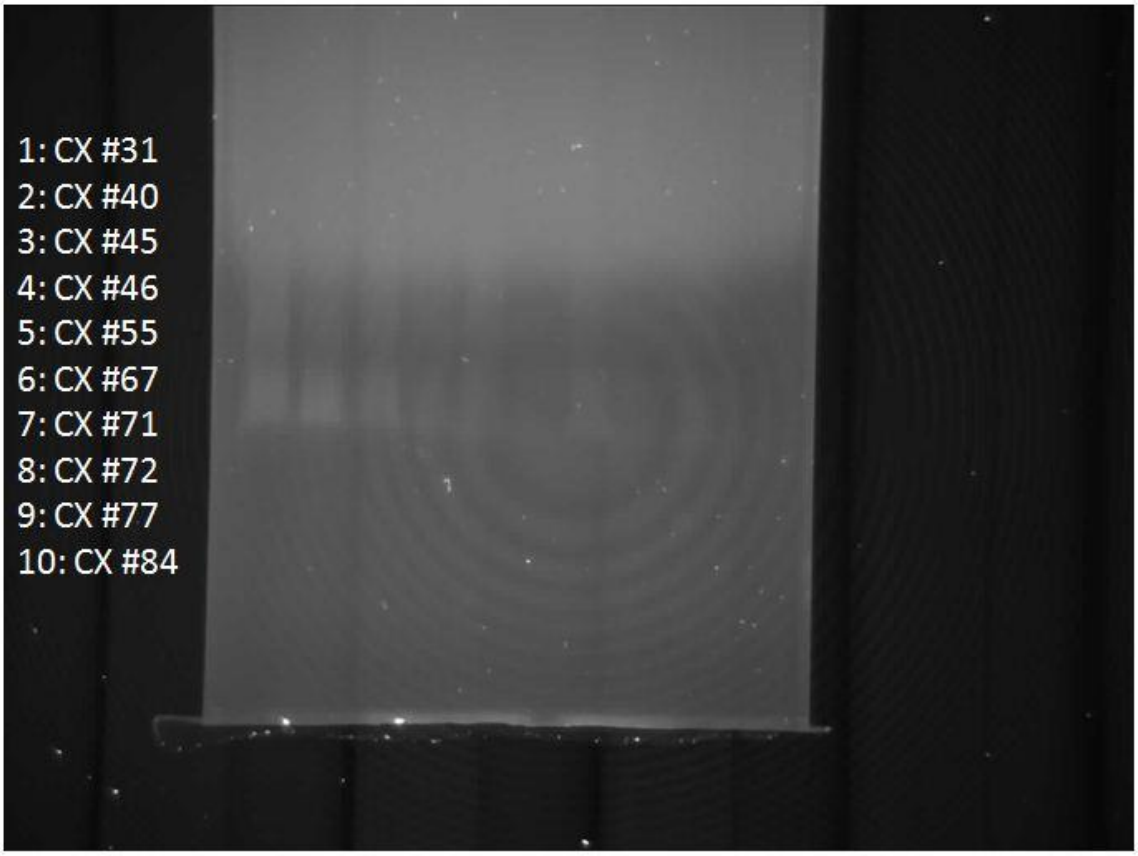

Figure 34. cDNA fragments from cortex samples at 1 hr post 1mg/kg DFP exposure. Exposure was extremely light but evidence of fragmented cDNA at bottom is clear.

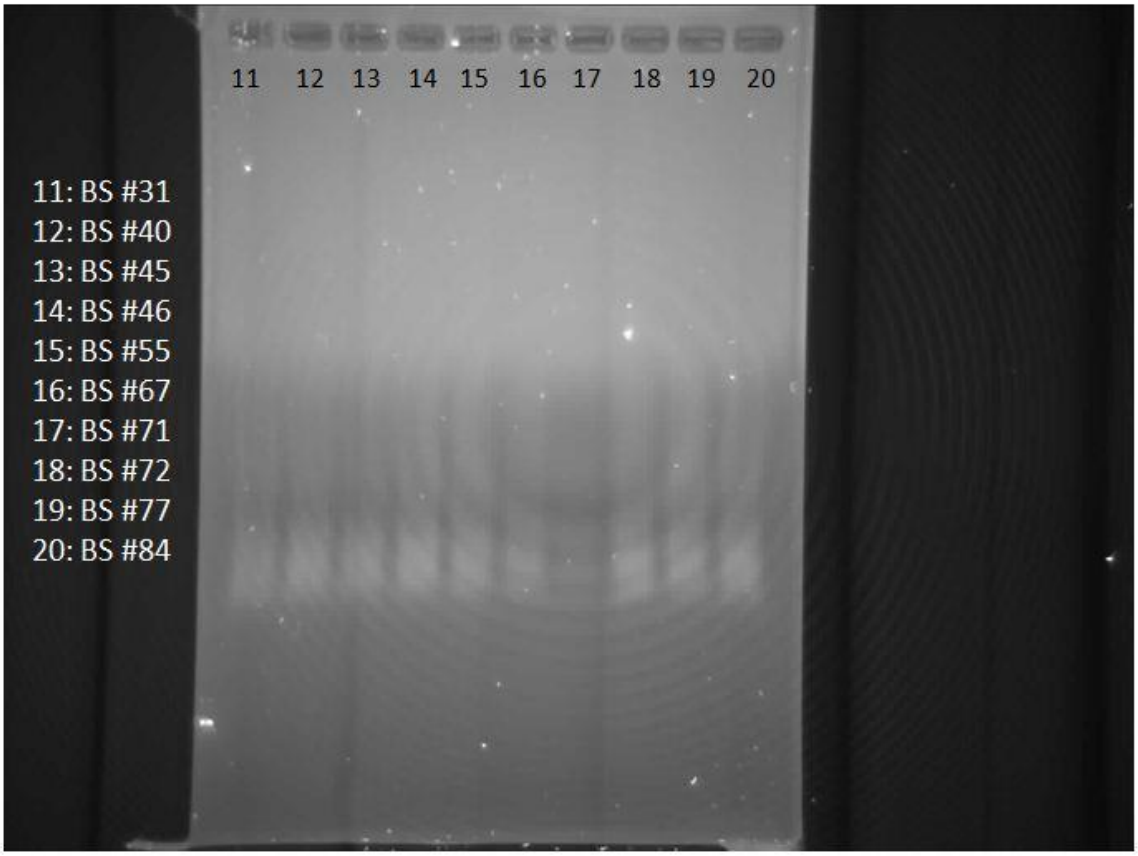

Figure 35. cDNA fragments from brainstem samples at 1 hr post 1mg/kg DFP exposure. Exposure was extremely light but evidence of fragmented cDNA at bottom is clear.

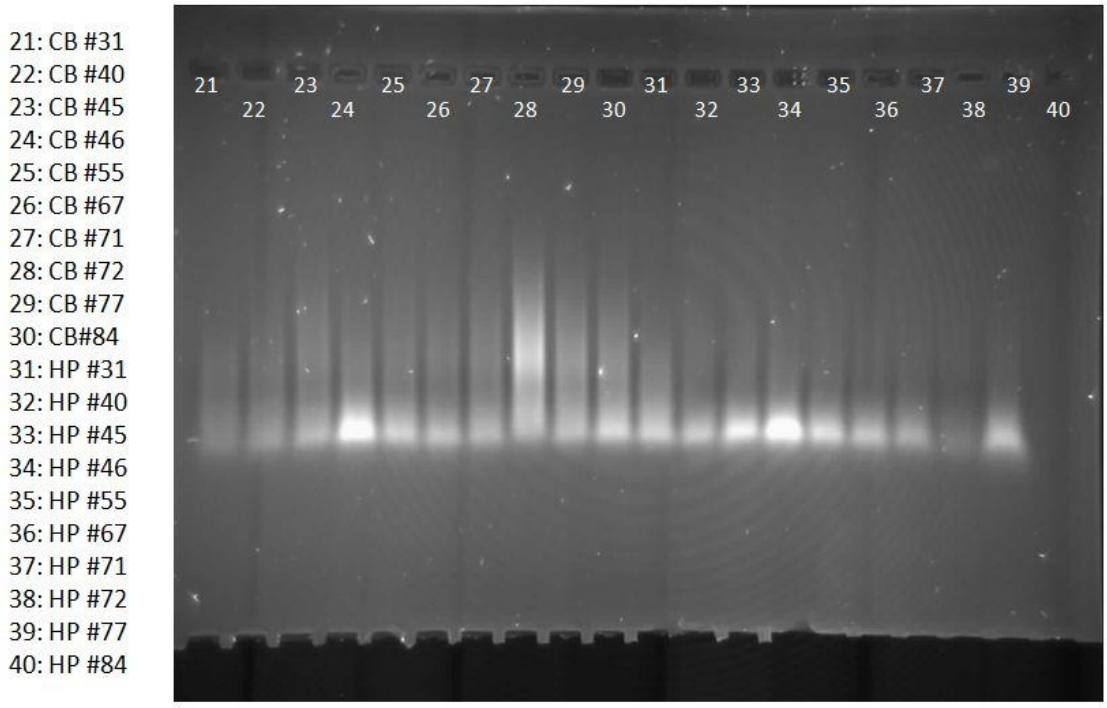

Figure 36. cDNA fragments from cerebellum and hippocampus samples at 1 hr post 1mg/kg DFP exposure.

VII. Appendix II

7.1 Quality control analysis of cortex gene array

Raw Data

The tabular text report for the raw data shows that sample 8 has the lowest pm_mean value among all the samples, while the raw signals of samples 3 and 5 exceed 400.

The signal histogram for the raw data is very uneven throughout. Sample 8 is really shifted to the left with a 2- to 3-fold lower signal overall.

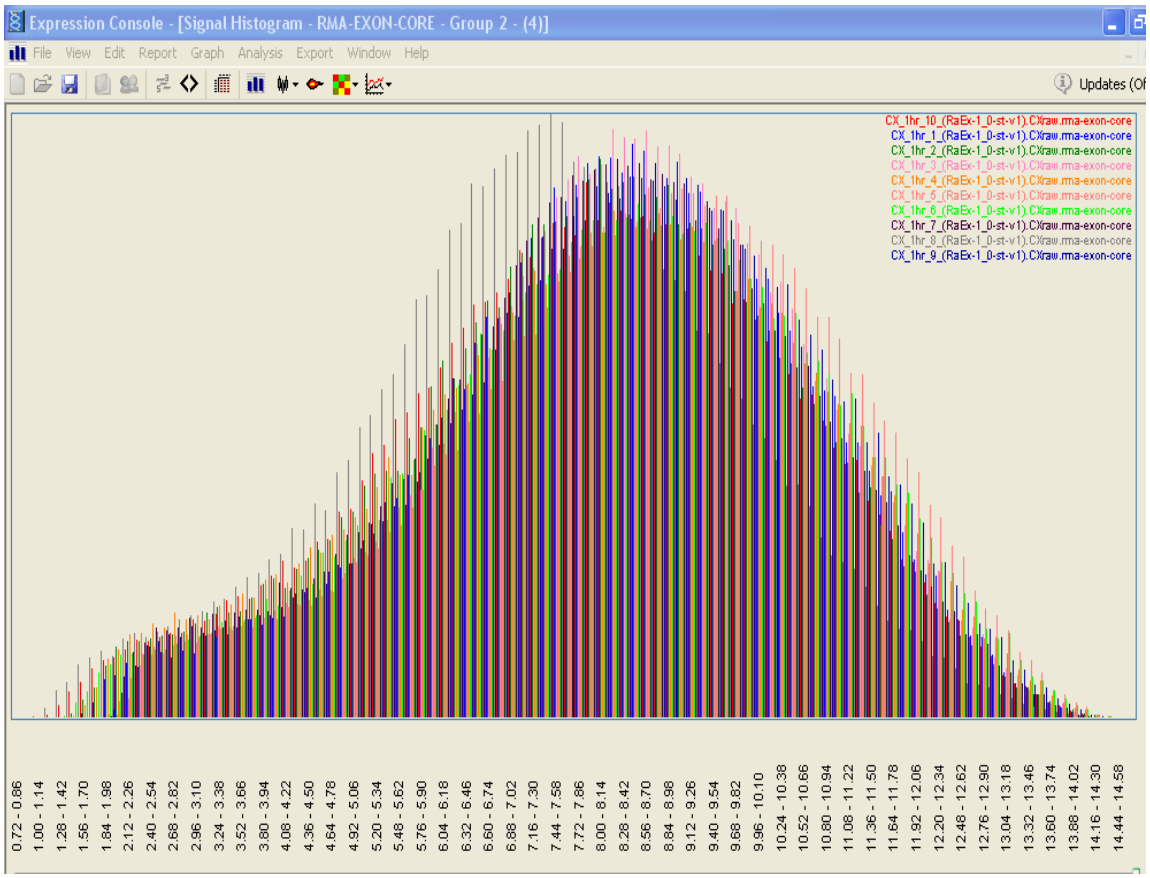

Figure 37. Signal histogram of raw cortex data.

The relative signal box plot of the raw data is very uneven. Samples 10, 2, and 8 fall below the median line, with sample 8 being the lowest and standing out more than the rest of the data set. Samples 3, 5, and 9 fall above the median line with sample 5 being the furthest away. Overall sample 8 looks like an outlier in this graph.

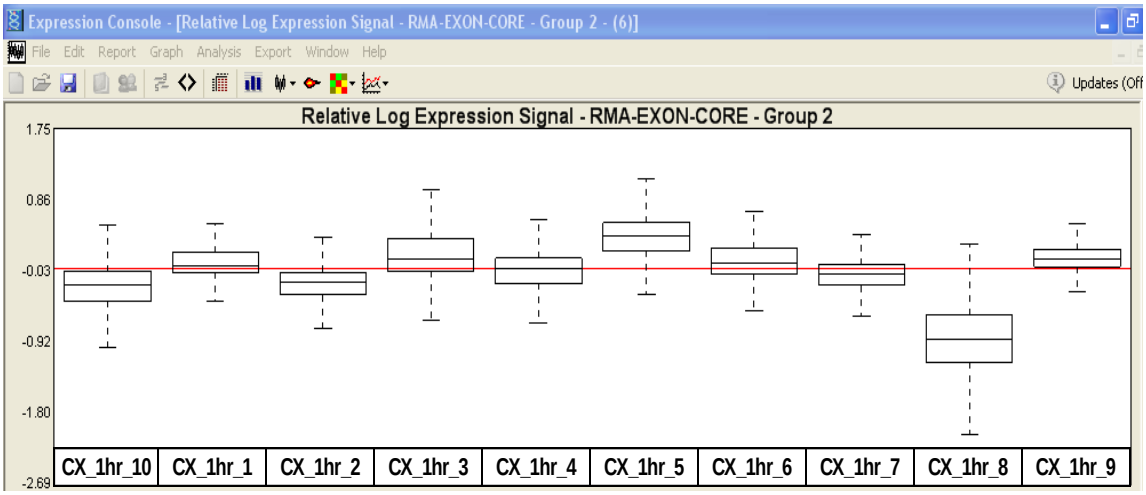

Figure 38. Relative signal box plot of raw cortex data.

The Pearson's correlation plot of the raw data shows all samples with correlation 0.966 or greater. Consistent with the result of the box plot, sample 8 shows the lowest correlation with the rest of this dataset, suggesting that it is probably an outlier.

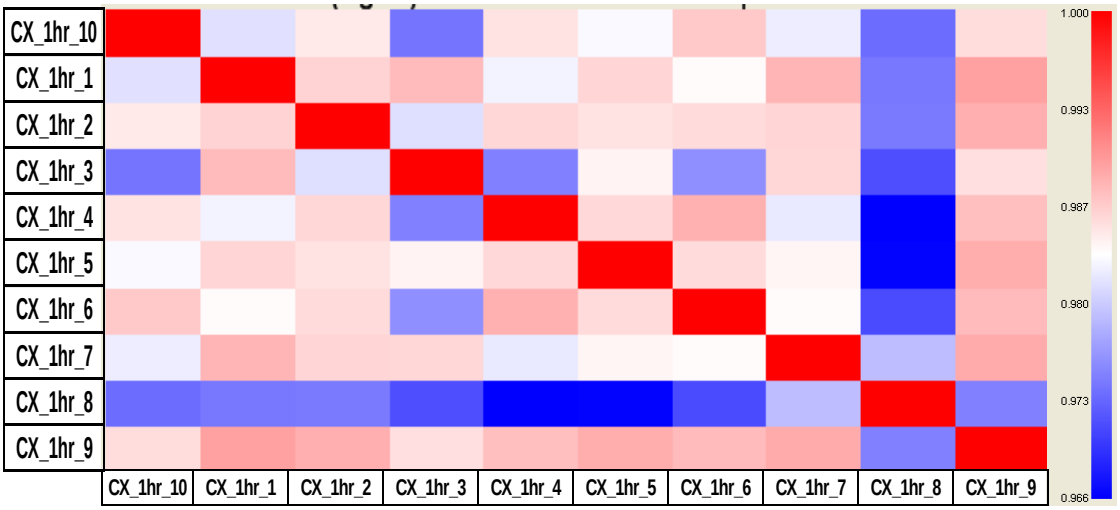

Figure 39. Pearson's correlation plot of raw cortex data.

Normalized Data

The tabular report for the normalized data shows that the %P of sample 8 is significantly lower than that of other samples, probably due to the overall low signal of this chip. Although sample 3 has the second highest overall signal level, it has the lowest pos_control_mean and dabg_pos_vs_neg_auc among all samples.

The signal histogram for the normalized data is much smoother than the raw signal histogram. There is some unevenness around the peak signal area but no chip seems to really stand out more than the others.

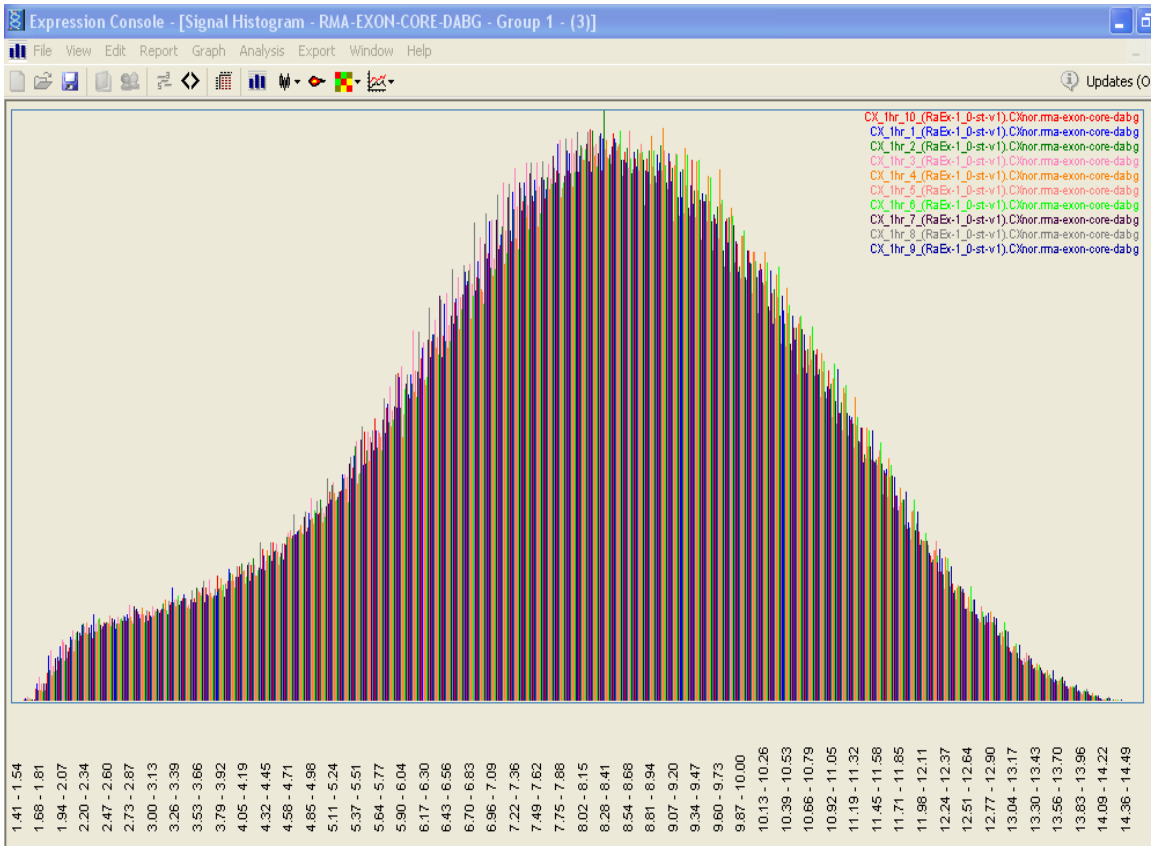

Figure 40. Signal histogram of normalized cortex data.

The relative signal box plot for the normalized data shows that after normalization most the samples are very close to the median line. Sample 3 is slightly below and sample 8 is much lower

than the rest of the samples and has a broader distribution. Sample 4 and 6 are slightly above the median line.

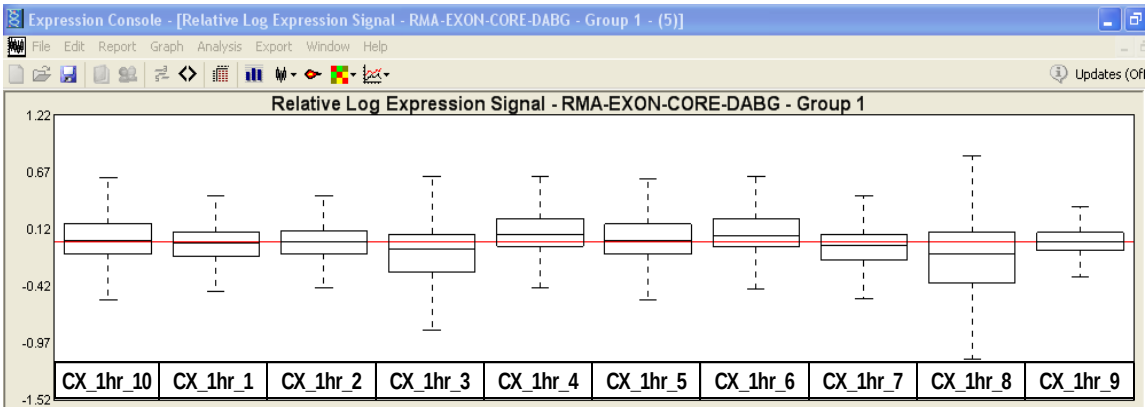

Figure 41. Relative signal box plot of normalized cortex data.

The Pearson's correlation plot shows that all samples have correlation 0.967 or greater. However, sample 8 has the lowest correlation with other samples in the dataset, followed by sample 3 with a slightly lower correlation with others.

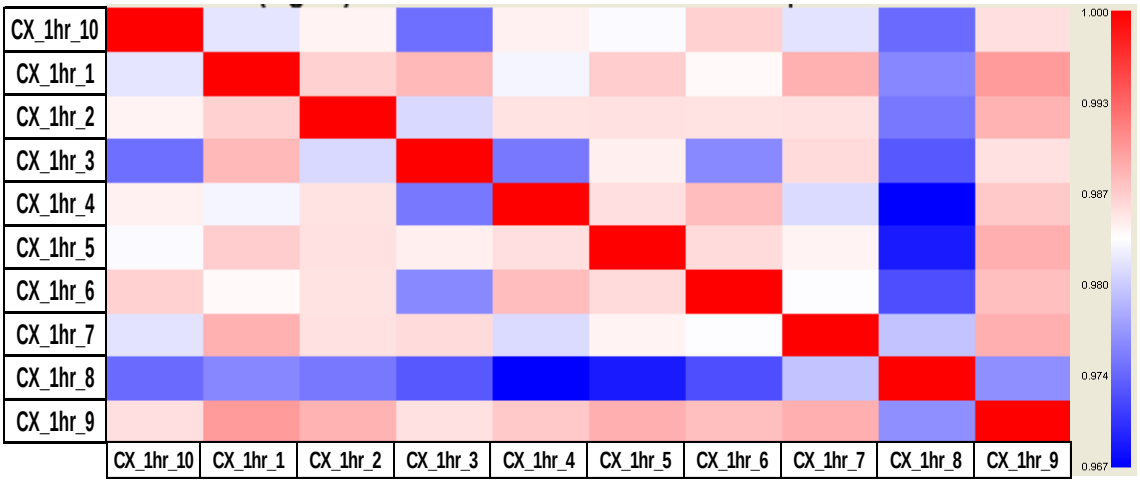

Figure 42. Pearson's correlation plot of normalized cortex data.

Comment and Suggestion

The signal of sample CX_1hr_8 is significantly lower than that of other chips even after normalization. Additionally, it shows the lowest correlation with other chips. As the quality of CX_1hr_8 is low, it should be excluded from the dataset. Sample CX_1hr_3 also shows a decreased correlation with other chips. However, considering the Pearson's correlation coefficient and the number of samples of the DFP treatment group left after exclusion of CX_1hr_8, it is decided to include CX_1hr_3 in the dataset.

7.2 Quality control analysis of brainstem gene array

Raw Data

The tabular text report for the raw data shows that the pm_mean values of samples BS_2hr_14 and BS_2hr_20 are less than 300. Other metrics appear to be okay.

The signal histogram for the raw data is somewhat uneven with several samples shifting slightly away from the main peak area. The peak of sample BS_2hr_20 has shifted noticeably to the left of the graph, indicating a weaker signal overall.

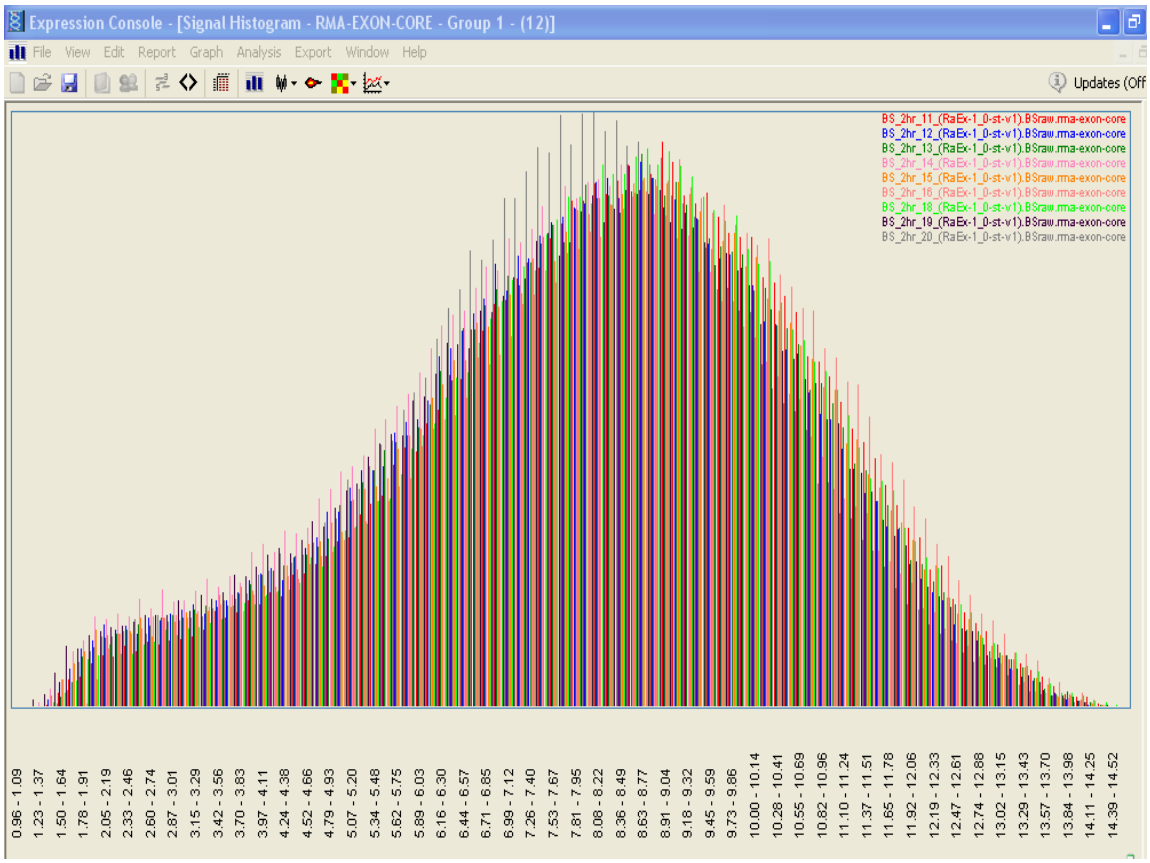

Figure 43. Signal histogram of raw brainstem data.

The relative signal box plot for the raw data is somewhat uneven with the majority of samples falling above or below the average median line. Samples BS_2hr_20 has a broader signal distribution than the rest of the data set.

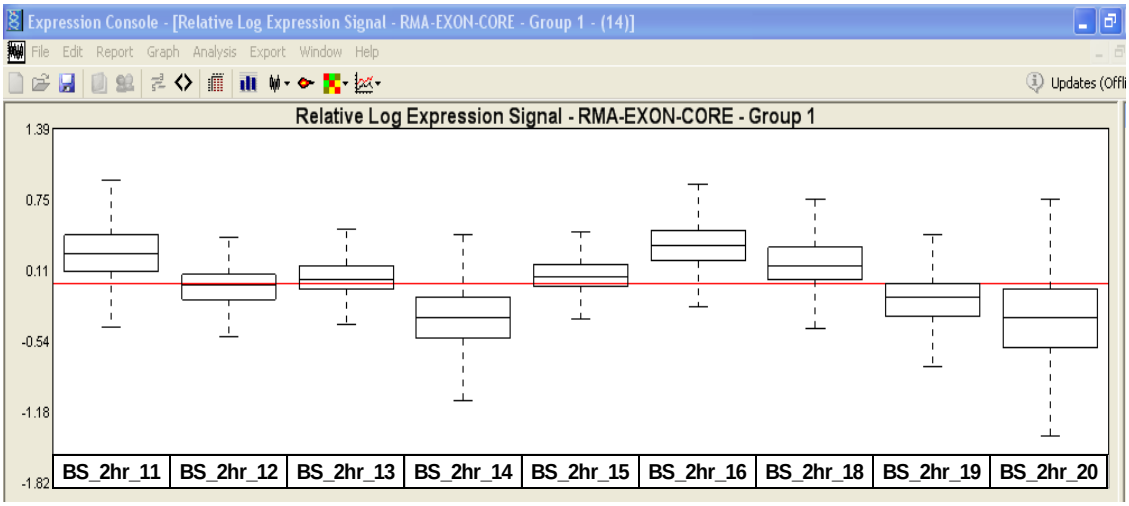

Figure 44. Relative signal box plot of raw brainstem data.

The Pearson's Correlation plot for the raw signals indicates that all samples have a good correlation with the lowest correlation coefficient being 0.977. Samples BS_2hr_14 and BS_2hr_20 appear to have a weaker correlation than the rest of the data set.

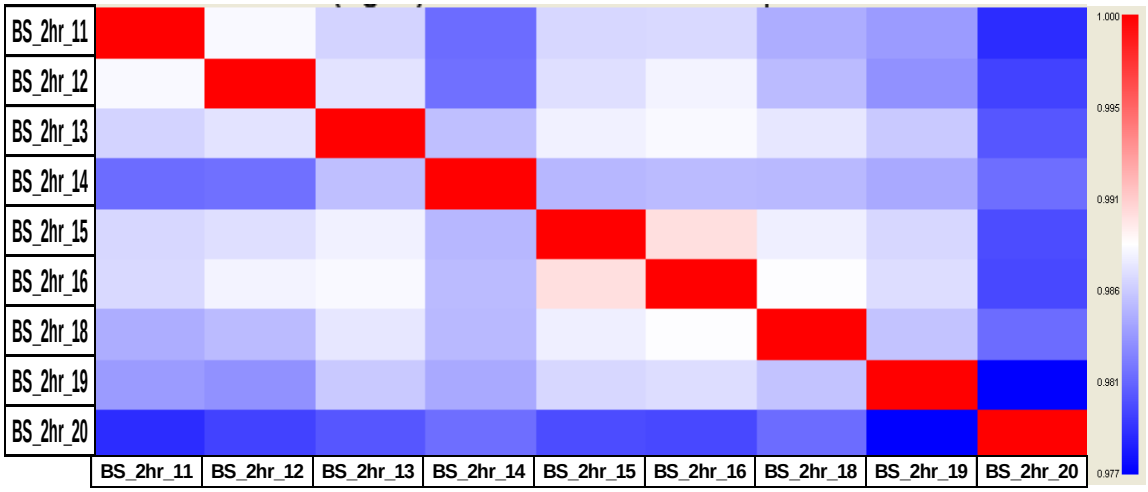

Figure 45. Pearson's correlation plot of raw brainstem data.

Normalized Data

The tabular text report shows that after normalization samples BS_2hr_14 and BS_2hr_20 have signal values very close to that of other chips. The background-corrected signal (pm_mean - bgrd_mean) of most samples (except BS_2hr_14 and BS_2hr_20) is ≥100. The quality of BS_2hr_20 is lower than that of other chips, based on the values of %P, pos_vs_neg_auc and dabg_pos_vs_neg_auc.

The signal histogram for normalized data is improved from the raw data histogram, however it is still a little uneven. The graph shows a significant amount of variation in the signal strength, particularly around the peak area.

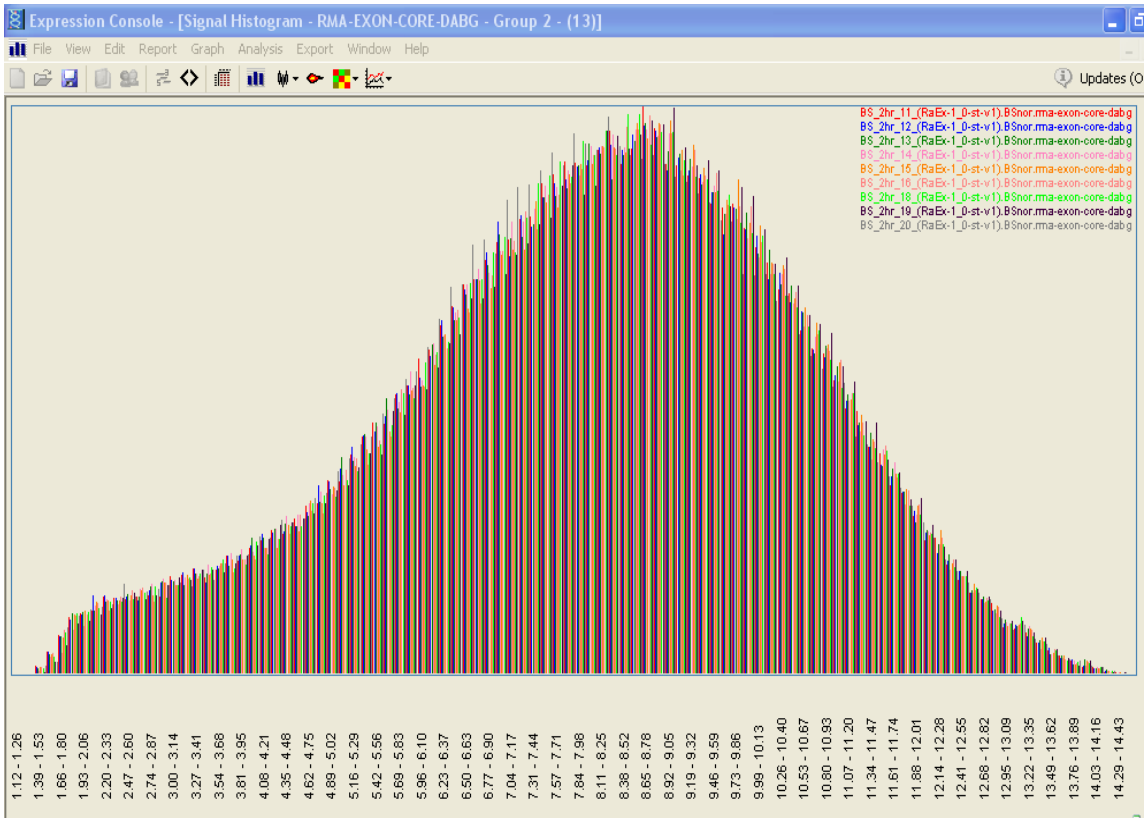

Figure 46. Signal histogram of normalized brainstem data.

The relative signal box plot for the normalized data is quite even with all samples falling closely to the median line. Sample BS_2hr_20 is the furthest from the median line, falling slightly below average. It also has the broadest signal distribution among all samples.

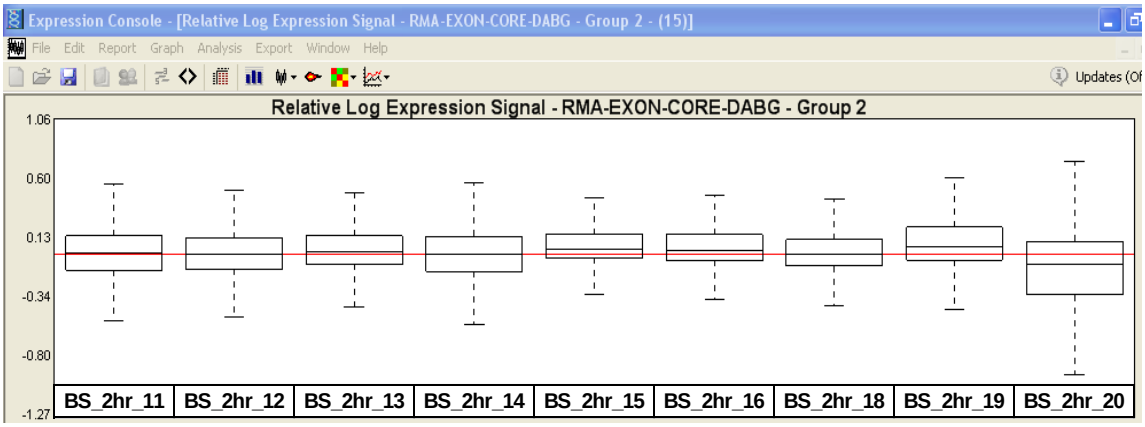

Figure 47. Relative signal box plot of normalized brainstem data.

The Pearson's Correlation plot for the normalized signals shows that all samples have a good correlation with the lowest correlation coefficient being 0.977. Samples BS_2hr_14 and BS_2hr_20 appear to have a lower correlation with other samples than the rest of the data set.

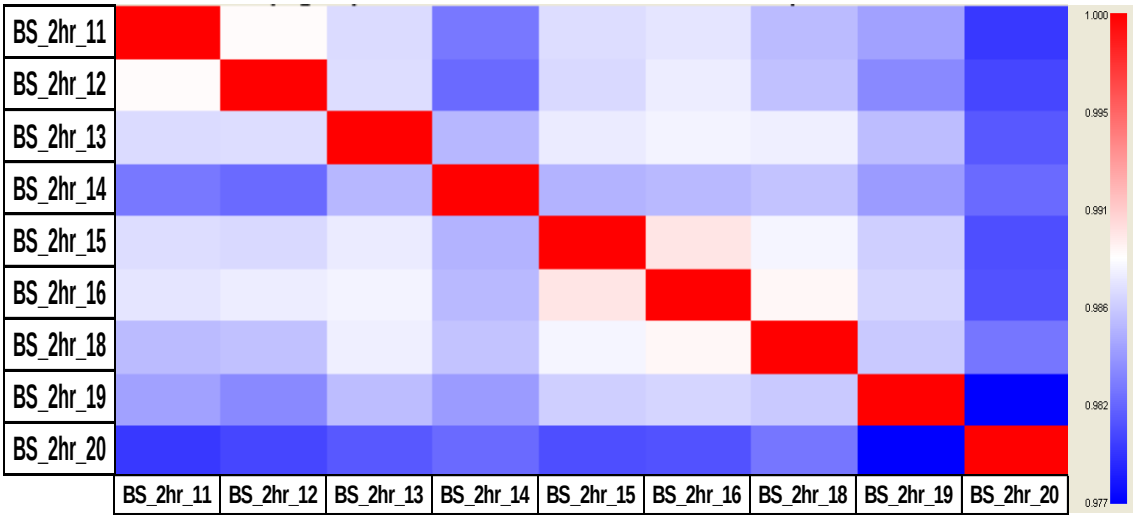

Figure 48. Pearson's correlation plot of normalized brainstem data.

Comment and Suggestion

After normalization the signals of the chips look reasonably consistent. The quality of BS_2hr_20 is lower than that of others. However, considering the Pearson's correlation coefficient and the number of samples in the DFP treatment group, it is recommended to include this sample in the dataset.

7.3 Quality control analysis of cerebellum gene array

Raw Data

The tabular text report for the raw data shows that sample CB_1hr_28 has a pm_mean value of 175 that is significantly lower than that of other samples.

The signal histogram for the raw data is somewhat uneven. It also shows multiple peaks suggesting variation in the signal intensity. Sample CB_1hr_28 has shifted noticeably away from the main peak to the left indicating a lower signal (it is at least 5-fold lower than other chips).

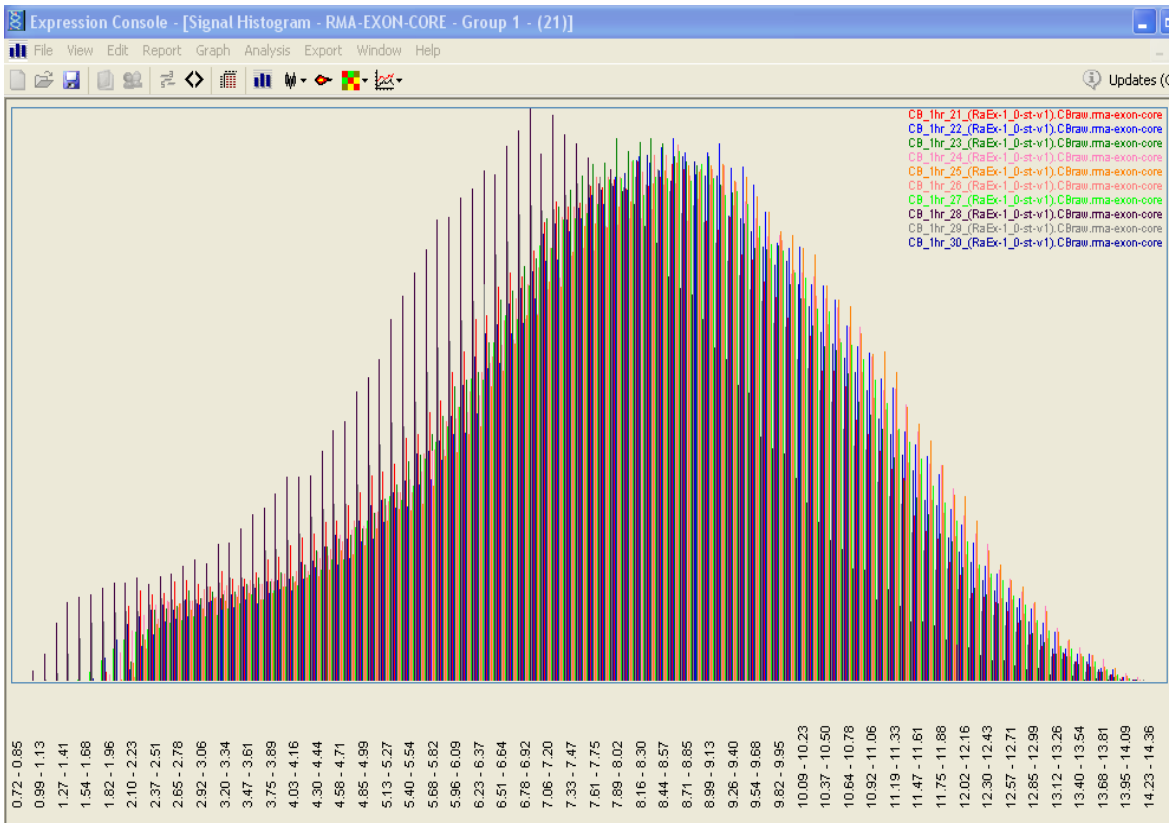

Figure 49. Signal histogram of raw cerebellum data.

The relative signal box plot for the raw is uneven with the majority of samples falling above or below the median line. Samples CB_1hr_28 and CB_1hr_29 have shifted the furthest from the median line with sample CB_1hr_28 showing the lowest signals, as well as a broad signal distribution.

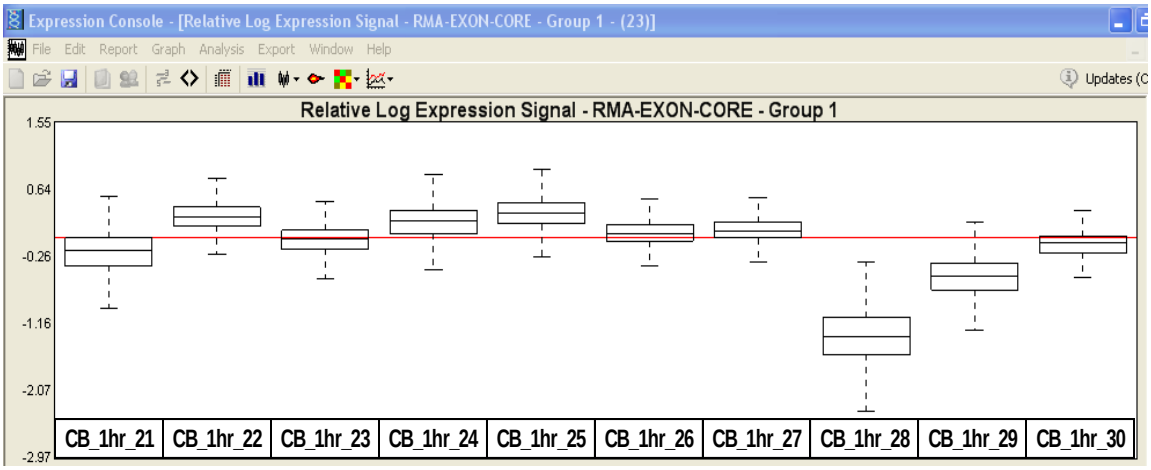

Figure 50. Relative signal box plot of raw cerebellum data.

The Pearson's correlation signal plot of the raw data shows that all samples have a good correlation with the lowest correlation coefficient being 0.972. Sample CB_1hr_28 has the lowest correlation of the data set, while sample CB_1hr_21 has a lower correlation than most of the data set.

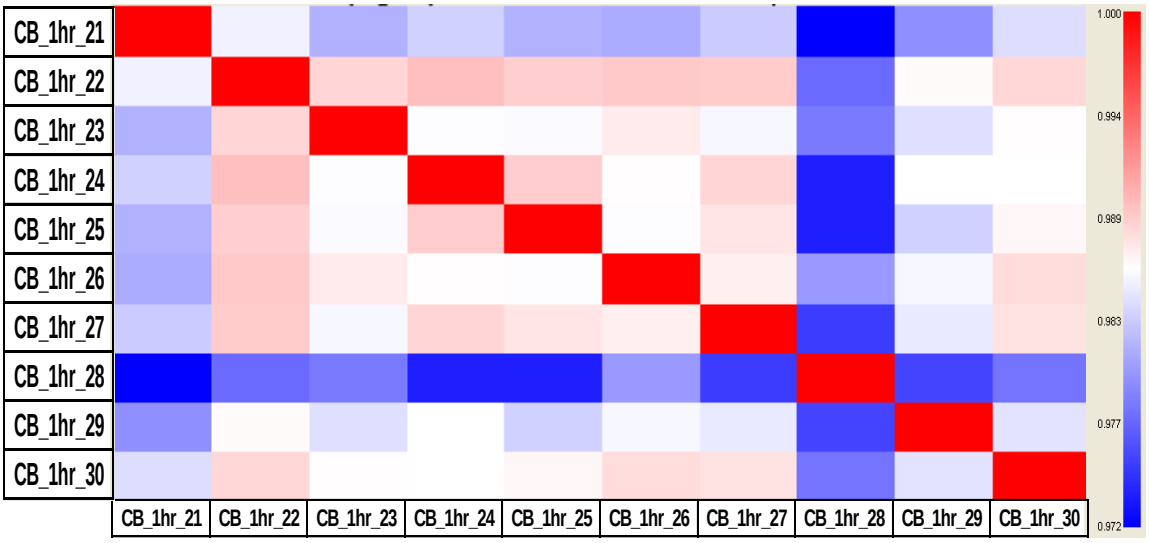

Figure 51. Pearson's correlation plot of raw cerebellum data.

Normalized Data

The tabular report for the normalized data shows that the sample CB_1hr_28 has a %P of 69.1, a value that is significantly lower than that of other samples. This is probably due to the low signal of CB_1hr_28. However, its pos_vs_neg_auc is about the same as that of other samples, while it has the highest dabg_pos_vs_neg_auc among all the samples.

The signal histogram for the normalized data is greatly improved from the plot of the raw data. However it is still a little uneven and shows a lot of variance in signal intensity.

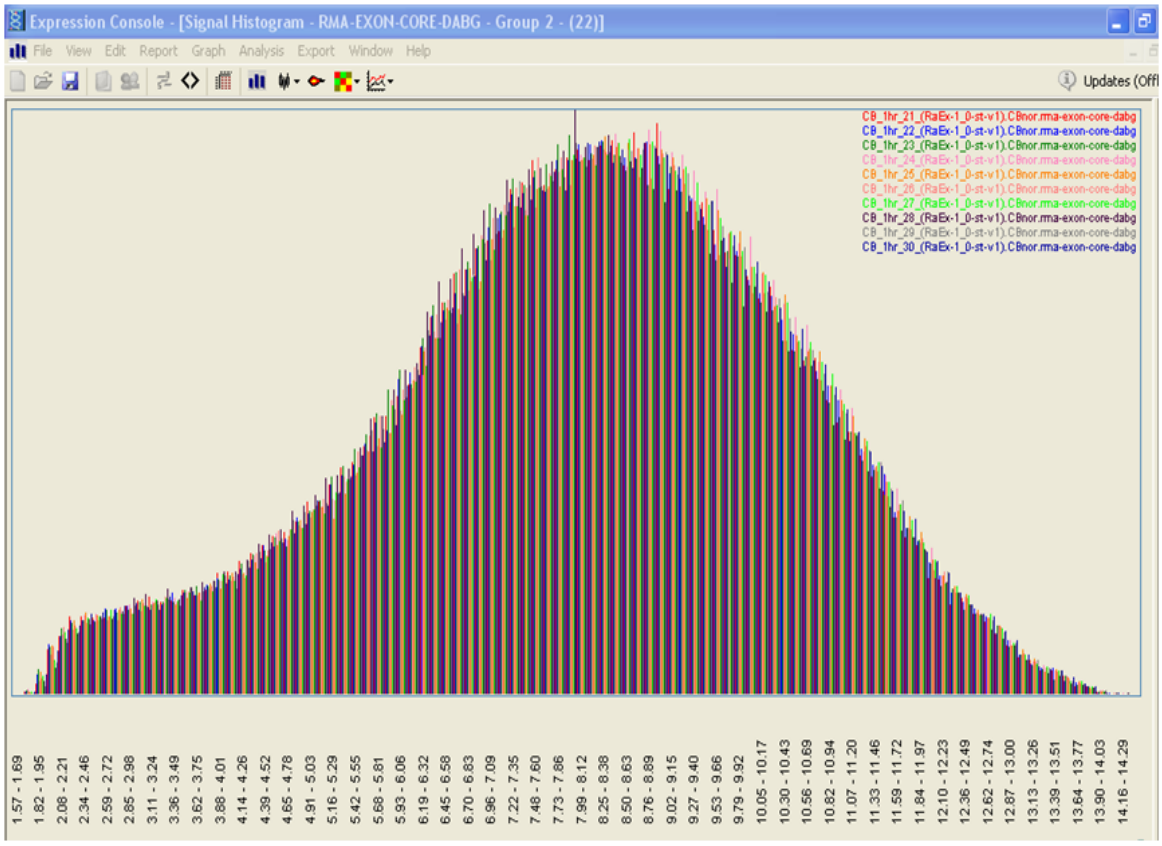

Figure 52. Signal histogram of normalized cerebellum data.

The relative signal box plot of the normalized data is quite even with most samples falling well on the median line. Sample CB_1hr_28 falls somewhat below this line and has the broadest

signal distribution among all samples. Sample CB_1hr_21 also has a slightly increased signal distribution in comparison to the rest of the data set.

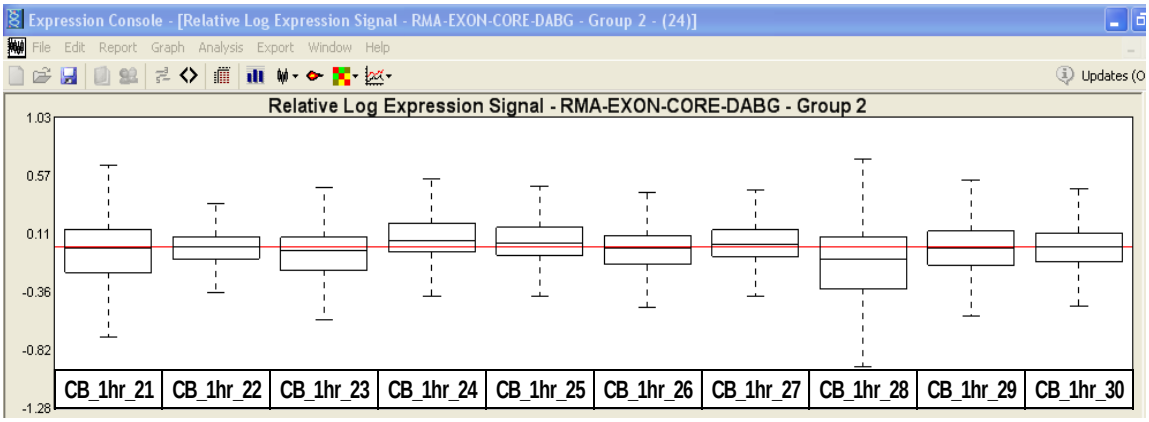

Figure 53. Relative signal box plot of normalized cerebellum data.

The Pearson's correlation plot for the normalized data shows that all samples have a good correlation with the lowest correlation coefficient being 0.972. Samples CB_1hr_21 and CB_1hr_28 appear to have lower correlations than the rest of the dataset.

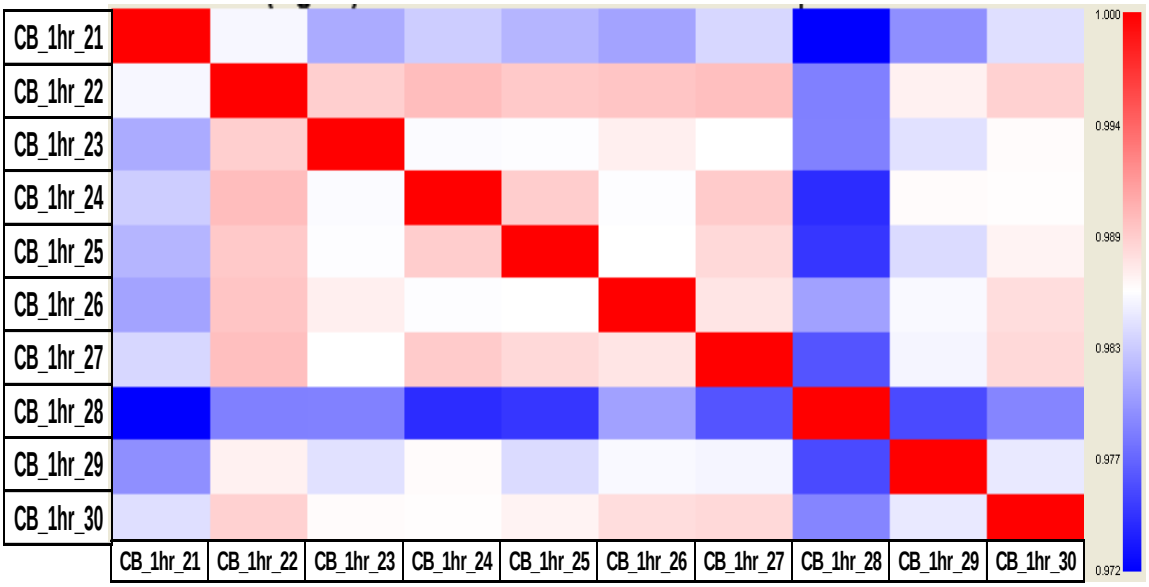

Figure 54. Pearson's correlation plot of normalized cerebellum data.

Comment and Suggestion

The signal of sample CB_1hr_28 is significantly lower than that of other chips even after normalization. Additionally, it shows the lowest correlation with other chips. Sample CB_1hr_21 also shows a decreased correlation with other chips. These two samples should probably be excluded from the dataset.

7.4 Quality control analysis of hippocampus gene array

Raw Data

The tabular text report for the raw data shows that although there are variations in the raw signals among the samples, the difference between the highest and the lowest samples is less than that observed in other brain regions.

The signal histogram for the raw data has some uneven peaks throughout but only one sample (HP_1hr_38) stands out significantly. This sample is shifted to the left of the rest and is an indicator of a weaker signal.

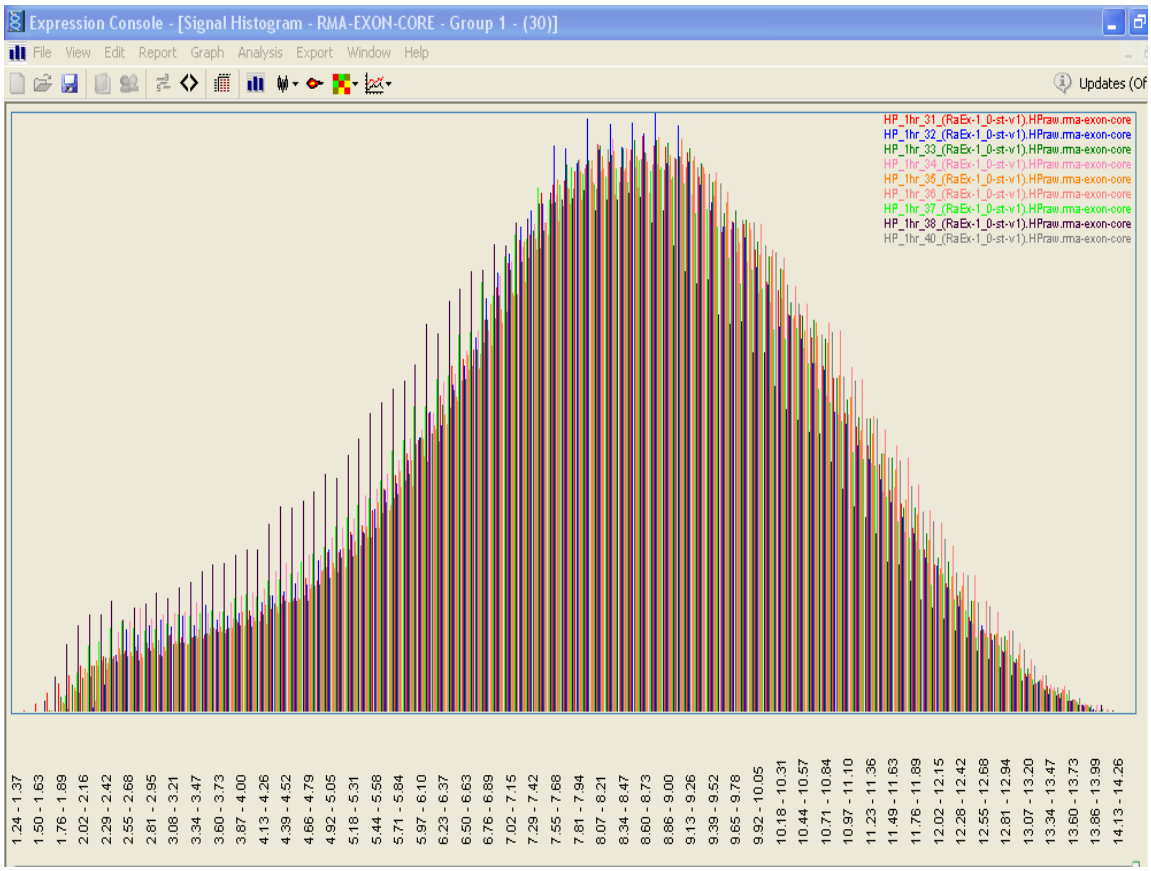

Figure 55. Signal histogram of raw hippocampus data.

The relative signal box plot for the raw data has some variation throughout with most of the sample staying close to the median line. Sample 38 is most noticeably below the median. Sample 37 is slightly below the median and samples 36 and 40 are slightly above the median.

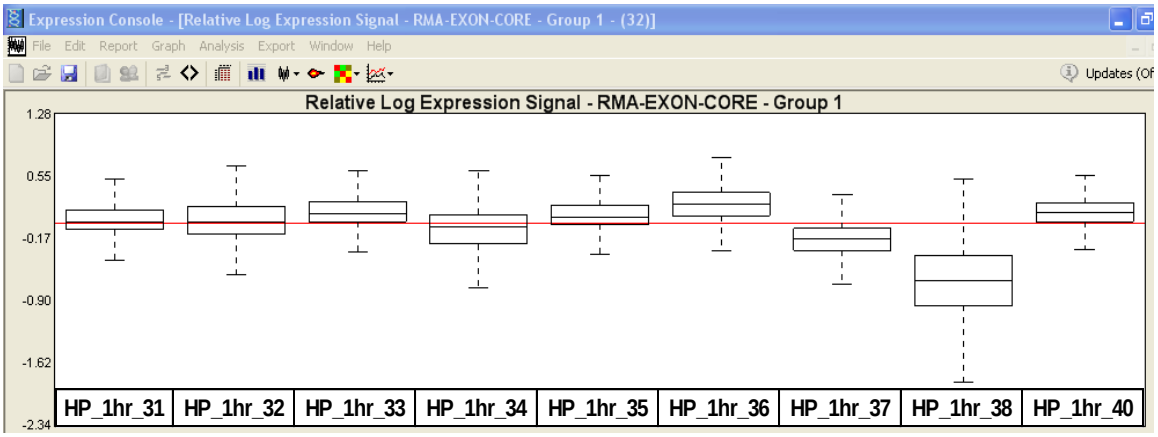

Figure 56. Relative signal box plot of raw hippocampus data.

The Pearson's correlation plot of the raw data shows that all samples have correlation coefficient of 0.964 or above. Sample 38 however shows much lower correlation values than the rest of the data set.

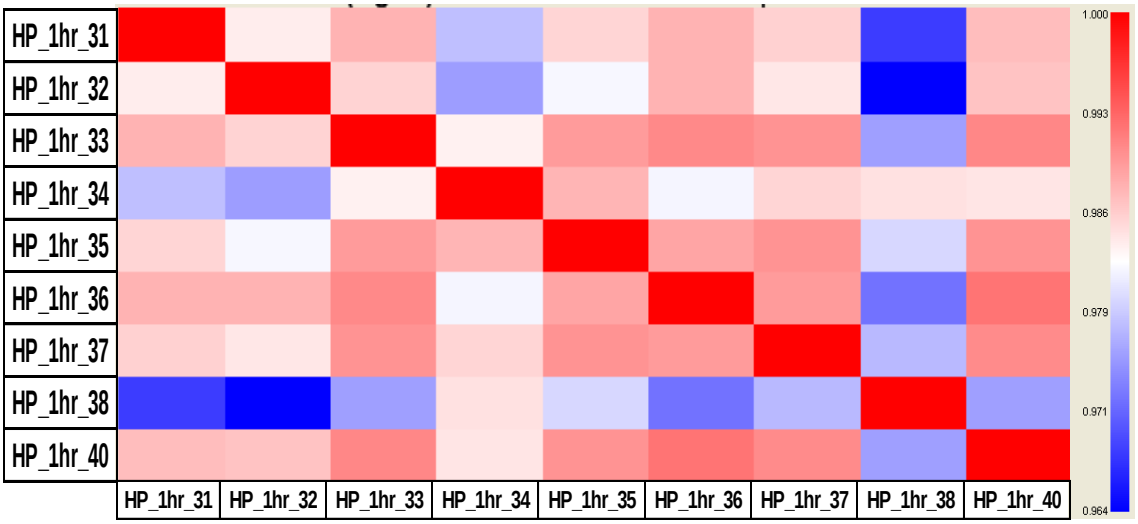

Figure 57. Pearson's correlation plot of raw hippocampus data.

Normalized Data

The tabular report for the normalized data shows that sample HP_1hr_38 has the lowest %P (~72), while that of HP_1hr_31 is the highest (>77). However, other QC metrics of HP_1hr_38

(including pos_vs_neg_auc and dabg_pos_vs_neg_auc, etc.) are very similar to that of other chips. HP_1hr_38 does show a lower correlation with other samples (the lowest being 0.964).

The signal histogram for the normalized data is much smoother then the raw signal histogram. Sample 32 is slightly shifted to the left but may not be considered as an outlier.

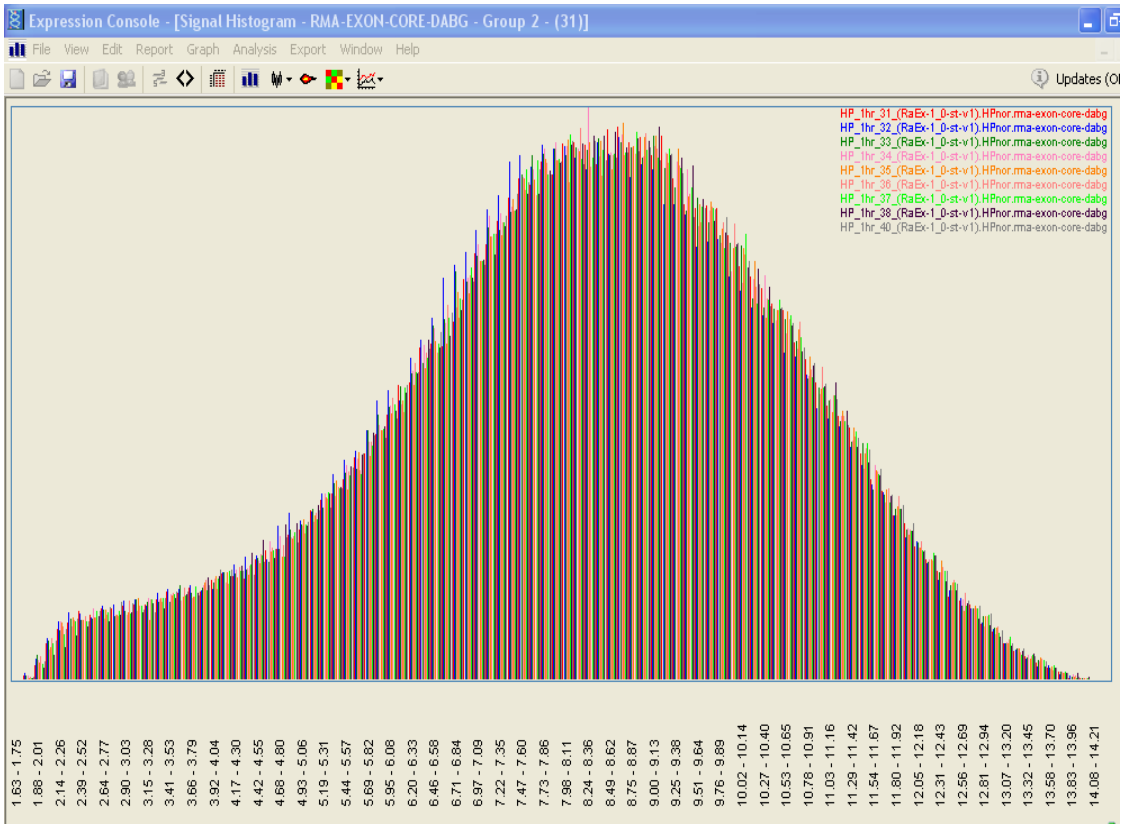

Figure 58. Signal histogram of normalized hippocampus data.

The relative signal box plot for the normalized data shows all samples falling very close to the median line. Sample 38 has a broader signal distribution when compared to the rest of the samples.

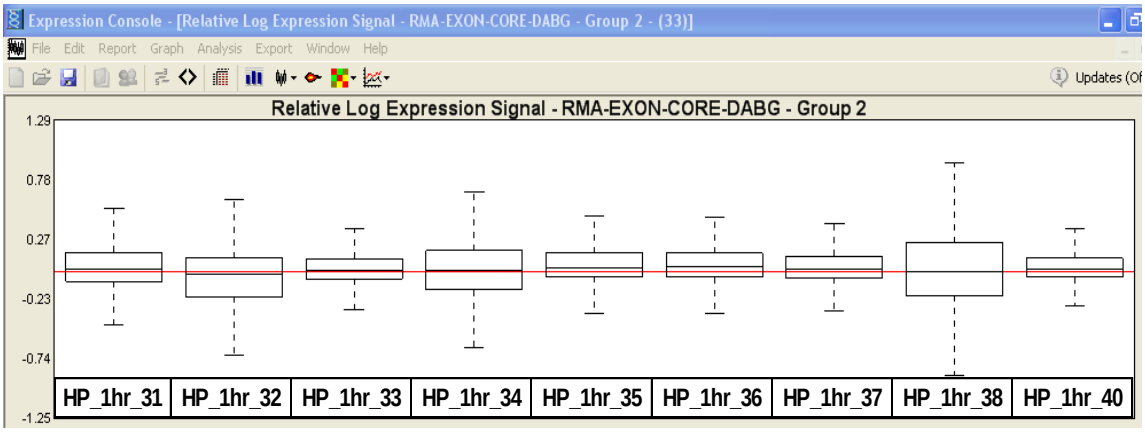

Figure 59. Relative signal box plot of normalized hippocampus data.

The Pearson's correlation plot of the normalized data looks much like that of the raw data. All samples have 0.965 or more and sample 38 shows the lowest correlation than the rest of the samples.

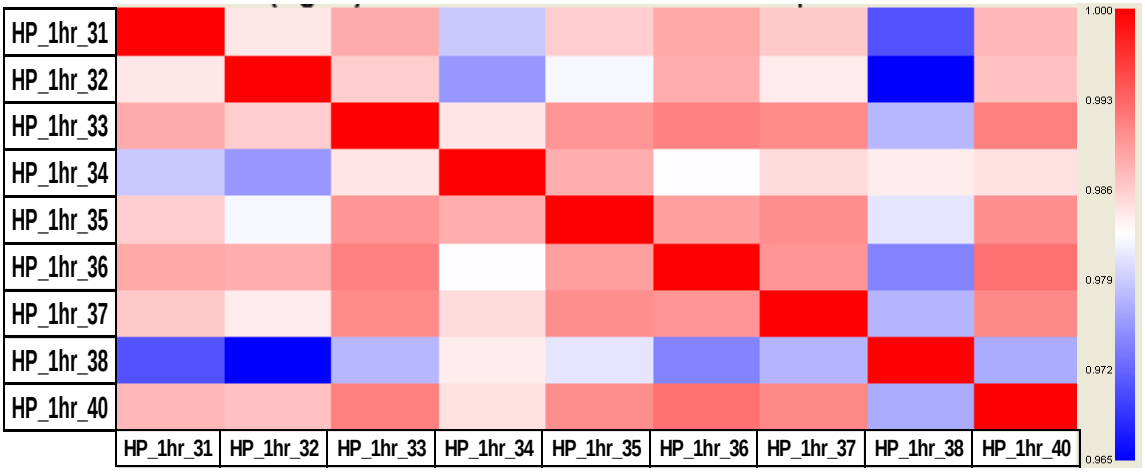

Figure 60. Pearson's correlation plot of normalized hippocampus data.

Comment and Suggestion

Although the raw signal of sample HP_1hr_38 is significantly lower than that of other chips, the normalization step did bring it up to the median line. However, it has a somewhat broader signal distribution than that of the others, as well as a lower correlation with other samples (especially

HP_1hr_31 and HP_1hr_32). Considering the quality of HP_1hr_38 and the numbers of samples in the control and DFP groups, HP_1hr_38 should probably be excluded from the dataset.

VIII. APPENDIX III

8.1 Differential gene expression in cortex

Table 19. List of significantly up- and down-regulated genes in the cortex at 1 hr post 1 mg/kg DFP exposure ($p<0.05$).

Gene Symbol	Transcript Cluster ID	Control P Call[a]	DFP P Call[a]	Fold Change[b]	Differential Gene Expression (p-val)
ly6g6e	7220633	A	P	1.2710	0.0062
rgd1563319_predicted	7058913	A	P	1.1680	0.0479
nmur2	7077638	A	P	1.0475	0.0183
clca2	7215247	A	P	1.0381	0.0091
pcolce	7101091	P	P	1.2000	0.0074
ptgds	7236819	P	P	1.1777	0.0492
ppapdc2	7040998	P	P	-1.1503	0.0068
chd6_predicted	7247512	P	P	-1.1503	0.0500
ppp1r9a	7250817	P	P	-1.1503	0.0212
stau1	7248027	P	P	-1.1503	0.0269
b3galt5_predicted	7087139	P	P	-1.1511	0.0041
ikbkap	7286561	P	P	-1.1511	0.0226
lats2_predicted	7138580	P	P	-1.1511	0.0487
ddx24	7309953	P	P	-1.1511	0.0232
gabrg3	7051876	P	P	-1.1511	0.0422
rgd1565966_predicted	7259993	P	P	-1.1511	0.0451
tparl	7124803	P	P	-1.1519	0.0279
arid4b	7165280	P	P	-1.1519	0.0222
rgd1311340_predicted	7060851	P	P	-1.1519	0.0364
loc315676	7345882	P	P	-1.1519	0.0486
rps6ka2	7027386	P	P	-1.1519	0.0154
loc500392	7282942	P	P	-1.1519	0.0351
ung	7103033	P	P	-1.1519	0.0132
mme	7194580	P	P	-1.1519	0.0014
crhr1	7072608	P	P	-1.1519	0.0425
lsm14a_predicted	7050065	P	P	-1.1519	0.0319
zc3h8	7244736	P	P	-1.1527	0.0497
loc682082	7120010	P	P	-1.1527	0.0415
map3k4_predicted	7027136	P	P	-1.1527	0.0040

cttnbp2	7262584	P	P	-1.1527	0.0321
olr59	7034855	P	P	-1.1527	0.0293
uble1a	7048375	P	P	-1.1535	0.0383
rgd1564821_predicted	7313538	P	P	-1.1535	0.0399
mtf2	7122533	P	P	-1.1535	0.0317
fcmd_predicted	7275208	P	P	-1.1535	0.0005
rab3c	7203733	P	P	-1.1543	0.0215
zfml_predicted	7255517	P	P	-1.1551	0.0452
fbxo34_predicted	7131094	P	P	-1.1551	0.0058
rgd1559742_predicted	7175146	P	P	-1.1551	0.0243
slco2b1	7054899	P	P	-1.1551	0.0277
loc499258	7190524	P	P	-1.1551	0.0024
anxa11	7142829	P	P	-1.1551	0.0482
cul5	7345821	P	P	-1.1551	0.0047
usp24_predicted	7278018	P	P	-1.1559	0.0415
rnf19_predicted	7326587	P	P	-1.1567	0.0159
slc16a7	7326050	P	P	-1.1567	0.0415
grik2	7224361	P	P	-1.1567	0.0150
rgd1308284_predicted	7201429	P	P	-1.1567	0.0422
tlk1_predicted	7240022	P	P	-1.1575	0.0042
rgd1308133_predicted	7328693	P	P	-1.1575	0.0127
psme4	7122317	P	P	-1.1575	0.0318
ppp3r1	7121341	P	P	-1.1583	0.0011
loc682319	7238202	P	P	-1.1583	0.0353
jmjd1a	7265928	P	P	-1.1591	0.0152
slc2a3	7269356	P	P	-1.1591	0.0487
ppp1r12a	7314682	P	P	-1.1591	0.0159
tcerg1_predicted	7169917	P	P	-1.1599	0.0312
ptgfrn	7212112	P	P	-1.1599	0.0219
pcdh8	7140465	P	P	-1.1599	0.0146
rgd1563278_predicted	7087855	P	P	-1.1599	0.0115
sdad1	7116943	P	P	-1.1599	0.0102
actr8_predicted	7143057	P	P	-1.1599	0.0313
mgc112775	7278605	P	P	-1.1607	0.0075
sorcs1_predicted	7063716	P	P	-1.1607	0.0091
rgd1564304_predicted	7233239	P	P	-1.1615	0.0229
mina	7092362	P	P	-1.1615	0.0327
pip3ap	7190771	P	P	-1.1615	0.0008
scyl2_predicted	7323630	P	P	-1.1615	0.0051
rgd1564243_predicted	7229382	P	P	-1.1623	0.0071
fxna	7061738	P	P	-1.1631	0.0214

rab11fip2_predicted	7064282	P	P	-1.1639	0.0184
pde4b	7277759	P	P	-1.1639	0.0001
rgd1561597_predicted	7231650	P	P	-1.1639	0.0338
appbp2	7080918	P	P	-1.1647	0.0159
loc361929	7193056	P	P	-1.1655	0.0171
rgd1560157_predicted	7263015	P	P	-1.1655	0.0251
gpr22_predicted	7305518	P	P	-1.1655	0.0281
asns	7262054	P	P	-1.1655	0.0463
hps6	7042520	P	P	-1.1663	0.0056
gabrd	7293733	P	P	-1.1663	0.0417
adam17	7305030	P	P	-1.1663	0.0182
klhl22_predicted	7095327	P	P	-1.1663	0.0005
snx13_predicted	7297384	P	P	-1.1672	0.0290
cybasc3	7039697	P	P	-1.1672	0.0004
ythdf3_predicted	7192186	P	P	-1.1672	0.0330
slc16a1	7197677	P	P	-1.1672	0.0235
pitrm1_predicted	7166245	P	P	-1.1672	0.0150
slc25a30	7140153	P	P	-1.1680	0.0443
rgd1308297	7141456	P	P	-1.1680	0.0137
loc294560	7367579	P	P	-1.1688	0.0122
ldha	7031732	P	P	-1.1688	0.0342
xpo1	7121841	P	P	-1.1688	0.0212
centb2	7088946	P	P	-1.1688	0.0221
strn4_predicted	7029119	P	P	-1.1696	0.0465
rgd1560288_predicted	7061550	P	P	-1.1696	0.0133
eif5b	7353614	P	P	-1.1696	0.0033
prpf31_predicted	7047524	P	P	-1.1704	0.0272
gyk	7381764	P	P	-1.1704	0.0156
ruvbl1	7255986	P	P	-1.1704	0.0324
rgd1308745_predicted	7230611	P	P	-1.1704	0.0291
loc686794	7107406	P	P	-1.1704	0.0282
rabep1	7069295	P	P	-1.1712	0.0265
rab14	7237876	P	P	-1.1720	0.0161
ets2	7087083	P	P	-1.1728	0.0002
sfrs8	7101643	P	P	-1.1736	0.0275
gdap1_predicted	7282454	P	P	-1.1736	0.0326
foxo1a	7193959	P	P	-1.1745	0.0434
rgd1309765_predicted	7145510	P	P	-1.1745	0.0035
csrp2bp_predicted	7233359	P	P	-1.1753	0.0181
zfp46_predicted	7280640	P	P	-1.1761	0.0005
unc13b	7274462	P	P	-1.1761	0.0254

tmem32_predicted	7384334	P	P	-1.1761	0.0061
actn1	7308330	P	P	-1.1761	0.0039
btbd15	7334334	P	P	-1.1769	0.0317
rgd1563920_predicted	7190584	P	P	-1.1769	0.0283
nfx1	7274267	P	P	-1.1769	0.0097
sema4f	7266506	P	P	-1.1777	0.0220
stxbp5l_predicted	7088544	P	P	-1.1785	0.0269
garnl1	7306743	P	P	-1.1785	0.0491
smpd3	7185072	P	P	-1.1794	0.0190
loc688502	7269834	P	P	-1.1794	0.0064
trpc5	7374009	P	P	-1.1794	0.0148
polr2b_predicted	7124650	P	P	-1.1794	0.0101
rad50	7077420	P	P	-1.1802	0.0389
slc25a29	7310462	P	P	-1.1802	0.0451
rgd1560891_predicted	7375722	P	P	-1.1802	0.0134
hes1	7094386	P	P	-1.1810	0.0044
acsl4	7374114	P	P	-1.1810	0.0001
bbs2	7178810	P	P	-1.1810	0.0332
ddx5	7083616	P	P	-1.1810	0.0021
cacna2d3	7148574	P	P	-1.1810	0.0036
rgd1562456_predicted	7204917	P	P	-1.1818	0.0100
ctns_predicted	7079678	P	P	-1.1818	0.0263
vps16	7232578	P	P	-1.1818	0.0381
rgd1563620_predicted	7158419	P	P	-1.1818	0.0462
smarca5_predicted	7180178	P	P	-1.1818	0.0438
rgd1304687_predicted	7311646	P	P	-1.1818	0.0266
txnl1	7176469	P	P	-1.1826	0.0267
slc4a11_predicted	7244936	P	P	-1.1826	0.0315
tmem33	7125361	P	P	-1.1835	0.0023
ocrl	7377457	P	P	-1.1843	0.0154
brd8	7174341	P	P	-1.1843	0.0201
ifnar1_predicted	7086751	P	P	-1.1843	0.0123
vps35	7179671	P	P	-1.1843	0.0019
rgd1309821_predicted	7285358	P	P	-1.1851	0.0053
phtf1	7197646	P	P	-1.1851	0.0415
wrnip1	7163963	P	P	-1.1851	0.0064
bhlhb9	7377146	P	P	-1.1859	0.0027
psip1	7288108	P	P	-1.1859	0.0104
wdsof1_predicted	7316378	P	P	-1.1867	0.0004
loc302855	7384409	P	P	-1.1867	0.0226
epha6_predicted	7087282	P	P	-1.1867	0.0091

tomm70a	7092521	P	P	-1.1876	0.0016
klf5	7134502	P	P	-1.1876	0.0441
neto2_predicted	7179618	P	P	-1.1876	0.0180
rgd1561347_predicted	7280055	P	P	-1.1884	0.0304
pik3c3	7168785	P	P	-1.1884	0.0222
usp11	7379200	P	P	-1.1884	0.0103
dcp2_predicted	7170052	P	P	-1.1892	0.0053
cdh8	7178411	P	P	-1.1892	0.0074
rgd1563192_predicted	7170080	P	P	-1.1900	0.0222
senp2	7094920	P	P	-1.1900	0.0196
sypl	7297253	P	P	-1.1909	0.0047
pank3_predicted	7066268	P	P	-1.1909	0.0098
loc362994	7320536	P	P	-1.1917	0.0387
ncoa6ip_predicted	7272299	P	P	-1.1917	0.0223
matk	7322009	P	P	-1.1917	0.0344
rgd1308916_predicted	7331805	P	P	-1.1925	0.0272
klhl9_predicted	7288433	P	P	-1.1925	0.0129
rgd1560736_predicted	7339286	P	P	-1.1925	0.0230
mtmr4_predicted	7070858	P	P	-1.1925	0.0226
herc3_predicted	7254229	P	P	-1.1925	0.0432
dapk1_predicted	7161563	P	P	-1.1925	0.0192
atp2c1	7349651	P	P	-1.1925	0.0027
ppil4_predicted	7024728	P	P	-1.1933	0.0018
cast	7201367	P	P	-1.1933	0.0493
rgd1560909_predicted	7353732	P	P	-1.1933	0.0283
lrrtm3_predicted	7222712	P	P	-1.1942	0.0153
smarca1_predicted	7384017	P	P	-1.1942	0.0467
hps3_predicted	7206804	P	P	-1.1942	0.0150
loc685009	7054929	P	P	-1.1942	0.0422
clcc1	7198031	P	P	-1.1950	0.0101
ddx46	7161974	P	P	-1.1950	0.0187
rgd1305020_predicted	7234434	P	P	-1.1950	0.0282
rpo1-2	7232482	P	P	-1.1958	0.0108
cdh9_predicted	7190970	P	P	-1.1958	0.0323
rtn4	7122174	P	P	-1.1958	0.0019
plk2	7189518	P	P	-1.1958	0.0120
agtpbp1_predicted	7155116	P	P	-1.1958	0.0097
nup155	7190518	P	P	-1.1966	0.0008
nol9	7281877	P	P	-1.1966	0.0265
pafah1b2	7345103	P	P	-1.1966	0.0289
cntn4	7256986	P	P	-1.1975	0.0066

loc606294	7222960	P	P	-1.1975	0.0102
cand1	7325522	P	P	-1.1975	0.0096
rgd1566090_predicted	7111046	P	P	-1.1975	0.0360
arntl	7035625	P	P	-1.1983	0.0096
bai3_predicted	7360518	P	P	-1.1983	0.0330
crlz1	7124168	P	P	-1.1983	0.0269
cspg6	7043235	P	P	-1.1991	0.0233
lnp_predicted	7240346	P	P	-1.1991	0.0053
loc682552	7370477	P	P	-1.1991	0.0492
zdhhc13	7031771	P	P	-1.2008	0.0459
rgd1307325	7151422	P	P	-1.2008	0.0115
ehmt2	7220672	P	P	-1.2008	0.0374
wbp4	7140489	P	P	-1.2016	0.0041
rgd1564397_predicted	7384188	P	P	-1.2016	0.0249
pcdhb13	7169550	P	P	-1.2033	0.0336
thap1	7152707	P	P	-1.2033	0.0045
grm8	7262990	P	P	-1.2050	0.0431
ctps_predicted	7290659	P	P	-1.2058	0.0111
stx7	7044991	P	P	-1.2066	0.0406
uck2	7113627	P	P	-1.2066	0.0198
epha7	7273556	P	P	-1.2066	0.0145
itch	7234287	P	P	-1.2066	0.0456
loc297530	7257651	P	P	-1.2075	0.0079
lmo7	7134690	P	P	-1.2075	0.0048
myo1b	7354333	P	P	-1.2075	0.0016
lzts1	7144503	P	P	-1.2075	0.0146
kpna3	7138937	P	P	-1.2083	0.0058
tollip_predicted	7058842	P	P	-1.2100	0.0165
rgd1307724_predicted	7104052	P	P	-1.2108	0.0012
rps6kb1	7081292	P	P	-1.2117	0.0392
gspt1	7064697	P	P	-1.2142	0.0118
atp5a1	7172368	P	P	-1.2142	0.0056
apaf1	7323725	P	P	-1.2150	0.0480
tgfbr1	7274897	P	P	-1.2159	0.0194
adss_predicted	7114537	P	P	-1.2159	0.0453
gpr88	7213152	P	P	-1.2167	0.0237
bhlhb5_predicted	7192231	P	P	-1.2176	0.0005
kremen1	7127825	P	P	-1.2176	0.0033
rgd1305255_predicted	7325674	P	P	-1.2184	0.0273
efnb2_predicted	7147985	P	P	-1.2193	0.0125
taok1	7070080	P	P	-1.2193	0.0338

col4a3bp_predicted	7188638	P	P	-1.2201	0.0044
tax1bp1	7253847	P	P	-1.2201	0.0461
gpr17	7174148	P	P	-1.2218	0.0041
cyp11b1	7328953	P	P	-1.2218	0.0414
clpx	7337301	P	P	-1.2226	0.0318
trpc4ap	7246986	P	P	-1.2235	0.0146
abcf2_predicted	7249579	P	P	-1.2235	0.0338
rgd1563798_predicted	7236146	P	P	-1.2243	0.0343
rgd1305386	7213641	P	P	-1.2286	0.0027
creld1	7257415	P	P	-1.2294	0.0205
loc362264	7235058	P	P	-1.2303	0.0442
aven_predicted	7231165	P	P	-1.2303	0.0369
yipf4	7303624	P	P	-1.2303	0.0054
kcnab1	7194678	P	P	-1.2329	0.0094
slc2a5	7281641	P	P	-1.2371	0.0164
plcl1	7354667	P	P	-1.2380	0.0353
dnajc10	7229289	P	P	-1.2406	0.0164
st8sia5	7172334	P	P	-1.2414	0.0463
papolg_predicted	7128938	P	P	-1.2414	0.0384
loc691335	7372942	P	P	-1.2431	0.0204
il1rapl1	7381802	P	P	-1.2475	0.0344
rdx	7336159	P	P	-1.2475	0.0075
loc306096	7140946	P	P	-1.2492	0.0111
wdr47	7198029	P	P	-1.2492	0.0056
tspan2	7197536	P	P	-1.2518	0.0122
hnrpr	7280644	P	P	-1.2527	0.0235
papd5_predicted	7183613	P	P	-1.2535	0.0139
rgd1305110_predicted	7128921	P	P	-1.2535	0.0190
atpaf1_predicted	7278598	P	P	-1.2553	0.0235
zbtb25	7308021	P	P	-1.2561	0.0254
dnaja2	7179628	P	P	-1.2561	0.0267
actn2_predicted	7159027	P	P	-1.2561	0.0068
ssb	7228467	P	P	-1.2570	0.0376
accn2	7320698	P	P	-1.2588	0.0026
pacsin3	7229978	P	P	-1.2614	0.0101
gucy1a3	7210088	P	P	-1.2614	0.0000
rgd1308557_predicted	7272431	P	P	-1.2623	0.0374
strn	7302571	P	P	-1.2640	0.0212
psmd11_predicted	7070233	P	P	-1.2675	0.0187
spock3_predicted	7150497	P	P	-1.2684	0.0121
loc683283	7266023	P	P	-1.2710	0.0245

rab3gap2	7108733	P	P	-1.2746	0.0247
ephb6	7253088	P	P	-1.2746	0.0426
gpc4	7384216	P	P	-1.2754	0.0094
idh3a	7336340	P	P	-1.2781	0.0335
rgs8	7106406	P	P	-1.2790	0.0340
vcpip1	7272087	P	P	-1.2843	0.0023
ap1g1	7180943	P	P	-1.2852	0.0249
rgd1563860_predicted	7381372	P	P	-1.2870	0.0255
zfyve20_predicted	7267350	P	P	-1.2906	0.0156
chordc1_predicted	7333276	P	P	-1.2941	0.0351
rgd1306526_predicted	7197758	P	P	-1.2941	0.0249
thumpd1	7056723	P	P	-1.3013	0.0270
akap5	7299483	P	P	-1.3022	0.0040
loc303067	7076750	P	P	-1.3041	0.0019
cse1l_predicted	7235503	P	P	-1.3068	0.0156
mtdh	7316024	P	P	-1.3077	0.0376
rgs9	7083866	P	P	-1.3077	0.0005
rbm34	7186753	P	P	-1.3095	0.0301
pdap1	7096516	P	P	-1.3213	0.0052
hrmt1l3	7031833	P	P	-1.3250	0.0271
ugt8	7213846	P	P	-1.3296	0.0170
scn4b	7335651	P	P	-1.3351	0.0232
st8sia1	7271000	P	P	-1.3435	0.0160
nlgn1	7206998	P	P	-1.3510	0.0034
pdyn	7244787	P	P	-1.5052	0.0441
rgd1564914_predicted	7294851	P	P	-1.6632	0.0153
rgd1308113	7138227	P	A	-1.0098	0.0086
card15_predicted	7183538	P	A	-1.0182	0.0459
syk	7162313	P	A	-1.0295	0.0309
mgam_predicted	7252877	P	A	-1.0353	0.0214
isg20l1_predicted	7033277	P	A	-1.0403	0.0150
cd80	7093567	P	A	-1.0497	0.0443
rhov	7243592	P	A	-1.0519	0.0289
ddx59	7105549	P	A	-1.0688	0.0480
arhgap27	7083177	P	A	-1.0703	0.0432
chd1_predicted	7027824	P	A	-1.0830	0.0247
rgd1564792_predicted	7249737	P	A	-1.0860	0.0081
cldn22_predicted	7151316	P	A	-1.1057	0.0020
rgd1563090_predicted	7172373	P	A	-1.1204	0.0235
chaf1b	7086975	P	A	-1.1212	0.0151
zfp294	7091191	P	A	-1.1258	0.0098

rgd1306565_predicted	7025395	P	A	-1.1527	0.0411
sart3_predicted	7099072	P	A	-1.1769	0.0179
aste1	7339953	P	A	-1.1835	0.0199

[a]Label refers to the presence call determined by Affymetrix software. For the signal detected by each probe set, the Affymetrix software uses 2 pieces of information: the level of the signal (expression level) and the quality of the signal (real signal versus background noise caused by cross hybridization). If the signal quality is low (detection p value > 0.05) then the software will make an absolute call of whether or not the gene is expressed regardless of the signal strength. A – absent; P – present.

[b]The Affymetrix software will make a fold change calculation based solely on the signal levels without consideration of the detection p values. Therefore, genes that are turned off or on will also show a fold change, although it is meaningless for these genes and can be ignored.

8.2 Differential gene expression in brainstem

Table 20. List of significantly up- and down-regulated genes in the brainstem at 1 hr post 1 mg/kg DFP exposure ($p<0.05$).

Gene Symbol	DFP Present (p-val)	Control P Call[a]	DFP P Call[a]	Fold Change[b]	Differential Gene Expression (p-val)
ccl11	0.0410	A	P	1.2518	0.0363
hpd	0.0484	A	P	1.1983	0.0340
slc23a1	0.0463	A	P	1.1696	0.0102
espn	0.0445	A	P	1.1423	0.0031
btnl8	0.0499	A	P	1.1127	0.0055
loc680712	0.0357	A	P	1.0996	0.0013
gucy2e	0.0272	A	P	1.0762	0.0467
slc2a2	0.0500	A	P	1.0519	0.0008
smyd1_predicted	0.0403	A	P	1.0432	0.0403
mgam_predicted	0.0323	A	P	1.0310	0.0139
hdmcp	0.0464	A	P	1.0288	0.0031
slc26a4	0.0433	A	P	1.0260	0.0081
kif12	0.0384	A	P	1.0210	0.0444
rgd1561153_predicted	0.0304	A	P	1.0161	0.0329
aanat	0.0401	P	P	1.2075	0.0020
olr1451_predicted	0.0107	P	P	1.1843	0.0149
gchfr	0.0148	P	P	1.1810	0.0321
rgd1566127_predicted	0.0022	P	P	1.1712	0.0483
oraov1_predicted	0.0243	P	P	1.1704	0.0060
ppig	0.0003	P	P	-1.4631	0.0432
zmpste24_predicted	0.0000	P	P	-1.3204	0.0382
rgd735140	0.0006	P	P	-1.3131	0.0377
rgd1307966_predicted	0.0013	P	P	-1.3022	0.0174
rgd1305001_predicted	0.0000	P	P	-1.2897	0.0116
stx1a	0.0223	P	P	-1.2861	0.0306
peflin	0.0026	P	P	-1.2746	0.0207
mip1	0.0090	P	P	-1.2702	0.0198
lypla1	0.0114	P	P	-1.2693	0.0160
adprtl1	0.0013	P	P	-1.2684	0.0306
loc499563	0.0016	P	P	-1.2658	0.0234
loc317279	0.0342	P	P	-1.2649	0.0009
tor1aip1	0.0000	P	P	-1.2640	0.0215
loc304725	0.0014	P	P	-1.2457	0.0184
atp11c_predicted	0.0017	P	P	-1.2329	0.0037

rgd1563556_predicted	0.0043	P	P	-1.2303	0.0063
cdh18_predicted	0.0006	P	P	-1.2286	0.0095
pctk2	0.0000	P	P	-1.2226	0.0465
oprk1	0.0015	P	P	-1.2226	0.0286
cacna2d3	0.0000	P	P	-1.2209	0.0185
rgd1562284_predicted	0.0047	P	P	-1.2150	0.0218
cntn6	0.0133	P	P	-1.2134	0.0419
trhr	0.0374	P	P	-1.2125	0.0368
rgd1306256_predicted	0.0060	P	P	-1.2066	0.0275
pgr	0.0173	P	P	-1.2066	0.0263
anapc4	0.0002	P	P	-1.2025	0.0296
lrrc7	0.0000	P	P	-1.2025	0.0407
loc679564	0.0021	P	P	-1.2016	0.0457
mllt3	0.0005	P	P	-1.2000	0.0098
ddx50	0.0014	P	P	-1.1991	0.0406
calb1	0.0000	P	P	-1.1983	0.0148
gabrg3	0.0000	P	P	-1.1975	0.0217
galnt13	0.0000	P	P	-1.1975	0.0286
rgd1310810	0.0005	P	P	-1.1966	0.0431
cul5	0.0000	P	P	-1.1950	0.0469
ppm1a	0.0000	P	P	-1.1942	0.0203
zc3h6_predicted	0.0002	P	P	-1.1925	0.0064
car7_predicted	0.0026	P	P	-1.1917	0.0455
sgtb	0.0001	P	P	-1.1900	0.0368
loc688502	0.0001	P	P	-1.1892	0.0051
jak2	0.0004	P	P	-1.1876	0.0444
tlk2	0.0010	P	P	-1.1867	0.0308
txndc4	0.0004	P	P	-1.1867	0.0310
taf5l	0.0085	P	P	-1.1867	0.0414
ipo7_predicted	0.0022	P	P	-1.1851	0.0336
csnk1g1	0.0008	P	P	-1.1843	0.0092
smarca1_predicted	0.0361	P	P	-1.1843	0.0213
hspa14	0.0069	P	P	-1.1826	0.0245
loc678810	0.0057	P	P	-1.1810	0.0281
rgd1307084	0.0167	P	P	-1.1810	0.0391
snapc1_predicted	0.0046	P	P	-1.1794	0.0055
slc30a1	0.0229	P	P	-1.1785	0.0237
cdkl1_predicted	0.0000	P	P	-1.1761	0.0480
rgd1306259_predicted	0.0064	P	P	-1.1753	0.0122
fkbp5	0.0032	P	P	-1.1753	0.0363
cnksr2	0.0000	P	P	-1.1745	0.0333

kcnt2	0.0031	P	P	-1.1736	0.0232
rgd1309058_predicted	0.0044	P	P	-1.1712	0.0301
rgd1563465_predicted	0.0000	P	P	-1.1704	0.0182
rgd1549725	0.0283	P	P	-1.1696	0.0138
lrrtm3_predicted	0.0000	P	P	-1.1696	0.0424
arf2	0.0194	P	P	-1.1688	0.0178
stk32c_predicted	0.0002	P	P	-1.1688	0.0275
loc689617	0.0072	P	P	-1.1688	0.0394
mobk1b	0.0011	P	P	-1.1672	0.0324
loc367153	0.0118	P	P	-1.1663	0.0096
gpr22_predicted	0.0002	P	P	-1.1655	0.0131
grpca	0.0471	P	P	-1.1655	0.0319
pigh_predicted	0.0159	P	P	-1.1631	0.0404
ahctf1_predicted	0.0000	P	P	-1.1623	0.0360
fez2	0.0190	P	P	-1.1615	0.0203
arntl	0.0114	P	P	-1.1591	0.0316
ift74	0.0006	P	P	-1.1591	0.0472
srm	0.0000	P	P	-1.1583	0.0152
papd4	0.0000	P	P	-1.1583	0.0336
pafah1b2	0.0000	P	P	-1.1567	0.0070
rab5a	0.0004	P	P	-1.1551	0.0034
rab3b	0.0016	P	P	-1.1551	0.0420
ssx2ip	0.0001	P	P	-1.1543	0.0167
loc682303	0.0124	P	P	-1.1535	0.0176
rgd1310137	0.0232	P	P	-1.1527	0.0036
lrfn5_predicted	0.0001	P	P	-1.1527	0.0153
xrn1_predicted	0.0040	P	P	-1.1519	0.0223
oxr1	0.0000	P	P	-1.1519	0.0103
soat	0.0477	P	P	-1.1511	0.0337
rgd1560796_predicted	0.0011	P	P	-1.1511	0.0092
klhl8_predicted	0.0000	P	P	-1.1511	0.0254
ckm	0.0530	P	A	-1.2702	0.0068
nov	0.1610	P	A	-1.2596	0.0359
loc361473	0.0531	P	A	-1.2371	0.0118
rnf6_predicted	0.0514	P	A	-1.1975	0.0260
usp12_predicted	0.0578	P	A	-1.1583	0.0439
dnmt2	0.0564	P	A	-1.1282	0.0431
daxx	0.0521	P	A	-1.1127	0.0282
camlg	0.0604	P	A	-1.1119	0.0270
zcchc11_predicted	0.0883	P	A	-1.1034	0.0404
rgd1308632	0.0538	P	A	-1.0981	0.0029

kcnn4	0.0705	P	A	-1.0762	0.0394
mrps9	0.0524	P	A	-1.0417	0.0052
loc288750	0.0518	P	A	-1.0217	0.0483
rgd1311358	0.0526	P	A	-1.0084	0.0425
rgd1564727_predicted	0.0512	P	A	-1.0014	0.0180

[a]Label refers to the presence call determined by Affymetrix software. For the signal detected by each probe set, the Affymetrix software uses 2 pieces of information: the level of the signal (expression level) and the quality of the signal (real signal versus background noise caused by cross hybridization). If the signal quality is low (detection p value > 0.05) then the software will make an absolute call of whether or not the gene is expressed regardless of the signal strength. A – absent; P – present.

[b]The Affymetrix software will make a fold change calculation based solely on the signal levels without consideration of the detection p values. Therefore, genes that are turned off or on will also show a fold change, although it is meaningless for these genes and can be ignored.

8.3 Differential gene expression in cerebellum

Table 21. List of significantly up- and down-regulated genes in the cerebellum at 1 hr post 1 mg/kg DFP exposure ($p<0.05$).

Gene Symbol	Transcript Cluster ID	Control P Call[a]	DFP P Call[a]	Fold Change[b]	Differential Gene Expression (p-val)
npas4	7059690	A	P	1.4409	0.0230
prss1	7253051	A	P	1.1851	0.0321
npy5r	7144617	A	P	1.1487	0.0358
loc682898	7373679	A	P	1.1479	0.0157
ubxd3	7292372	A	P	1.1400	0.0108
pex11c_predicted	7096062	A	P	1.1368	0.0104
rom1	7060215	A	P	1.1034	0.0019
mpo	7070870	A	P	1.1004	0.0197
loc686178	7152914	A	P	1.0981	0.0275
loc686966	7142343	A	P	1.0935	0.0190
loc682124	7115871	A	P	1.0468	0.0470
dusp2	7232331	A	P	1.0353	0.0124
col27a1	7275821	A	P	1.0154	0.0445
nr4a2	7239111	P	P	1.5476	0.0346
fos	7300295	P	P	1.5021	0.0359
rgd1305207	7320961	P	P	1.4113	0.0319
nr4a3	7274931	P	P	1.3232	0.0333
dusp1	7066011	P	P	1.2843	0.0289
tessp5	7340732	P	P	1.2518	0.0208
tnfrsf4	7282381	P	P	1.1892	0.0176
mafg	7085198	P	P	1.1769	0.0161
zfp206_predicted	7065316	P	P	1.1753	0.0026
trib1	7317342	P	P	1.1623	0.0383
heyl_predicted	7279240	P	P	1.1599	0.0189
rgd1560065_predicted	7200445	P	P	-1.3822	0.0007
eif3s6	7327087	P	P	-1.3794	0.0259
cbr4	7150589	P	P	-1.3538	0.0119
morf4l2	7383689	P	P	-1.3351	0.0074
rgd1304686	7039157	P	P	-1.3268	0.0106
pin1_predicted	7333428	P	P	-1.3186	0.0395
jtb	7196390	P	P	-1.3113	0.0146
hbxip_predicted	7197893	P	P	-1.3013	0.0055
cmpk	7290094	P	P	-1.2977	0.0323
idi1	7166170	P	P	-1.2941	0.0013

tmem22	7349372	P	P	-1.2941	0.0326
atox1	7077604	P	P	-1.2941	0.0380
cox4i2	7233997	P	P	-1.2843	0.0430
arl4a	7305953	P	P	-1.2781	0.0109
mki67ip	7104286	P	P	-1.2719	0.0269
rps7	7305265	P	P	-1.2605	0.0168
sult1a1	7057289	P	P	-1.2579	0.0176
tmem49	7081108	P	P	-1.2509	0.0125
crtam_predicted	7344444	P	P	-1.2501	0.0134
gnmt	7352038	P	P	-1.2492	0.0250
loc499779	7237617	P	P	-1.2466	0.0416
loc363484	7376206	P	P	-1.2457	0.0299
rnut1	7336565	P	P	-1.2440	0.0457
rgd1565441_predicted	7376584	P	P	-1.2431	0.0256
ssr3	7209291	P	P	-1.2423	0.0018
chic2_predicted	7117936	P	P	-1.2414	0.0044
rnf138	7168316	P	P	-1.2406	0.0036
akr7a2	7280974	P	P	-1.2397	0.0036
ttpa	7273147	P	P	-1.2388	0.0428
paip1_predicted	7190069	P	P	-1.2337	0.0093
march2	7322862	P	P	-1.2286	0.0225
cldn12_predicted	7250545	P	P	-1.2243	0.0112
rgd1563459_predicted	7068965	P	P	-1.2218	0.0249
tmco1	7107464	P	P	-1.2218	0.0388
txnl2	7037921	P	P	-1.2209	0.0398
timp1	7379138	P	P	-1.2176	0.0398
slc2a10_predicted	7235412	P	P	-1.2167	0.0183
mettl6	7148827	P	P	-1.2159	0.0084
taf11	7221138	P	P	-1.2150	0.0244
loc362129	7238414	P	P	-1.2142	0.0020
loc301117	7370407	P	P	-1.2125	0.0498
mnat1	7299267	P	P	-1.2117	0.0147
znf593_predicted	7291854	P	P	-1.2117	0.0149
loc362304	7249784	P	P	-1.2108	0.0043
rgd1310794	7250681	P	P	-1.2100	0.0281
alkbh3	7242031	P	P	-1.2100	0.0480
cbx7	7329878	P	P	-1.2075	0.0313
fcgr3	7113955	P	P	-1.2075	0.0377
sub1	7205179	P	P	-1.2050	0.0061
cldnd1	7092399	P	P	-1.2025	0.0159
cyb5	7172808	P	P	-1.2016	0.0129

rgd1562933_predicted	7371886	P	P	-1.2008	0.0220
rgd1562794_predicted	7173122	P	P	-1.2008	0.0445
dap3	7210715	P	P	-1.1991	0.0242
loc498396	7120252	P	P	-1.1983	0.0199
gclm	7198646	P	P	-1.1975	0.0409
tsc22d3	7383864	P	P	-1.1950	0.0274
tmem19	7325131	P	P	-1.1942	0.0275
ppil3	7362531	P	P	-1.1942	0.0360
psma6	7298286	P	P	-1.1925	0.0446
bbs4_predicted	7346390	P	P	-1.1917	0.0053
wdr12	7362759	P	P	-1.1917	0.0109
eef1b2_predicted	7355235	P	P	-1.1909	0.0069
ms4a6b	7060488	P	P	-1.1884	0.0083
orc4l	7238623	P	P	-1.1876	0.0308
hsf2	7219178	P	P	-1.1876	0.0396
il13ra1	7378996	P	P	-1.1867	0.0319
rgd1563824_predicted	7027009	P	P	-1.1851	0.0477
atp5f1	7212517	P	P	-1.1843	0.0209
rgd1307449	7365763	P	P	-1.1835	0.0254
rsbn1_predicted	7197644	P	P	-1.1818	0.0148
lrrc35	7344567	P	P	-1.1818	0.0164
mrpl46	7053246	P	P	-1.1810	0.0063
rchy1	7117001	P	P	-1.1810	0.0409
rap2ip	7072450	P	P	-1.1802	0.0024
slc25a20	7340393	P	P	-1.1802	0.0125
metrn	7075592	P	P	-1.1802	0.0364
trim50	7101332	P	P	-1.1794	0.0438
atp5c1	7159732	P	P	-1.1785	0.0155
ilkap	7365239	P	P	-1.1761	0.0047
hmgn1	7092107	P	P	-1.1761	0.0201
tmem138	7060322	P	P	-1.1761	0.0353
cdh7	7104008	P	P	-1.1753	0.0144
eif4a1	7079103	P	P	-1.1753	0.0425
cd74	7170979	P	P	-1.1736	0.0303
d123	7159989	P	P	-1.1720	0.0087
gsbs	7254092	P	P	-1.1712	0.0283
gabra4	7118216	P	P	-1.1704	0.0176
rgd1310320	7110414	P	P	-1.1704	0.0195
psma3	7299062	P	P	-1.1704	0.0338
resp18	7363941	P	P	-1.1696	0.0168
rgd1304748	7142414	P	P	-1.1696	0.0291

tprkb	7255679	P	P	-1.1696	0.0432
nme2	7081660	P	P	-1.1688	0.0027
rgd1311925_predicted	7085130	P	P	-1.1688	0.0231
bap1_predicted	7143236	P	P	-1.1688	0.0358
tada2l	7080793	P	P	-1.1680	0.0141
rgd1311161	7151445	P	P	-1.1680	0.0185
ercc8_predicted	7189404	P	P	-1.1672	0.0371
galnt11	7260392	P	P	-1.1663	0.0330
pcmt1	7043913	P	P	-1.1663	0.0377
mrps12_predicted	7049346	P	P	-1.1647	0.0467
atp1b3	7349069	P	P	-1.1631	0.0122
fbxo22	7336427	P	P	-1.1623	0.0052
loc293589	7038162	P	P	-1.1623	0.0414
surf1	7237053	P	P	-1.1623	0.0446
morf4l1	7114379	P	P	-1.1623	0.0405
rgd1306583	7203374	P	P	-1.1615	0.0263
rgd1309784	7337926	P	P	-1.1615	0.0206
taldo1	7038449	P	P	-1.1607	0.0119
dhx40	7081133	P	P	-1.1607	0.0450
rgd1559909_predicted	7290921	P	P	-1.1599	0.0031
isgf3g	7131960	P	P	-1.1599	0.0490
rgd1304890	7208620	P	P	-1.1599	0.0195
dnajc9_predicted	7129918	P	P	-1.1583	0.0495
rgd1310953	7181438	P	P	-1.1583	0.0140
cops3	7078117	P	P	-1.1583	0.0377
tpst1	7101571	P	P	-1.1567	0.0033
za20d3	7053926	P	P	-1.1567	0.0134
rgd1565289_predicted	7375643	P	P	-1.1567	0.0292
khdrbs3	7317826	P	P	-1.1559	0.0157
rgd1304592_predicted	7271008	P	P	-1.1543	0.0337
dnaja2	7179628	P	P	-1.1535	0.0160
yipf4	7303624	P	P	-1.1527	0.0124
rgd1563352_predicted	7050869	P	P	-1.1527	0.0212
eif3s4	7342899	P	P	-1.1511	0.0264
rgd1559901_predicted	7033268	P	P	-1.1511	0.0094
lmcd1_predicted	7257290	P	P	-1.1511	0.0004
cct4	7121804	P	P	-1.1511	0.0020
prei3	7354648	P	P	-1.1511	0.0253
loc500947	7333100	P	P	-1.1503	0.0367
loc685243	7349579	P	A	-1.2380	0.0206
glipr1	7324926	P	A	-1.2252	0.0056

pi4k2b	7126173	P	A	-1.2075	0.0121
loc500893	7318137	P	A	-1.1313	0.0077
rgd1560328_predicted	7039654	P	A	-1.1235	0.0282
apoh	7073093	P	A	-1.0920	0.0240
chek1	7344093	P	A	-1.0770	0.0426
rgd1304719	7301961	P	A	-1.0267	0.0155

[a]Label refers to the presence call determined by Affymetrix software. For the signal detected by each probe set, the Affymetrix software uses 2 pieces of information: the level of the signal (expression level) and the quality of the signal (real signal versus background noise caused by cross hybridization). If the signal quality is low (detection p value > 0.05) then the software will make an absolute call of whether or not the gene is expressed regardless of the signal strength. A – absent; P – present.

[b]The Affymetrix software will make a fold change calculation based solely on the signal levels without consideration of the detection p values. Therefore, genes that are turned off or on will also show a fold change, although it is meaningless for these genes and can be ignored.

8.4 Differential gene expression in hippocampus

Table 22. List of significantly up- and down-regulated genes in the hippocampus at 1 hr post 1 mg/kg DFP exposure ($p<0.05$).

Gene Symbol	Transcript Cluster ID	Control P Call[a]	DFP P Call[a]	Fold Change[b]	Differential Gene Expression (p-val)
pex11c_predicted	7096062	A	P	1.1511	0.0315
rgd1564139_predicted	7226812	A	P	1.1352	0.0327
cpa6_predicted	7271972	A	P	1.1251	0.0299
rgd1307392_predicted	7300366	A	P	1.0951	0.0027
rgd1311565	7149614	A	P	1.0815	0.0129
slc1a6	7322521	A	P	1.0607	0.0282
rgd1560814_predicted	7131980	P	P	1.3068	0.0132
rragd_predicted	7273845	P	P	1.1591	0.0253
ptges2_predicted	7226278	P	P	-1.1503	0.0219
rgd1561074_predicted	7338955	P	P	-1.1503	0.0385
hrmt1l1	7217751	P	P	-1.1519	0.0313
dhrs7b	7068301	P	P	-1.1535	0.0249
tmie_predicted	7350260	P	P	-1.1535	0.0037
loc307798	7184960	P	P	-1.1535	0.0125
rgd1560783_predicted	7319486	P	P	-1.1543	0.0215
rgd1305276	7169645	P	P	-1.1551	0.0347
rgd1305110_predicted	7128921	P	P	-1.1559	0.0364
trpc3	7207698	P	P	-1.1567	0.0296
birc2	7341989	P	P	-1.1567	0.0123
loc500392	7282942	P	P	-1.1575	0.0126
armcx6	7383569	P	P	-1.1599	0.0025
cdh22	7247856	P	P	-1.1599	0.0109
vps45	7211615	P	P	-1.1607	0.0159
heyl_predicted	7279240	P	P	-1.1607	0.0121
fastk	7249610	P	P	-1.1615	0.0397
loc503000	7281575	P	P	-1.1623	0.0461
nfkbib	7049352	P	P	-1.1623	0.0165
rab34	7080062	P	P	-1.1639	0.0416
dvl1	7282328	P	P	-1.1655	0.0126
rgd1311433_predicted	7074692	P	P	-1.1688	0.0377
dffa	7281533	P	P	-1.1696	0.0237
erp29	7098469	P	P	-1.1704	0.0135
mfng	7329632	P	P	-1.1704	0.0016
sdhb_predicted	7281072	P	P	-1.1712	0.0367

ppm1f	7095530	P	P	-1.1753	0.0075
loc298018	7275427	P	P	-1.1769	0.0262
il3ra	7100909	P	P	-1.1769	0.0100
ctbp2	7058050	P	P	-1.1769	0.0435
abo	7237043	P	P	-1.1785	0.0112
moap1	7309897	P	P	-1.1818	0.0345
rps6ka4_predicted	7059970	P	P	-1.1818	0.0214
rgd1564019_predicted	7237711	P	P	-1.1818	0.0396
map2k2	7322049	P	P	-1.1859	0.0237
rgd1311900_predicted	7120197	P	P	-1.1867	0.0443
dpp10	7110544	P	P	-1.1909	0.0084
gli1	7326245	P	P	-1.1958	0.0225
rgd1305631_predicted	7096970	P	P	-1.1983	0.0071
cd320	7312950	P	P	-1.2050	0.0016
arv1_predicted	7182053	P	P	-1.2100	0.0226
abhd14a	7349759	P	P	-1.2117	0.0084
loc499798	7227487	P	P	-1.2125	0.0170
zfp207	7070228	P	P	-1.2193	0.0485
psmb8	7220914	P	P	-1.2235	0.0018
crip2	7302155	P	P	-1.2260	0.0131
prkg2	7116627	P	P	-1.2269	0.0258
ddx47	7259105	P	P	-1.2277	0.0404
sult1a1	7057289	P	P	-1.2294	0.0300
tmem22	7349372	P	P	-1.2303	0.0072
ubadc1	7236927	P	P	-1.2329	0.0480
irak1bp1_predicted	7338594	P	P	-1.2337	0.0476
hdgfrp3	7053729	P	P	-1.2397	0.0453
mrps12_predicted	7049346	P	P	-1.2406	0.0166
rgd1307475	7137537	P	P	-1.2466	0.0230
rab3b	7278266	P	P	-1.2475	0.0059
fabp3	7279978	P	P	-1.2501	0.0184
pcbp2	7373866	P	P	-1.2509	0.0355
znf593_predicted	7291854	P	P	-1.2509	0.0127
mrpl9	7196794	P	P	-1.2561	0.0275
mgc94555	7135395	P	P	-1.2588	0.0081
loc498029	7073939	P	P	-1.2614	0.0497
rgd1562933_predicted	7371886	P	P	-1.2684	0.0410
ke2	7217033	P	P	-1.2799	0.0350
exosc5_predicted	7029832	P	P	-1.2816	0.0027
loc499947	7248407	P	P	-1.2852	0.0275
camk2d	7198855	P	P	-1.2861	0.0175

ndn	7032357	P	P	-1.2950	0.0040
igfbp6	7321003	P	P	-1.2977	0.0046
mpst	7318588	P	P	-1.3086	0.0498
bri3	7100296	P	P	-1.3140	0.0498
ahcy	7246923	P	P	-1.3296	0.0210
rgd1563497_predicted	7051164	P	P	-1.3538	0.0390
resp18	7363941	P	P	-1.3890	0.0410
map1lc3a	7234297	P	P	-1.4006	0.0279
aqp11	7054680	P	P	-1.4152	0.0273
stard10	7034633	P	P	-1.4499	0.0438
unc119	7079952	P	P	-1.4917	0.0354
coch_predicted	7298004	P	A	-1.2277	0.0141
mafk	7100653	P	A	-1.1591	0.0126
syde1_predicted	7312686	P	A	-1.1527	0.0114
eif1b_predicted	7341468	P	A	-1.1503	0.0187
rgd1566118_predicted	7216807	P	A	-1.1400	0.0219
umps	7088755	P	A	-1.1329	0.0260
myocd	7078672	P	A	-1.1282	0.0089
rgd1307688	7267004	P	A	-1.1196	0.0404
mppe1_predicted	7176727	P	A	-1.1165	0.0020
zcchc11_predicted	7278195	P	A	-1.1127	0.0158
ankrd32_predicted	7201470	P	A	-1.1042	0.0431
cdc25a	7340628	P	A	-1.1019	0.0177
rgd1308612	7236250	P	A	-1.0845	0.0097
ltk_predicted	7243627	P	A	-1.0845	0.0143
traf2_predicted	7236836	P	A	-1.0519	0.0067
rgd1564500_predicted	7339142	P	A	-1.0475	0.0166
ormdl2_predicted	7321465	P	A	-1.0417	0.0384
rnf125_predicted	7168309	P	A	-1.0295	0.0242
sfrp4	7164977	P	A	-1.0182	0.0289

[a]Label refers to the presence call determined by Affymetrix software. For the signal detected by each probe set, the Affymetrix software uses 2 pieces of information: the level of the signal (expression level) and the quality of the signal (real signal versus background noise caused by cross hybridization). If the signal quality is low (detection p value > 0.05) then the software will make an absolute call of whether or not the gene is expressed regardless of the signal strength. A – absent; P – present.

[b]The Affymetrix software will make a fold change calculation based solely on the signal levels without consideration of the detection p values. Therefore, genes that are turned off or on will also show a fold change, although it is meaningless for these genes and can be ignored.

IX. APPENDIX IV

The analyses of cortex lipid extracts from the 48 hr time point were compromised by faulty proton decoupling, creating spectra that contained signals with incomplete or absent decoupling. Therefore, it was impossible to quantify the lipid signals accurately. Because the PtdC signal was quantified from the ^{13}C spectra and used as the internal standard for the ^{31}P spectra signal quantification, the values derived from the phospholipid spectra were also suspect. The decoupling parameters were adjusted and decoupling was restored. The $CDCl_3$ from the small amount of lipid extract that was unused from the initial analysis was evaporated, vials were re-weighed and the remaining lipid was reconstituted with 550 µL of $CDCl_3$. Five hundred microliters were transferred to 5 mm NMR tubes and re-analyzed. Metabolite concentrations were normalized back to the original weight of tissue, although the full amount of lipid from the tissue was not available. Results from the first, non-decoupled analysis and second, decoupled analyses are shown in Table 22. These results are qualitative and are only meaningful relative to the samples that were run together (i.e. control and DFP for the first analysis). The data suggest that, at 48 hr post DFP exposure, the lipid profiles did not change significantly from control.

Table 23. Changes in lipid metabolite concentrations in the cortex 48 hr post 1 mg/kg DFP dose.

	Metabolite Concentration (µmol/g tissue)			
	First Analysis[a]		Second Analysis[b]	
Metabolite	**Control**	**DFP**	**Control**	**DFP**
Total Tissue Weight (g)	0.81 ± 0.03	0.78 ± 0.04	0.81 ± 0.03	0.78 ± 0.04
Phosphatidic acid	0.5 ± 0.06	0.6 ± 0.1	0.09 ± 0.06	0.09 ± 0.03
Cardiolipin	4.0 ± 0.6	3.4 ± 1.7	0.23 ± 0.12	0.22 ± 0.06
Ethanolamine plasmalogen	41.0 ± 2.9	47.9 ± 12.5	2.7 ± 1.4	2.7 ± 1.0
Choline plasmalogen	2.3 ± 1.8	[e]	0.14 ± 0.11	0.12 ± 0.05
Phosphatidylserine	30.8 ± 3.4	40.0 ± 9.2	1.4 ± 0.5	1.5 ± 0.6
Phosphatidyl-ethanolamine	64.4 ± 8.3	75.7 ± 13.0	2.6 ± 0.8	2.5 ± 0.9
Phosphatidylinositol	6.8 ± 1.0	9.5 ± 2.6	0.3 ± .1	0.3 ± 0.1
Phosphatidylcholine	111.7 ± 9.8	132.6 ± 29.1	5.9 ± 2.2	5.7 ± 2.1
Sphingomyelin	14.6 ± 3.3	24.7 ± 12.8	0.5 ± 0.2	0.5 ± 0.2
Cholesterol[c]	172.2 ± 22.1	207.6 ± 32.1	8.4 ± 4.3	9.4 ± 2.9
n3 Fatty acids	40.8 ± 8.9	52.4 ± 12.5	3.5 ± 1.3	3.2 ± 1.3
n6 Fatty acids	52.1 ± 7.0	75.2 ± 28.8	5.3 ± 1.8	5.0 ± 2.2
Polyunsaturated fatty acids[d]	430.7 ± 52.4	529.8 ± 107.0	28.7 ± 10.1	28.0 ± 11.2
Total fatty acids	440.3 ± 56.1	518.6 ± 96.5	36.5 ± 12.0	35.5 ± 14.1

[a]First analysis denotes initial NMR analysis of lipid extract where decoupling parameters were faulty.

[b]Second analysis denotes subsequent NMR analysis of remaining lipid extract after decoupling parameters were corrected. Lipid concentration was low, resulting in poor signal to noise ratio.

[c]Average of 2 cholesterol carbon signals for the first analysis (C18 at 12.5 ppm and C19 at 19.7 ppm) and 3 cholesterol carbon signals for the second analysis (C18 at 12.5 ppm, C19 at 19.7 ppm and C14 at 57.2 ppm).

[d]Polyunsaturated fatty acid signal intensity is subject to changes in both concentration and composition

[e]Unable to quantify signal because of poor resolution